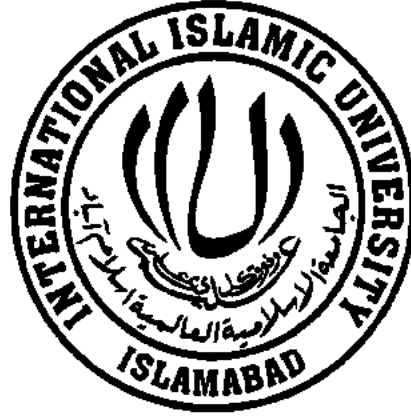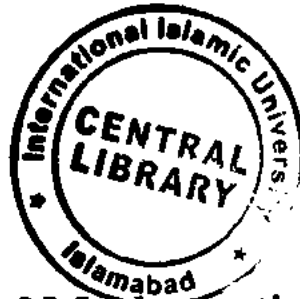# Numerical Study of Oblique Stagnation Point Flow of Non-Linear Fluids

By

Abuzar Ghaffari

Reg. No. 8-FBAS/PHDMA/S12

Department of Mathematics and Statistics
Faculty of Basic and Applied Sciences
International Islamic University
Islamabad, Pakistan

2016

phD
514.24
ABN

1. Fluid dynamics — Mathematical

models

Numerical Study of Oblique Stagnation Point Flow of Non-Linear Fluids

By

Abuzar Ghaffari

Supervised By

Dr. Tariq Javed

Department of Mathematics and Statistics
Faculty of Basic and Applied Sciences
International Islamic University
Islamabad, Pakistan
2016

Numerical Study of Oblique Stagnation Point Flow of Non-Linear Fluids

A dissertation

submitted in the partial fulfillment of the

requirements for the degree of

DOCTOR OF PHILOSOPHY

IN

MATHEMATICS

Submitted By

Abuzar Ghaffari

Supervised By

Dr. Tariq Javed

. il.

**Department of Mathematics and Statistics
Faculty of Basic and Applied Sciences
International Islamic University
Islamabad, Pakistan
2016**

. .t

Certificate

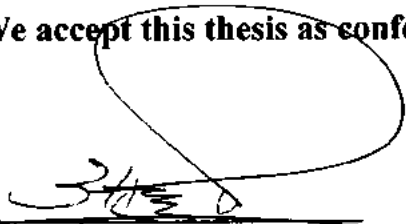# Numerical study of oblique stagnation point flow of non-linear fluids

By
Abuzar Ghaffari

A THESIS SUBMITTED IN THE PARTIAL FULFILLMENT OF THE
REQUIREMENTS FOR THE DEGREE OF THE
DOCTOR OF PHILOSOPHY IN MATHEMATICS

We accept this thesis as conforming to the required standard

1. _____
   Prof. Dr. Tasawar Hayat
   External Examiner

2. _____
   Dr. Rab Nawaz
   External Examiner

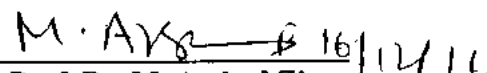3. _____
   Prof. Dr. M. Sajid, TI
   Internal Examiner

4. _____
   Dr. Tariq Javed
   Supervisor

5. _____
   Prof. Dr. M. Arshad Zia
   Chairman

Department of Mathematics and Statistics
Faculty of Basic and Applied Sciences
International Islamic University, Islamabad
Pakistan
2016

Declaration

I, hereby declare that this thesis neither as a whole nor as a part there of has been copied from any source. It is further declared that I have developed this thesis and the accompanied report entirely based on my personal efforts made under the sincere guidance of my supervisor. No portion of the work presented in this report has been submitted in support of any other degree or qualification of this or any other university or institute of learning, if found I should stand responsible.

Signature:

Name: **Abuzar Ghaffari**

Registration No.: **8-FBAS/PHDMA/S12**

v

Dedicated

To

*My Beloved Father **Muhammad Bashir***

&

My Respected Supervisor

Dr. Tariq Javed

Acknowledgment

Preface

Most of engineering and industrial problems are modeled in terms of nonlinear partial/ordinary differential equations. The exact/analytic solution of which is extremely difficult or nearly impossible. In these situations, the numerical methods are very helpful to find an approximate solution. In this thesis, we presented the numerical studies of oblique stagnation point flow for different Newtonian/non-Newtonian fluid models. Various physical aspects such as oscillating surface, vertical oscillating stretching surface, oscillating free stream, stretching sheet, MHD effect, radiation effect, oblique stagnation point flow through porous medium and heat transfer through nanofluids near stagnation point, are also investigated. The governing non-linear differential equation are solved by means of very efficient numerical techniques such as shooting method, finite difference method and spectral collocation method.

Chapter one includes, some basic information about the fluid models which are used in the whole study and literature review on orthogonal/oblique stagnation point flow is provided.

In chapter two, the study of unsteady oblique stagnation point flow due to an oscillating flat plate and oscillating free stream has been carried out. The governing partial differential equations are transformed to three coupled dimensionless, nonlinear partial differential equations. The system of equations is solved numerically by using well-known implicit finite difference scheme named as Keller-box method. The effects of pertinent parameters namely magnetic parameter, Prandtl number and impinging angle on the flow and heat transfer characteristics are illustrated through graphs. The contents of this chapter are published in **Canadian Journal of Physics 93(10) (2015) 1138-1143**.

In chapter three, a numerical study is carried out for the steady two-dimensional boundary layer flow of an incompressible Maxwell fluid in the region of oblique stagnation point over a stretching surface. The governing equations are transformed to dimensionless boundary layer

viii

equations. The reduced system of ordinary differential equations is simulated by mean of parallel shooting method. The effects of emerging dimensionless parameters are presented through graphs. Moreover, streamlines are drawn to predict the flow behavior near the stagnation point region. The contents of this chapter are published online in **Journal of Mechanics 32(2) (2016) 175-184**.

Chapter four addresses the non-linear radiation effect on the two-dimensional oblique stagnation point flow in a porous medium. Constitutive equations of viscoelastic second grade fluid are employed in the mathematical development of the relevant problem. The resulting nonlinear system is solved using Chebyshev Spectral Newton Iterative Scheme (CSNIS). Impact of sundry variables on the quantities of interest like skin friction and Nusselt number are discussed. Difference between linear and nonlinear radiation is discussed and streamlines for various values of obliqueness and porosity parameters are shown and their analysis is made. The analysis presented in this chapter is published online in **Transport in Porous Media 113(1) (2016) 245-266**.

Chapter 5 includes the study of enhancement of thermal conductivity of elastico-viscous fluid filled with nanoparticles due to the implementation of radiation and convective boundary condition. The flow is considered impinging obliquely over a stretching sheet near a stagnation point. The governing partial differential equations are transformed into a system of ordinary differential equations by employing suitable similarity transformations. Solution of the resulting equations is computed numerically using Chebyshev Spectral Newton Iterative Scheme (CSNIS). Effects of involving parameters on the flow and heat transfer characteristics are observed and shown through graphs. The findings of this chapter are published in **Thermal Science DOI:10.2298/TSCI150411163G**.

In chapter 6, the influence of radiation on the mixed convection flow of Walter's B fluid

ix

in the neighborhood of nonaligned stagnation point over a vertical oscillating flat plate has been investigated. The plate is assumed to be heated with sinusoidal surface temperature. It is further assumed that the plate is stretched linearly along the x-axis. The governing partial differential equations are transformed into dimensionless form. The obtained dimensionless partial differential equations are solved numerically using Chebyshev Spectral Newton Iterative Scheme (CSNIS). The variation of Prandtl and radiation parameter is handled through effective Prandtl number. The detailed discussion is made in this chapter with help of tables and graphs. The results of this chapter are submitted in **International Journal of Mechanical Sciences**

In chapter 7, heat transfer analysis of an unsteady oblique stagnation point flow of elastico-viscous fluid over an oscillating-stretching surface, heated due to sinusoidal wall temperature is presented. The governing partial differential equations are transformed into dimensionless form. The solution of obtained partial differential equations is computed numerically using Chebyshev Spectral Newton Iterative Scheme (CSNIS). The variation of skin friction coefficient and local Nusselt number are discussed for the wide range of time and various pertinent parameters. The contents of this chapter are published in **Journal of Molecular Liquids 219 (2016) 748-755.**

Contents

Nomenclature

a, b, c	Positive dimensional constants
a/c	Velocities ratio parameter
B_0	Strength of uniform magnetic field
Bi	Biot number
C	Solutal concentration
C_∞	Ambient solutal concentration
C_f	Skin friction coefficient
c_p	Specific heat constant
C_w	Solutal concentration at the wall
D_B	Brownian diffusion coefficient
D_T	Thermophoretic diffusion coefficient
f	Dimensionless normal component of flow
g	Dimensionless oblique component of flow
h_f	Convective heat transfer coefficient
K	Porosity parameter
k, k_f	Thermal conductivity of the fluid
k_1	Darcy permeability parameter
k_{eff}	Combined thermal conductivity of the fluid and porous medium
k_s	Thermal conductivity of solid
k_o	Elasticity of fluid
M	Dimensionless magnetic parameter
N_b	Brownian motion parameter
N_t	Thermophoresis parameter

Nu	Nusselt number
p	Pressure
Pr	Prandtl number
q_m	Mass flux at the wall
q_r	Radiative heat flux
q_w	Heat flux at the wall
Rd	Radiation conduction parameter or Planck number
Re_x	Local Reynolds number
Sc	Schmidt number
Sh_x	Local Sherwood number
T	Temperature of the fluid
t	Time
T_∞	Ambient fluid temperature
T_f	Temperature of the hot fluid
T_s	Temperature of solid
T_w	Surface temperature
$\bar{u}, \bar{v}$	Dimensional velocity components in $\bar{x}$ and $\bar{y}$ directions
u, v	Dimensionless velocity components in x and y directions
U_e	Free stream velocity
U_w	Velocity at the wall
We	Weissenberg number
x_s	Location of stagnation point
$\bar{x}, \bar{y}$	Coordinates along and normal to the surface in dimensional form
x, y	Coordinates along and normal to the surface in dimensionless form

Greek symbols

α	Obliqueness angle
α_1, α_2	Normal stress moduli
α_r	Rosseland mean absorption
β	Maxwell fluid parameter
β_T	Thermal expansion coefficient
$\beta*$	Unsteady parameter
γ	Obliqueness parameter
θ	Dimensionless temperature
θ_w	Surface Heating Parameter
ϕ	Dimensionless concentration
σ	Electrical conductivity
σ_{SB}	Stephan- Boltzmann constant
σ_s	Scattering coefficient
τ	Stress tensor
τ^*	Effective heat capacity of nanoparticle materials to heat capacity of the fluid.
τ_w	Wall shear stress
ψ	Stream function
ν	Kinematic viscosity
μ	Dynamic viscosity
Ω	Frequency of oscillation
ε	Amplitude of the plate oscillation
ε_1	Amplitude of imposed temperature oscillation
ρ	Fluid density

λ_1	Relaxation time of the material
$(\rho c)_f$	Heat capacity of the fluid
$(\rho c)_p$	Effective heat capacity of the nanoparticle material

Chapter 1

Introduction

In this chapter, fundamental knowledge related to research presented in this thesis in forth-coming chapters is provided for better understanding of the readers.

1.1 Fluid mechanics

Fluid mechanics is the branch of science which deals with the behavior of liquids and gases at rest or in motion. The term fluid in everyday life commonly refers to liquids, but through the definition, a substance that can easily gain the shape of its container is fluid or a substance is said to be fluid if it deforms continuously under the action of shear stress, no matter how small the shear stress may be, gases are also considered as fluid. Applications of fluid mechanics involves variety of mechanisms, ranging from blood flow in capillaries to flow of oil in huge pipelines and from flight of birds to supersonic airplanes. Even one can say that for all bodies in motion there is an associated fluid flow. Science of fluid mechanics is neither new nor biblical; however, most of the progress we are seeing, was made in the 20th century. Fluid mechanics and basic engineering were always integral parts of human evolution. Ancient civilizations built ships, sails, irrigation systems and food-management structures, all requiring

some basic understanding of fluid flow.

All the physical phenomena are in some way related to the laws of fluid mechanics. Application of these laws to fluid flow problems in terms of mathematics, results in the partial differential equations such as continuity equation, the equations of motion and the energy equation. These equations, for incompressible fluid flow are as follows

$$\nabla.V = 0, \tag{1.1}$$

$$\rho\frac{dV}{dt} = \nabla.\tau + \rho f, \tag{1.2}$$

$$\rho c_p\frac{dT}{dt} = \nabla.(k\nabla T) + \tau : \nabla V, \tag{1.3}$$

If we include the idea of mass transfer in fluid flow then we have another equation which can be written as

$$\rho c_p\frac{dC}{dt} = \nabla.(d\nabla C), \tag{1.4}$$

In above equations, term $\tau : \nabla V$ represents the viscous dissipation, ρ is the density, ∇ is the gradient operator, V is the velocity vector, τ is the stress tensor, f represent the body forces, c_p is the specific heat, T is the temperature, k is the thermal conductivity of the fluid, C is the species concentration for mass transfer, D is the diffusivity for mass and d/dt is the material derivative.

1.2 Newtonian fluids

The fluids in which the applied shear stress at every point is linearly proportional to the strain rate are considered as Newtonian fluids. In mathematical term for a unidirectional flow, it is represented by

$$\tau_{xy} \propto \frac{du}{dy}, \tag{1.5}$$

9

or

$$\tau_{xy} = \mu \frac{du}{dy},$$
(1.6)

where μ is the constant of proportionality commonly known as dynamic viscosity. The above relation is known as Newton's law of viscosity. For a Newtonian fluid, the stress tensor is given by $\tau = -p\mathbf{I} + \mathbf{S}$ where p is the pressure, $\mathbf{I}$ is the identity tensor and $\mathbf{S}$ is the extra stress tensor defined as $\mathbf{S} = \mu\mathbf{A}_1$, where $\mathbf{A}_1$ represents the first Rivlin-Ericksen tensor and is defined as

$$\mathbf{A}_1 = \mathbf{L} + \mathbf{L}^*,$$
(1.7)

where $\mathbf{L}$ represents the velocity gradient and $\mathbf{L}^*$ represents its transpose.

1.3 Non-Newtonian fluids

If the relationship between the applied shear stress and the rate of strain is non-linear the fluid is termed as non-Newtonian fluid. These fluids are very important due to their applications in industries including civil, metallurgical, mining and chemical engineering. Many fluids in nature have very complex behavior and cannot be studied on the basis of Newtonian fluid model only. It is therefore, different models are presented to predict the behavior of non-Newtonian fluids namely Power law model, Sisko model, Casson model, Maxwell model, Second grade model and Walter's B model etc. The rheological effects in the present thesis are captured on the basis of constitutive relationship of Maxwell, second grade and Walter's B fluids.

1.4 Mathematical models for non-Newtonian fluid flow

Different mathematical models have been proposed to study the behavior of fluid flow in different geometries. The models which are studied in this thesis are explained as follows:

1.4.1 Maxwell fluid

The rheological equation of Maxwell fluid model is

$$S + \lambda_1 \frac{DS}{Dt} = \mu A_1 \tag{1.8}$$

where λ_1 is the relaxation time of the material, which is duration of the time over which significant stress persist after termination of deformation. D/Dt is the contravariant convective derivative [80] defined as

For a contravariant vector

$$\frac{DS}{Dt} = \frac{dS}{dt} - LS \tag{1.9}$$

For a contravariant tensor of rank 2

$$\frac{DS}{Dt} = \frac{dS}{dt} - LS - SL^* \tag{1.10}$$

1.4.2 Second grade fluid

Extra stress tensor in second grade fluid obeys

$$S = \mu A_1 + \alpha_1 A_2 + \alpha_2 A_1^2, \tag{1.11}$$

where A_2 is the second Rivilin-Erickson tensor defined by the following relation

$$A_2 = \frac{dA_1}{dt} + A_1 L + L^* A_1, \tag{1.12}$$

For thermodynamically compatible second grade fluids one must have

$$\mu \geq 0, \quad \alpha_1 \geq 0, \quad \alpha_1 + \alpha_2 = 0. \tag{1.13}$$

11

1.4.3 Walter's B fluid

The stress deformation relation for a Walter's B fluid is given by

$$\mathbf{S} = \mu \mathbf{A}_1 - 2k_0 \frac{D\mathbf{A}_1}{Dt}, \qquad (1.14)$$

where

$$\frac{D\mathbf{A}_1}{Dt} = \frac{\partial \mathbf{A}_1}{\partial t} + (\mathbf{V}.\nabla)\mathbf{A}_1 - \mathbf{A}_1.\mathbf{L} - \mathbf{L}^{*}.\mathbf{A}_1. \qquad (1.15)$$

1.5 Literature review

In fluid mechanics, when fluid strikes to a rigid surface then velocity of fluid eventually become zero at a point commonly known as stagnation point. The flow in the neighborhood of stagnation point is called stagnation point flow. The two-dimensional stagnation point flow was first encountered by Hiemenz [1], also known as the Hiemenz flow. He reduced the governing partial differential equations to a nonlinear third order ordinary differential equation by means of the similarity transformation and found an exact solution of the obtained ordinary differential equation. Howarth [2] studied the steady two-dimensional boundary layer flow past an obstacle by means of various methods and provided an improved form of the Hiemenz solution. Goldstein [3] observed that Hiemenz solution satisfies the full Navier Stokes equations as well as the boundary layer equations. Various authors extended the stagnation flow in different ways. Homann [4] extented the work of Hiemenz [1] by considering the axisymmetric stagnation point flow. In the middle of last century, Howarth [5] extended the two-dimensional stagnation point flow on a general (three dimensional) surface. He modeled the boundary layer ordinary differential equations containing a single parameter c. For $c = 0$ corresponds to the two-dimensional flow and $c = 1$ corresponds to the axial flow. He computed the solution for the

12

various values of c between 0 and 1. Davey [6] numerically simulated the three dimensional stagnation point flow, where the external flow is assumed to be irrotational with components $\{ax, by, -(a+b)z\}$ with a and b are constants where $a > 0 > b$. He reported that the flow has boundary layer character and for $b/a < -0.4294$ the boundary layer flow is reversed. Eckert [7] has performed the heat transfer analysis in stagnation point flow and it was observed that the maximum heat transfer occurs in stagnation point region. Nachtsheim and Swigert [8] numerically investigated the stagnation point flow in boundary layer region. They solve the boundary value problem by first setting into initial value problem and then supplied a suitable initial guess which satisfies the condition defined at second point. The developed initial value problem was encountered by Adams-Moulton integration scheme by using least-square convergence criterion to get the unique solution. They concluded that the, applied method is insensitive to the initial guess and converges rapidly. The stagnation point flow over oscillatory walls was examined by Rott [9], in which he considered the case where the plate performed periodic oscillations in its flown plane. During the same era, Glauert [10] attempted the two-dimensional time dependent potential flow over oscillating surfaces. In this study, he not only considered the flow over oscillating plate but also extended his study for the oscillating cylinder. He reduced the Navier-Stokes equations in the form of boundary layer equations and then used similarity transformation. He solved the obtained ordinary differential equation by series method for large and small values of frequency parameter upto the enough number of terms to ensure the accuracy. He also oberved that the obtained solution satisfies the full Navier-Stokes equations. Watson [11] generalized Rotts and Glauerts work [9, 10] by allowing the periodic oscillations to be replaced by an arbitrary transverse motion. He approximated the solution by means of different techniques according to the situation. For this purpose, by means of Laplace transform method (for the case of moving wall from the rest), expansions of the velocity for

13

large and small times are expressed in terms of the velocity of the wall. Further, he expressed that how Pohlhausen type of method can be used. Stuart [12] studied the double boundary layer oscillatory viscous flow and considered case of flow generated by a circular cylinder oscillating along a diameter where the free stream velocity was assumed as a function of time. He found the asymptotic solution of the considered problem and made qualitative agreement with experimental results obtained by Schlichting [83]. Pedley [13] studied the stagnation point flow problem by considering the time dependent sinusoidal free stream velocity. Nusselt number and skin friction coefficient are calculated by means of two expansion asymptotically, a regular one for small values of $\varepsilon_1(x) = wx/U_0(x)$ and, a singular one (requiring the use of matched asymptotic expansions) for large values of ε_1. The main difference of his work with earlier authors is that the amplitude of the oscillating velocity can be considered as large. He calculated the numerical values for different emerging parameter. The boundary layer time dependent Hiemenz flow was also discussed by Grosch and Salwen [14]. They gave approximate solution for low and high frequency oscillation parameter . The approximated results are validated through numerical scheme and they found good agreement with the previous results. Merchant and Davis [15] summarized the work of Pedley [13] and Grosch and Salwen [14], extending it to consider the case where the dimensionless frequency parameter is large and the oscillatory component is much larger than the mean component. In this work, much attention is focused on the steady streaming generated in this flow with strongly non-parallel streamlines. Hazel and Pedley [16] considered an unsteady orthogonal oscillating two-dimensional stagnation point flow approaching an oscillating wall.

During the last few decades, enormous research activities in the area of stagnation point flow have been considered by many researchers in different directions having to its applications in engineering and industries. An analytical solution for steady, two dimensional

, n

stretching sheet was originated by Crane [17]. He assumed that velocity of stretching sheet is proportional to distance from the silt. This phenomena is widely encountered in many industrial applications such as materials manufacturing by polymer extrusion, wire drawing such as springs, paper clips, spokes for wheels, and stringed musical instruments, continuous stretching of plastic films, artificial fibers, hot rolling, glass fiber, metal extrusion and metal spinning, cooling of metallic sheets or electronic chips, and many others. The idea of Crane was extended by many researchers by incorporating different physical aspects such as Gupta and Gupta [18] considered the heat and mass transfer over an impermeable stretching sheet. Wang [19–21] considered three dimensional flow over a stretching sheet, flow due to a stretching cylinder and flow due to time dependent stretching sheet. Moreover, stagnation point flow over stretching sheet has gained the attention of many scientists and engineers. Chiam [22] was among the earlier scientists who considered stagnation point flow towards a stretching plate. In his study, he considered different cases of the flow like two dimensional normal/oblique stagnation point flow and axisymmetric normal/oblique stagnation point flow over stretchable sheet. Mahapatra and Gupta [23] discussed the magnetic effect near the stagnation point over a stretchable sheet. He observed the behavior of fluid flow within the boundary layer, with transverse boundary and of no boundary layer cases. In an other study, Mahapatra and Gupta [24] observed the rate of heat transfer near the stagnation point region. Nazar et al. [25] studied stagnation point flow of a micropolar fluid towards a stretching sheet. They reduced the partial differential equation into ordinary differential equation and then solved numerically by using finite difference scheme. They observed that the skin friction coefficient is lower for boundary layer and higher for transverse boundary layer flow. Similarly, the velocity of the fluid is decreasing function of K in case of boundary layer and increasing function of K in case of transverse boundary layer flow. Furthermore, Layek et al. [26] considered mass transfer

15

in stagnation point region by assuming permeable heated stretching sheet. Hayat et al. [27] consider stagnation point flow over a nonlinear stretching. Zhu et al. [28], Shit et al. [29], Bhattacharyya [30] and many others have discussed the stagnation point flow over a stretching surfaces by incorporating different aspects.

Orthogonal stagnation point flow has been interesting study area for the researcher but the less attention was devoted to oblique stagnation-point flows. Oblique stagnation-point flow appears when fluid strikes on a rigid surface at an arbitrary angle. From a mathematical point of view, such flow is obtained by combining orthogonal stagnation point flow with a shear flow parallel to the wall. The study of steady two-dimensional oblique stagnation-point flow of a Newtonian fluid was first elaborated by Stuart [31]. He first reduced the problem into system of ordinary differential equations by using similarity transformation and then found the exact solution. Following the Stuart, Tamada [32] considered steady two-dimensional stagnation point flow impinging obliquely to the plane wall. He found analytical solution of the problem and comparison is presented with existing solutions. He also sketched the stream lines to predict the fluid flow behavior. The work of Tamada, was extended by Chiam [33] with addition of moving plane wall. He found numerical solution of the problem by assuming the constant velocity of the moving sheet and considered the same stream function as reported by Tamada [32]. He obtained the result for both stationary and moving plate and for case of stationary sheet the results are compared with previous studies. Dorrepaal [34] revisited the work of Stuart [31] and Tamada [32] and found the similarity solution for two dimensional oblique stagnation point flow. In his study, he assumed the stream function in terms of impinging angle α and for $\alpha = 0$ the problem reduces to the orthogonal stagnation point flow. Lyell and Cronin [35] presented finite element solution of premixed laminar flame extinction in the region of orthogonal and oblique stagnation point flow. For case of orthogonal stagna-

16

tion flow, they compared finite element solution with previously investigated by Runge- Kutta. They found that, except in the case of Levis number unity, the effect of shear was to shift the reaction region closer to the wall. Labropulu et al. [36] extended the work of Dorrepaal [34] by considering the flat plate as permeable. They found that, suction helps to penetrate the fluid in wall, while blowing helps to shift the stagnation point and this shifting of stagnation point depends upon the magnitude of the blowing. Tilley and Weidman [37], investigated the impingement of two fluid flows forming a flat interface. They solved the governing equations numerically using shooting method with fourth order Runge- Kutta scheme and missing initial conditions are calculated through Newton-Raphson method. Amaouche and Boukari [38] investigated oblique stagnation point flow over an inclined heated flat plate. They found that buoyancy induced convection flow acts to either reinforced or oppose the fluid flow. Weidman and Putkaradze [39] studied the axisymmetric flow on a circular cylinder where the fluid is impinging to the surface. In this study they consider incorrect outer pressure filed for the case of circular cylinder. Later, in ref. [40] they presented a correct solution of their problem by considering a valid outer pressure field. Labropulu and Chinichian [41] considered time dependent oblique stagnation point flow of non-Newtonian fluid. In their article, they used constitutive equations of Walters B fluid model and assumed that the plate is oscillating with velocity $U cos t$. In last decade, Reza and Gupta [42] generalized the problem of an oblique stagnation point flow over a stretching sheet by Chiam [33] to include surface stretching rate different from that of the stagnation-point flow. In that paper, they have ignored the displacement thickness parameter and the pressure gradient parameter. This was partially rectified in a paper by Lok et al. [43]. Later, Reza and Gupta [44] gave a correct solution of steady oblique stagnation point flow over a stretching sheet. They found that the flow has a boundary layer behavior when free stream velocity is greater than stretching velocity and it has an inverted

17

boundary layer structure when free stream velocity is less than stretching velocity. Recently, Drazin and Riley [45], Mahapatra et al. [46], Tooke and Blyth [47], Grosan et al. [48], Singh et al. [49] and several others (see refs. [50–54]) have done notable work on oblique stagnation point flows.

In recent years, study of nanofluids gathered a lot of attentions due to their enormous applications. Many researchers contributed in this area due its significance in pharmaceutical and food processes, hyperthermia, fuel cells, microelectronics, hybrid-powered engines, coolants for advanced nuclear Power Plants [55] and many others. The basic idea of using nano-sized particle to enhance the thermal conductivity of the fluid was given by Maxwell [56]. Choi [57] was the first who introduce the term nanofluid in 1995. He studied the characteristics of nanofluids and deduced that the thermal conductivity of the base fluid (water, oil, bio-fluids, organic liquids, ethylene glycol etc.) can be enhanced by introducing metallic particles (average size about 10 nanometers). Nano-particles are made of different metals (Al, Cu, Ag, Au, Fe), metal carbides (SiC) non-metals (graphite carbon nanotubes), oxides (Al_2O_3, CuO, TiO_2), nitrides (AlN, SiN) etc. In 2006, Buongiorno [58] has studied the convective transport in fluid and he considered seven slip mechanisms (thermophoresis, diffusiophoresis, Brownian diffusion, inertia, Magnus effect, gravity and fluid drainage) to discuss the relative velocity of the fluid and nano-particles and he concluded that among these seven slip mechanisms only two are important. Recently Kuznetsov and Nield [59] studied the gravity driven flow by considering the buongiorno model to capture the Brownian motion and thermophoresis effects of the nanoparticles. After using the similarity transformation, they solved the reduced ordinary differential equations analytically and observed the variation in Nusselt number due to various emerging parameters like Lewis number Le, buoyancy-ratio number Nr, Brownian motion number Nb, thermophoresis number Nt and Prandtl number Pr. In an article, Kuznetsov and

18

Nield [60] considered the natural convection flow of nanofluid by considering the double diffusion effects (regular diffusion and cross-diffusion terms). Makinde and Aziz [61] studied the heat transfer in nanofluid past a stretching sheet by assuming the convective boundary conditions. The transport equations include the effects of Brownian motion and thermophoresis. They found numerical results by means of shooting method for various dimensionless parameters like, Lewis number Le, Prandtl number Pr, thermophoresis parameter Nt, Brownian motion parameter Nb and convection Biot number Bi. Hassani et al. [62] analytically investigated the boundary layer flow of nanofluid by means of HAM. They found the results in form of Nusselt and Sherwood numbers for different pertinent parameters. From the analysis, they found that heat transfer rate is a decreasing function of each dimensionless parameter while the mass transfer rate is found an increasing function for Pr and decreasing function for small Pr. There is extensive literature available on the topic through different aspects. Few representative recent studies on the topic may be seen in the refs. [63–75].

Chapter 2

Heat transfer analysis of unsteady MHD oblique stagnation point flow

In this chapter, heat transfer analysis of unsteady oblique stagnation point flow due to an oscillating flat plate and oscillating free stream has been carried out. The governing boundary layer equations are transformed to three coupled dimensionless nonlinear partial differential equations, here stream function is expressed as Hiemenz and tangential components. The equations are solved numerically by using well-known implicit finite difference scheme named as Keller-box method. To ensure the accuracy of obtained results, the comparison of numerical results is made with the results available in the literature. It is observed that the obtained solution is highly accurate and analysis is valid. The effects of pertinent parameters namely magnetic parameter, Prandtl number and impinging angle on the flow and heat transfer characteristics are illustrated through graphs.

20
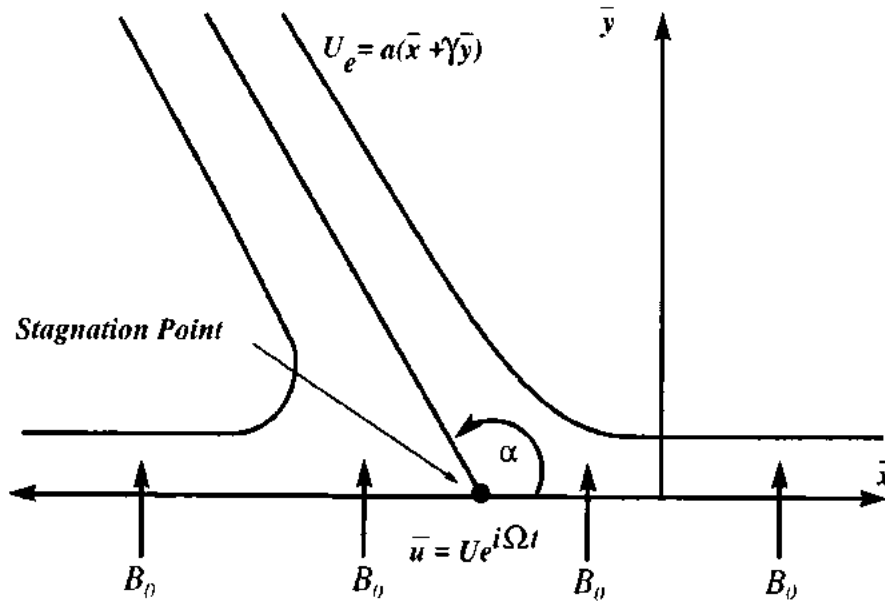
(a)

(b)
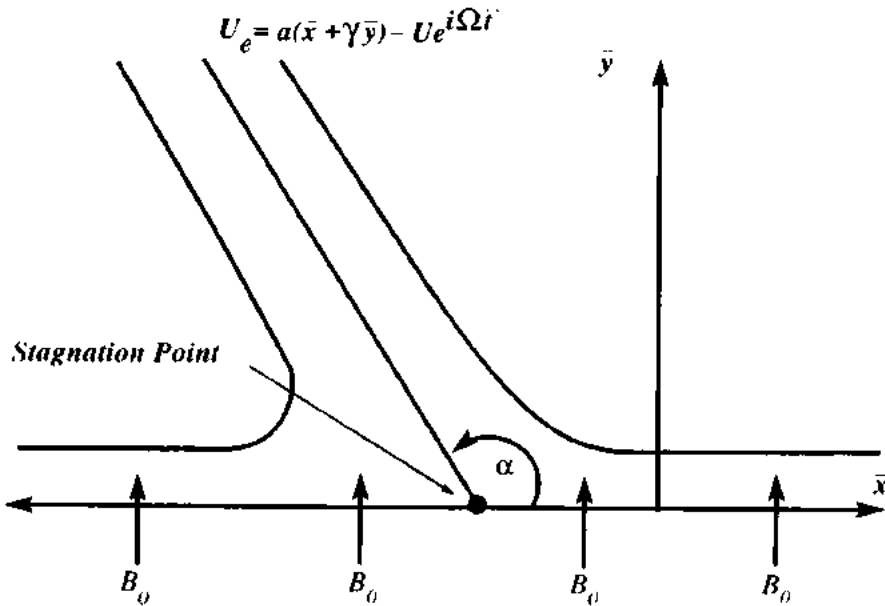
Figure 2.1: Geometery of the flow (a) due to oscillating plate (b) due to oscillating free stream

2.1 Mathematical formulation

Consider the unsteady MHD laminar, incompressible flow of a viscous fluid impinging obliquely

on an infinite flat plate oscillating in its own plane. The Cartesian coordinates $(\bar{x}, \bar{y})$ fixed in

21

space are taken, where the $\bar{x}$—axis is considered along the plate and the $\bar{y}$—axis is normal to it. The external magnetic field of uniform strength B_0 is applied in the direction of $\bar{y}$-axis with the low magnetic Reynolds number assumption is imposed so that the induced magnetic field can be neglected in comparison to the applied magnetic field. Commonly, the effect of Joule heating becomes more important for sufficiently strong applied magnetic field, but for small magnetic interaction parameter these heating effects can be neglected. The physical model and coordinate system are shown in Fig. 2.1. Under these assumptions, the continuity, the Navier-Stokes and the energy equations are given by

$$\frac{\partial \bar{u}}{\partial \bar{x}} + \frac{\partial \bar{v}}{\partial \bar{y}} = 0, \tag{2.1}$$

$$\frac{\partial \bar{u}}{\partial \bar{t}} + \bar{u}\frac{\partial \bar{u}}{\partial \bar{x}} + \bar{v}\frac{\partial \bar{u}}{\partial \bar{y}} = -\frac{1}{\rho}\frac{\partial p}{\partial \bar{x}} + \nu\left(\frac{\partial^2 \bar{u}}{\partial \bar{x}^2} + \frac{\partial^2 \bar{u}}{\partial \bar{y}^2}\right) - \frac{\sigma B_0^2}{\rho}\bar{u}, \tag{2.2}$$

$$\frac{\partial \bar{v}}{\partial \bar{t}} + \bar{u}\frac{\partial \bar{v}}{\partial \bar{x}} + \bar{v}\frac{\partial \bar{v}}{\partial \bar{y}} = -\frac{1}{\rho}\frac{\partial p}{\partial \bar{y}} + \nu\left(\frac{\partial^2 \bar{v}}{\partial \bar{x}^2} + \frac{\partial^2 \bar{v}}{\partial \bar{y}^2}\right), \tag{2.3}$$

$$\frac{\partial T}{\partial \bar{t}} + \bar{u}\frac{\partial T}{\partial \bar{x}} + \bar{v}\frac{\partial T}{\partial \bar{y}} = \frac{k}{\rho c_p}\frac{\partial^2 T}{\partial \bar{y}^2}, \tag{2.4}$$

where $\bar{u}$ and $\bar{v}$ are the $\bar{x}$ and $\bar{y}$ components of velocity respectively, t is time, ν be the kinematic viscosity, σ be the electrical conductivity, B_0 be the strength of uniform magnetic field, ρ be the density of the fluid, T be the temperature of fluid, c_p is the specific heat and k is the thermal conductivity of the fluid. The boundary conditions in case of oscillating plate and in case of oscillating free stream with the time dependent velocity are given by

For oscillating plate:

$$\bar{u} = Ue^{i\Omega t}, \ \bar{v} = 0, \ T = T_w \quad \text{at} \quad \bar{y} = 0.$$
$$\bar{u} = a(\bar{x} + \gamma \bar{y}), \ T = T_\infty \quad \text{as} \quad \bar{y} \to \infty, \tag{2.5}$$

For oscillating free stream:

$$\bar{u} = 0, \ \bar{v} = 0, \ T = T_w \quad \text{at} \quad \bar{y} = 0,$$
$$\bar{u} = U_e, \ T = T_\infty \quad \text{as} \quad \bar{y} \to \infty, \tag{2.6}$$

22

where T_w is the wall temperature, T_∞ is the ambient temperature, $U_e = a(\bar{x} + \gamma\bar{y}) - Ue^{i\Omega\bar{t}}$ is the oscillating free stream velocity, a is the constant having dimension inverse of time, Ω represents the frequency of oscillation, U is the amplitude of the oscillating velocity and γ is the non-dimensional constant characterizing the obliqueness of oncoming flow. After eliminating pressure p from Eqs. (2.2) and (2.3), we get

$$\frac{\partial^2 \bar{u}}{\partial \bar{t} \partial \bar{y}} - \frac{\partial^2 \bar{v}}{\partial \bar{t} \partial \bar{x}} + \frac{\partial \bar{u}}{\partial \bar{y}}\frac{\partial \bar{u}}{\partial \bar{x}} + \bar{u}\frac{\partial^2 \bar{u}}{\partial \bar{y} \partial \bar{x}} + \frac{\partial \bar{v}}{\partial \bar{y}}\frac{\partial \bar{u}}{\partial \bar{y}} + \bar{v}\frac{\partial^2 \bar{u}}{\partial \bar{y}^2} - \frac{\partial \bar{u}}{\partial \bar{x}}\frac{\partial \bar{v}}{\partial \bar{x}} - \bar{u}\frac{\partial^2 \bar{v}}{\partial \bar{x}^2} -$$

$$\frac{\partial \bar{v}}{\partial \bar{x}}\frac{\partial \bar{v}}{\partial \bar{y}} - \bar{v}\frac{\partial^2 \bar{v}}{\partial \bar{y} \partial \bar{x}} = v\left(\frac{\partial^3 \bar{u}}{\partial \bar{y} \partial \bar{x}^2} + \frac{\partial^3 \bar{u}}{\partial \bar{y}^3} - \frac{\partial^3 \bar{v}}{\partial \bar{x}^3} - \frac{\partial^3 \bar{v}}{\partial \bar{x} \partial \bar{y}^2}\right) - \frac{\sigma B_0^2}{\rho}\frac{\partial \bar{u}}{\partial \bar{y}}. \qquad (2.7)$$

Following Takemitsu and Matunobu [76], the stream function is chosen of the following form

$$\psi^* = a\left(\bar{x}\bar{f}(\bar{y}) + \bar{g}(\bar{y}, t)\right) \qquad (2.8)$$

The boundary conditions reduced to

For oscillating plate:

$$\bar{f} = \bar{g} = 0, \; \bar{f}_{\bar{y}} = 0, \; \bar{g}_{\bar{y}} = \frac{U}{a}e^{i\Omega\bar{t}} \quad \text{at} \quad \bar{y} = 0,$$

$$\bar{f} \sim \bar{y}, \; \bar{g} \sim (1/2)\gamma\bar{y}^2, \; T \rightarrow T_\infty \quad \text{as} \quad \bar{y} \rightarrow \infty, \qquad (2.9)$$

For oscillating free stream:

$$\bar{f} = \bar{g} = 0, \quad \bar{f}_{\bar{y}} = 0, \quad \bar{g}_{\bar{y}} = 0 \quad \text{at} \quad \bar{y} = 0,$$

$$\bar{f} \sim \bar{y}, \; \bar{g} \sim (1/2)\gamma\bar{y}^2 - \frac{U}{a}\bar{y}e^{i\Omega\bar{t}}, \; T \rightarrow T_\infty \quad \text{as} \quad \bar{y} \rightarrow \infty, \qquad (2.10)$$

using Eq. (2.8) we get

$$\bar{u} = \frac{\partial \psi^*}{\partial \bar{y}} = a\left(\bar{x}\bar{f}_{\bar{y}} + \bar{g}_{\bar{y}}\right), \; \bar{v} = -\frac{\partial \psi^*}{\partial \bar{x}} = -a\bar{f}, \qquad (2.11)$$

where the suffix denotes partial differentiation with respect to $\bar{y}$. After substituting Eqs. (2.8) and (2.11) in Eq. (2.7), we obtain the following equation:

$$\bar{g}_{\bar{y}\bar{y}\bar{t}} + a\left\{\left(\bar{x}\bar{f}_{\bar{y}\bar{y}} + \bar{g}_{\bar{y}\bar{y}}\right)\bar{f}_{\bar{y}} + \bar{f}_{\bar{y}\bar{y}}\left(\bar{x}\bar{f}_{\bar{y}} + \bar{g}_{\bar{y}}\right) - \bar{f}_{\bar{y}}\left(\bar{x}\bar{f}_{\bar{y}\bar{y}} + \bar{g}_{\bar{y}\bar{y}}\right) - \bar{f}\left(\bar{x}\bar{f}_{\bar{y}\bar{y}\bar{y}} + \bar{g}_{\bar{y}\bar{y}\bar{y}}\right)\right\}$$

$$= v\left(\bar{x}\bar{f}_{\bar{y}\bar{y}\bar{y}\bar{y}} + \bar{g}_{\bar{y}\bar{y}\bar{y}\bar{y}}\right) - \frac{\sigma B_0^2}{\rho}\left(\bar{x}\bar{f}_{\bar{y}\bar{y}} + \bar{g}_{\bar{y}\bar{y}}\right), \qquad (2.12)$$

23

Equating like powers of x, we have

$$a\left(2\bar{f}_{\bar{y}}\bar{f}_{\bar{y}\bar{y}} - \bar{f}\bar{f}_{\bar{y}\bar{y}\bar{y}} - \bar{f}_{\bar{y}}\bar{f}_{\bar{y}\bar{y}}\right) = \nu\bar{f}_{\bar{y}\bar{y}\bar{y}\bar{y}} - \frac{\sigma B_0^2}{\rho}\bar{f}_{\bar{y}\bar{y}}, \qquad (2.13)$$

$$\bar{g}_{\bar{y}\bar{y}\bar{t}} + a\left(\bar{g}_{\bar{y}\bar{y}}\bar{f}_{\bar{y}} + \bar{g}_{\bar{y}}\bar{f}_{\bar{y}\bar{y}} - \bar{f}\bar{g}_{\bar{y}\bar{y}\bar{y}} - \bar{f}_{\bar{y}}\bar{g}_{\bar{y}\bar{y}}\right) = \nu\bar{g}_{\bar{y}\bar{y}\bar{y}\bar{y}} - \frac{\sigma B_0^2}{\rho}\bar{g}_{\bar{y}\bar{y}}. \qquad (2.14)$$

Integrating Eqs. (2.13) and (2.14) with respect to $\bar{y}$ and applying the free stream conditions on obtains

For oscillating plate:

$$a\left(\left(\bar{f}_{\bar{y}}\right)^2 - \bar{f}\bar{f}_{\bar{y}\bar{y}} - 1\right) = \nu\bar{f}_{\bar{y}\bar{y}\bar{y}} - \frac{\sigma B_0^2}{\rho}\left(\bar{f}_{\bar{y}} - 1\right), \qquad (2.15)$$

$$\bar{g}_{\bar{y}\bar{t}} + a\left(\bar{f}_{\bar{y}}\bar{g}_{\bar{y}} - \bar{f}\bar{g}_{\bar{y}\bar{y}}\right) = \nu\bar{g}_{\bar{y}\bar{y}\bar{y}} - \frac{\sigma B_0^2}{\rho}\left(\bar{g}_{\bar{y}} - \gamma\bar{y}\right). \qquad (2.16)$$

For oscillating free stream:

$$a\left(\left(\bar{f}_{\bar{y}}\right)^2 - \bar{f}\bar{f}_{\bar{y}\bar{y}} - 1\right) = \nu\bar{f}_{\bar{y}\bar{y}\bar{y}} - \frac{\sigma B_0^2}{\rho}\left(\bar{f}_{\bar{y}} - 1\right), \qquad (2.17)$$

$$\bar{g}_{\bar{y}\bar{t}} + a\left(\bar{f}_{\bar{y}}\bar{g}_{\bar{y}} - \bar{f}\bar{g}_{\bar{y}\bar{y}}\right) = \nu\bar{g}_{\bar{y}\bar{y}\bar{y}} - \frac{\sigma B_0^2}{\rho}\left(\bar{g}_{\bar{y}} - \gamma\bar{y} + \frac{U}{a}e^{i\Omega\bar{t}}\right) - Ue^{i\Omega\bar{t}} - \left(\frac{U}{a}\right)i\Omega e^{i\Omega\bar{t}}. \qquad (2.18)$$

Introducing the non-dimensional variables as follows:

$$\bar{y} = \left(\frac{\nu}{a}\right)^{\frac{1}{2}}y, \bar{t} = \frac{t}{\Omega}, \bar{f}(\bar{y}) = \left(\frac{\nu}{a}\right)^{\frac{1}{2}}f(y), \bar{g}(\bar{y},\bar{t}) = \left(\frac{\nu}{a}\right)g(y,t), T = T_\infty + (T_w - T_\infty)\theta, \quad (2.19)$$

the Eqs. (2.15) - (2.18) and (2.4) with boundary conditions reduce to the following dimensionless form

For oscillating plate:

$$f''' + ff'' - (f')^2 - M(f' - 1) + 1 = 0, \qquad (2.20)$$

$$g''' + fg'' - f'g' - \beta^*\overset{\bullet}{g} - M(g' - \gamma y) = 0, \qquad (2.21)$$

For oscillating free stream:

$$f''' + ff'' - (f')^2 - M(f' - 1) + 1 = 0, \qquad (2.22)$$

$$g''' + fg'' - f'g' - \beta^*\overset{\bullet}{g} - M(g' - \gamma y + \varepsilon e'') = (1 + i\beta^*)\varepsilon e'' \qquad (2.23)$$

24

Energy equation

$$\frac{1}{Pr}\theta'' + f\theta' - \beta^* \overset{\bullet}{\theta} = 0,$$ (2.24)

and the boundary conditions in dimensionless variables are

For oscillating plate:

$$f = g = 0, \ f' = 0, \ g' = \varepsilon e^{it}, \ \theta = 1 \ \text{at} \ y = 0, t \ge 0,$$

$$f' = 1, \ g'' = \gamma, \ \theta = 0 \ \text{as} \ y \to \infty, t \ge 0,$$ (2.25)

For oscillating free stream:

$$f = g = 0, \ f' = 0, \ g' = 0, \ \theta = 1 \ \text{at} \ y = 0,$$

$$f' = 1, \ g' = \gamma y - \varepsilon e^{it}, \ \theta = 0 \ \text{as} \ y \to \infty.$$ (2.26)

where prime denotes differentiation with to y and $\bullet$ denotes differentiation with respect to t and $M = \sigma B_0^2/\rho a$ is the magnetic parameter, $Pr = \mu c_p/k$ is the Prandtl number, $\beta^* = \Omega/a$ is the unsteady parameter and $\varepsilon = U/(v a)^{1/2}$ is the amplitude of the oscillating velocity in dimensionless form . The drag force at the surface in form of skin friction coefficient C_f is given by

$$C_f = \frac{\tau_w}{\rho U^2} \quad , \tau_w = \mu \left(\frac{\partial \bar{u}}{\partial \bar{y}} \right)_{\bar{y}=0},$$ (2.27)

$$(\varepsilon \cos t)^2 C_f = x f''(0) + \frac{\partial^2 g}{\partial y^2}(0, t),$$ (2.28)

where $\bar{x}$ has been replaced by a non-dimensional variable $x = (a v)^{1/2}\bar{x}$. The non-dimensional stream function and velocity components are

$$\psi = \frac{\psi^*}{v} = x f(y) + g(y, t),$$ (2.29)

$$u = \frac{\bar{u}}{\sqrt{va}} = x f'(y) + \frac{\partial g}{\partial y},$$ (2.30)

$$v = \frac{\bar{v}}{\sqrt{va}} = -f(y)$$ (2.31)

25

In Fig. (2.1), the dividing stream line making angle α with the plate. The dividing stream line is a straight line whose slope can be found by substituting $\psi = 0$ as discussed in [34]

For oscillating plate:

$$\psi = xy + \frac{1}{2}\gamma y^2 = 0, \ \Rightarrow \ y = \left(-\frac{2}{\gamma}\right)x. \tag{2.32}$$

above equation implies that slope of the dividing streamline is

$$slope = -\frac{2}{\gamma}. \tag{2.33}$$

Hence the relationship between shearing parameter γ and impinging angle over an oscillating plate is

$$\alpha = \tan^{-1}\left(-\frac{2}{\gamma}\right). \tag{2.34}$$

For oscillating free stream:

$$\psi = xy + \frac{1}{2}\gamma y^2 - \varepsilon e^{it} = 0, \ \Rightarrow \ y = \left(-\frac{2}{\gamma}\right)x + \frac{2}{\gamma}\varepsilon e^{it}, \tag{2.35}$$

The slope of dividing streamline in case of oscillating free stream is $(-2/\gamma)$ where $\left(2\varepsilon e^{it}/\gamma\right)$ represents the $y-$intercept. So the relation between α and γ is same as given in Eq. (2.34).

2.2 Keller box scheme

The numerical solution of nonlinear partial differential Eqs. (2.20)–(2.24) with boundary conditions (2.25) and (2.26) is found by implementing an implicit finite difference scheme named as Keller box method having second order accuracy. This numerical method is highly accurate and rapid convergent. The details of the method is well explained by Cebeci and Bradshaw [77] and Keller and Cebeci [78]. For implementation of this numerical scheme, we first convert the higher order differential equations into the system of first order differential

equations. For this purpose, new dependent variables $U(y)$, $V(y)$, $P(y,t)$, $Q(y,t)$ and $R(y,t)$ are introduced. So the equation for oscillating plate i.e Eqs(2.20, 2.21, 2.24) with boundary conditions (2.25) in the form of first order differential equations can be represented as

$$f' = U,$$

$$\left(f'' =\right) U' = V,$$

$$g' = P,$$

$$\left(g'' =\right) P' = R.$$

Thus Eqs. (2.20) and (2.21) reduces to the following form

$$V' + fV - U^2 - M(U - 1) + 1 = 0,$$

$$R' + fR - UP - \beta^* \frac{\partial P}{\partial t} - M(P - \gamma y) = 0,$$

Energy equation:

$$\theta' = Q$$

$$\frac{1}{Pr} Q' + fQ - \beta^* \frac{\partial \theta}{\partial t} = 0$$

and boundary conditions (2.25) become

$$f = g = 0, U = 0, P = \varepsilon e^{it}, \theta = 1 \quad \text{at} \quad y = 0, t \geq 0,$$

$$U = 1, R = \gamma, \theta = 0 \quad \text{as} \quad y \to \infty, t \geq 0,$$

The infinite domain $[0, \infty)$ is truncated to $[0, L]$ where L is taken as sufficiently large. This truncated region is discritized into small rectangular elements on the (y, t) plane and net points are denoted as

$$y^0 = 0, \quad y^n = y^{n-1} + \Delta y, \quad n = 1,2,3,\ldots,N.$$

$$t_0 = 0, \quad t_j = t_{j-1} + \Delta t, \quad j = 1,2,3,\ldots,M.$$

Here n and j are positive integers on the (y, t) plane Δy and Δt are the widths of meshing variables. The approximate quantities of $f(y)$, $U(y)$, $V(y)$, $g(y,t)$, $P(y,t)$, $Q(y,t)$ and $R(y,t)$ at the net points (y_n, t_j) are called net functions. The derivatives in y and t-directions are replaced by the central difference formulae like:

$$\frac{\partial}{\partial y} \left(\right)\Big|_j^{n-1/2} = \frac{1}{\Delta y}\left(\left(\right)_j^n - \left(\right)_j^{n-1}\right), \quad \frac{\partial}{\partial t}\left(\right)\Big|_j^{n-1/2} = \frac{1}{\Delta t}\left(\left(\right)_j^n - \left(\right)_{j-1}^n\right)$$

and the values of the functions are replaced by its mean value as

$$\left(\right)_j^{n-1/2} = \frac{1}{2}\left(\left(\right)_j^n + \left(\right)_j^{n-1}\right), \quad \left(\right)_{j-1/2}^n = \frac{1}{2}\left(\left(\right)_j^n + \left(\right)_{j-1}^n\right).$$

For handling the non-linearity of resulting algebraic equations, Newton's linearization process is performed. For $(i+1)$th iterations the unknown functions are written as

$$f_j^{i+1} = f_j^i + \delta f_j^i, \quad U_j^{i+1} = U_j^i + \delta U_j^i, \quad V_j^{i+1} = V_j^i + \delta V_j^i,$$

$$g_j^{i+1} = g_j^i + \delta g_j^i, \quad P_j^{i+1} = P_j^i + \delta P_j^i, \quad R_j^{i+1} = R_j^i + \delta R_j^i,$$

$$\theta_j^{i+1} = \theta_j^i + \delta \theta_j^i, \quad Q_j^{i+1} = Q_j^i + \delta Q_j^i$$

After linearization, obtained system of linear algebraic equations is solved by using tri-diagonal block elimination method. Similar procedure can be adopted for the equation of flow and heat transfer due to oscillating free stream.

28

2.3 Results and Discussion

2.3.1 For oscillating plate

For the case of oscillating plate, system of differential equations (2.20), (2.21) and (2.24) subject to the boundary conditions (2.25) is solved numerically, first for the steady case i.e. for $t = 0$ by using Keller-box method and we proceed for $t = \pi/4$, $\pi/2$ and π by assuming the solution at $t = 0$ as an initial guess. The step size Δy in y and the edge of the boundary layer y_∞ is adjusted for different values of the parameters like M, Pr, and γ to maintain accuracy of the results. The step size $\Delta y = 0.01$ and $\Delta t = \pi/36$ are kept fixed for the present numerical study. To ensure the accuracy of our obtained results, a comparison of the values of $f''(0)$ against M is made with that of Ariel [79] and Grosan et al. [48] in Table 2.1. It shows that the obtained results are accurate and are in good agreement with that of previous studies. The results for velocity and temperature profiles have been discussed through graphs. Fig. 2.2 shows the behavior of stream function $\psi(x,y)$ for two different values of the magnetic parameter M when $\gamma=1, \beta=2, \varepsilon =1$ and $Pr=0.7$ against x. Fig. 2.2(a-d) illustrate the streamlines for $t =0$, $\pi/4$, $\pi/2$ and π respectively. The dash lines represent streamlines in the absence of magnetic field i.e. $M=0$ [76] and the solid lines show the streamlines in the presence of magnetic field when $M=2$. It is observed that the application of magnetic field helps to translate the stagnation point. It is also noted that the streamlines come closer to the plate and the boundary layer thickness reduces which indicates the increase in the velocity occur due to the presence of magnetic field. The Fig. 2.3 (a-d) represent the velocity profiles for the values of $t=0$, $\pi/4$, $\pi/2$ and π respectively. It is seen that the velocity increases with the increase in the value of M. It has also been noticed that the velocity at the wall oscillates between -1 to 1 for different values of t. Fig. 2.4 shows the velocity profile $u(x,y)$ for various values of the constant shear parameter

γ when $x=1, M=0$, $\beta^*=2$ $\varepsilon =1$ and Pr=0.7. Fig. 2.4 (a-d) show the velocity profiles for $t =0$, $\pi/4$, $\pi/$ and π respectively. An increase in the velocity u has been observed by increasing the value of γ. An oscillation in the velocity at the wall from -1 to 1 has been observed. Fig.2.5 shows the temperature profile $\theta(y,t)$ for various values of the magnetic parameter $M=0, 1, 2, 5$ when $t = 0, \gamma = 2, \beta^* = 2, \varepsilon = 1$ and $Pr=0.7$. It is observed that an increase in the value of magnetic parameter M decreases the thickness of the thermal boundary layer. Fig. 2.6 shows the temperature profile $\theta(y,t)$ for different values of the Pr at $t = 0, \gamma = 2, \beta^* = 2, \varepsilon = 1$. The dashed lines are for magnetic parameter $M=0$ and solid lines for magnetic parameter $M=2$. The increase in the value of Prandtl number reduces the thermal boundary layer thickness. It is also observed that there is no effect of unsteadiness on the temperature.

2.3.2   For oscillating free stream

For the case of oscillating free stream, system of differential equations (2.22), (2.23) subject to the boundary conditions (2.26) is solved numerically by using Keller-box method as described above. Fig. 2.7(a-d) shows the stream function $\psi(x, y)$ for two different values of the magnetic parameter M at $\gamma = 2, \beta^* = 2, \varepsilon = 1$ and Pr $= 0.7$ where $t =0$, $\pi/4$, $\pi/2$ and π respectively. The dash lines represent streamlines in the absence of magnetic field i.e. $M = 0$ and the solid lines show the streamlines in the presence of magnetic field i.e. $M = 2$. It is observed that at different time steps, the location of stagnation point can be made closer to the reference point and the streamlines become closer to the wall by applying magnetic field. Also it reduces the boundary layer thickness. Fig. 2.8(a-d) represents the steam lines for $\varepsilon = 0$ (the dashed lines) and $\varepsilon = 2$ (the solid lines) where $\gamma = 1, \beta^* = 2$, Pr $= 0.7$ and $M = 2$ at $t =0$, $\pi/4$, $\pi/2$ and π are fixed respectively. It is seen that the stagnation point oscillates between 1.5 and -2.5 with -0.5 as its mean value at different time steps. The Fig. 2.9(a-d) show the variation of

non-dimensional velocity profiles $u(x = 1, y)$ for different values of $M = 0, 0.5, 1, 2$ where $\gamma = 1, \beta^* = 2, \varepsilon = 1$ and $Pr = 0.7$. It is noted that there is a slight increase in the velocity with the increase in values of magnetic field at the different time steps $t = 0, \pi/4, \pi/2$ and π. In Fig. 2.10(a-d), variation of the non-dimensional velocity $u(x = 1, y)$ for different values of $\varepsilon = 0, 1, 2, 5$ where $\gamma = 1, \beta^* = 2, M = 2$ and $Pr = 0.7$ has been illustrated at the different time steps $t = 0, \pi/4, \pi/2$ and π respectively. For $t = 0$ and $\pi/4$, increase in ε results in decrease of the velocity $u(x, y)$ while for $t = \pi/2$ and π, the velocity $u(x = 1, y)$ increases with increase in the value of ε. Fig. 2.11 shows the value of skin friction coefficient against t for different values of ε while $M = 2, \gamma = 2, \beta^* = 2$ and $x = 1$. It is noted that the amplitude of oscillation in values of the skin friction coefficient increases with increase in ε. Fig. 2.12 illustrate the behavior of the skin friction coefficient for different values of γ against t when $M = 2, x = 1, \beta^* = 2$ and $\varepsilon = 1$. It is observed that with an increase in values of the γ, the values of skin friction coefficient increases but oscillates with the same amplitude. Fig. 2.13 expresses the trend of the skin friction coefficient for different values of magnetic parameter M against the values of t when $\gamma = 2, x = 1, \beta^* = 2$ and $\varepsilon = 1$. With increase in values of M, periodic increase in the skin friction coefficient has been observed. It is also noted that amplitude of oscillation of the skin friction coefficient increases by increasing M.

Table 2.1: Comparison of the variation of $f''(0)$ for the different values of M with the results obtained by Ariel [79] and Grosan et al. [48], when $\gamma = 0, \beta^* = 0, \varepsilon = 0$.
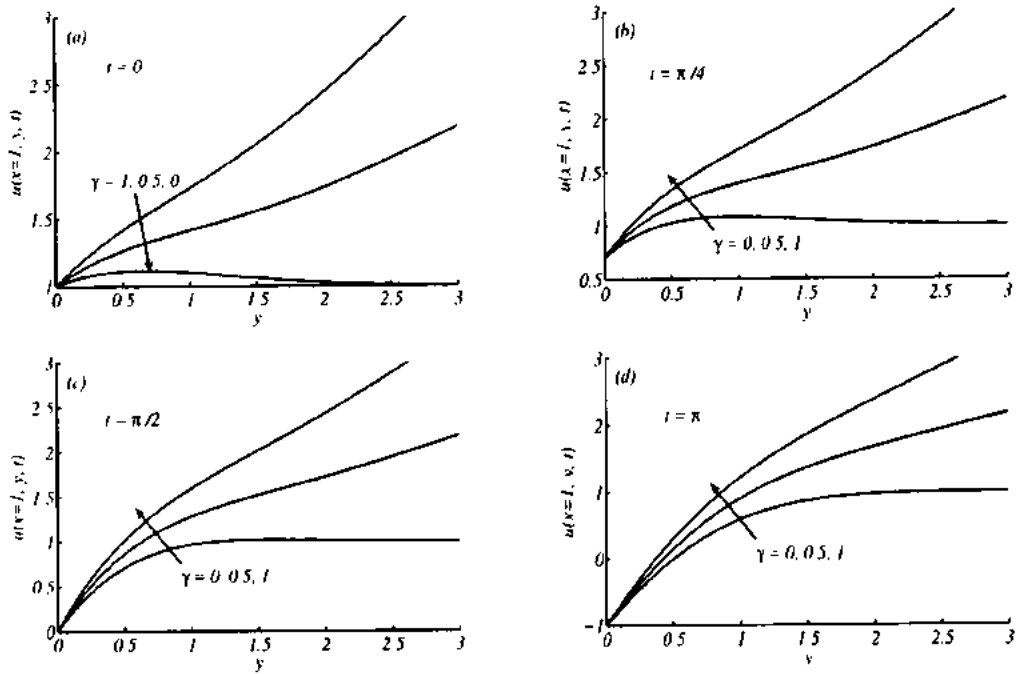
| M	Ariel [79]	Grosan et al. [48]	Present study
0.0	1.232588	1.232588	1.232597
0.16	1.295368	1.295368	1.295377
0.64	1.467976	1.467976	1.467987
1.00	1.585331	1.585331	1.585342
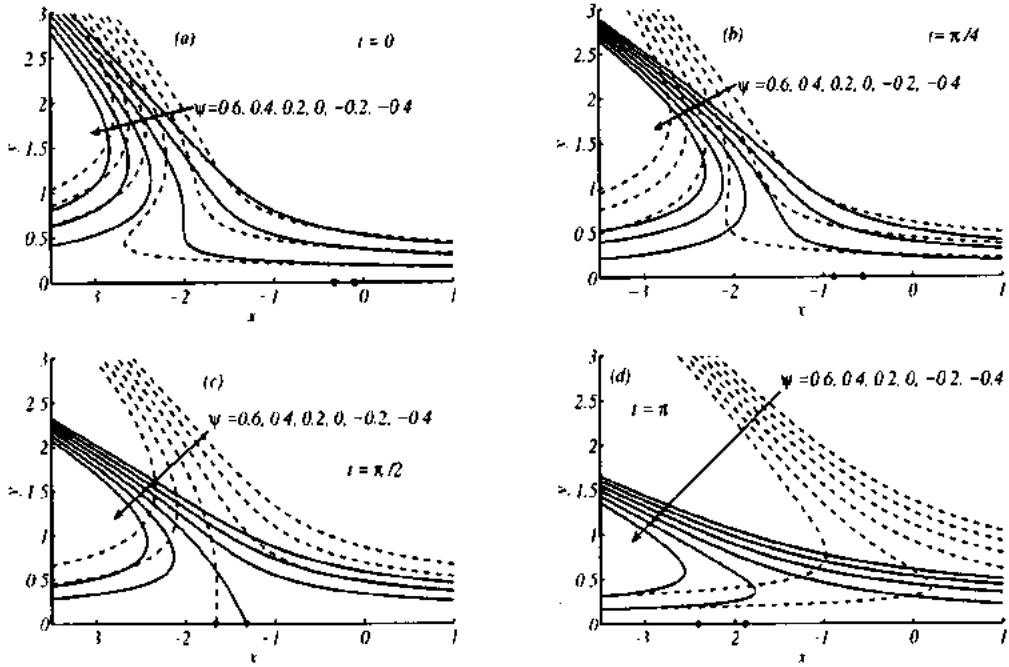
Figure 2.2: Streamlines for (a) $t = 0.0$, (b) $t = \pi/4$, (c) $t = \pi/2$ and (d) $t = \pi$ with $M = 0$ (dashed lines) and $M = 2$ (solid lines) while $\gamma = 1$, $\beta^* = 2$, $\varepsilon = 1$ and $Pr = 0.7$.
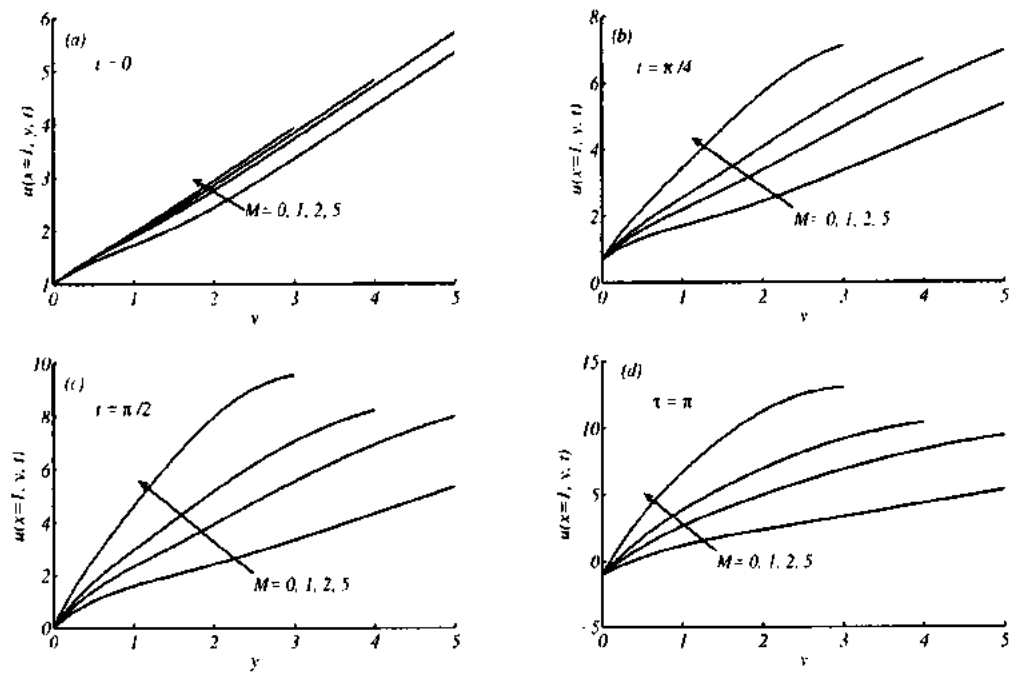
Figure 2.3: Velocity profile u for different values of M while $x = 1, \gamma = 1, \beta^* = 2, \varepsilon = 1$ and $Pr = 0.7$ at (a) $t = 0.0$, (b) $t = \pi/4$, (c) $t = \pi/2$ and (d) $t = \pi$.

32

Figure 2.4: Velocity profile u for different values of γ while $x = 1, M = 1, \beta^* = 2, \varepsilon = 1$ and

$Pr = 0.7$ at **(a)** $t = 0.0$, **(b)** $t = \pi/4$, **(c)** $t = \pi/2$ and **(d)** $t = \pi$.
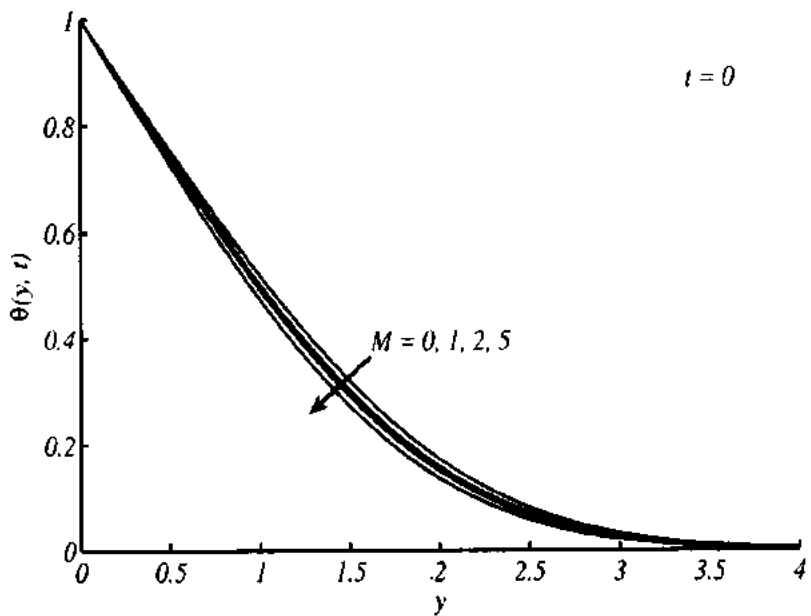
Figure 2.5: The temperature profile $\theta(y, t)$ for different values of M at $t = 0$.

33

Figure 2.6: The temperature profile $\theta(y, t)$ for different values of Pr at $t = 0$.
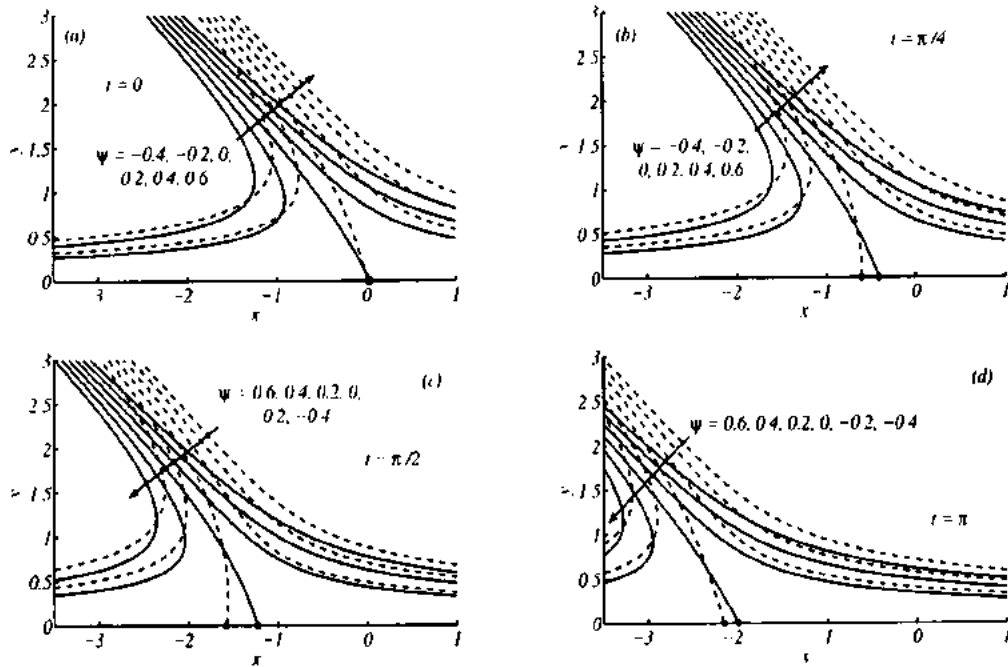
Figure 2.7: Streamlines for **(a)** $t = 0.0$, **(b)** $t = \pi/4$, **(c)** $t = \pi/2$ and **(d)** $t = \pi$ with $M = 0$ (dashed lines) and $M = 2$ (solid lines) while $\gamma = 2, \beta^* = 2, \varepsilon = 1$ and $Pr = 0.7$.
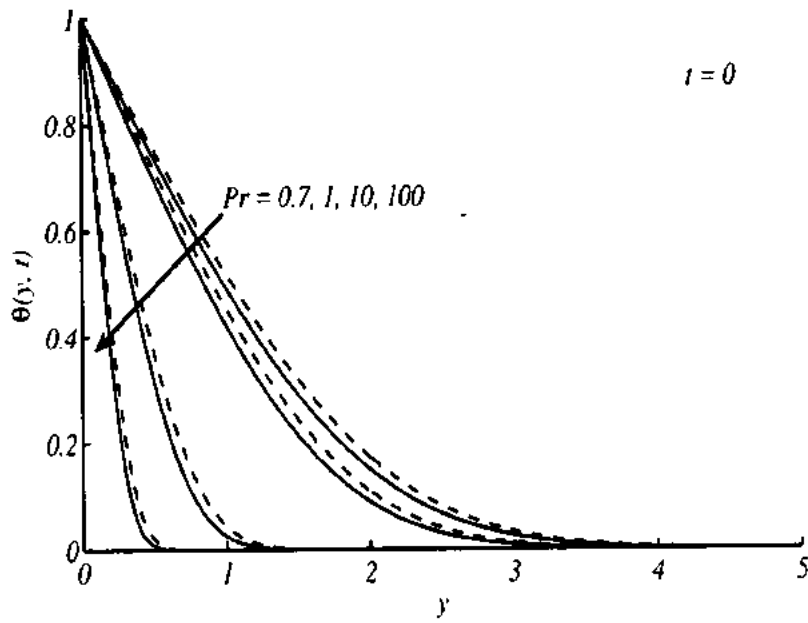
Figure 2.8: Streamlines for **(a)** $t = 0.0$, **(b)** $t = \pi/4$, **(c)** $t = \pi/2$ and **(d)** $t = \pi$ with $\varepsilon = 0$ (dashed lines) and $\varepsilon = 2$ (solid lines) while $\gamma = 1$, $\beta^* = 2$, $M = 2$ and $Pr = 0.7$.
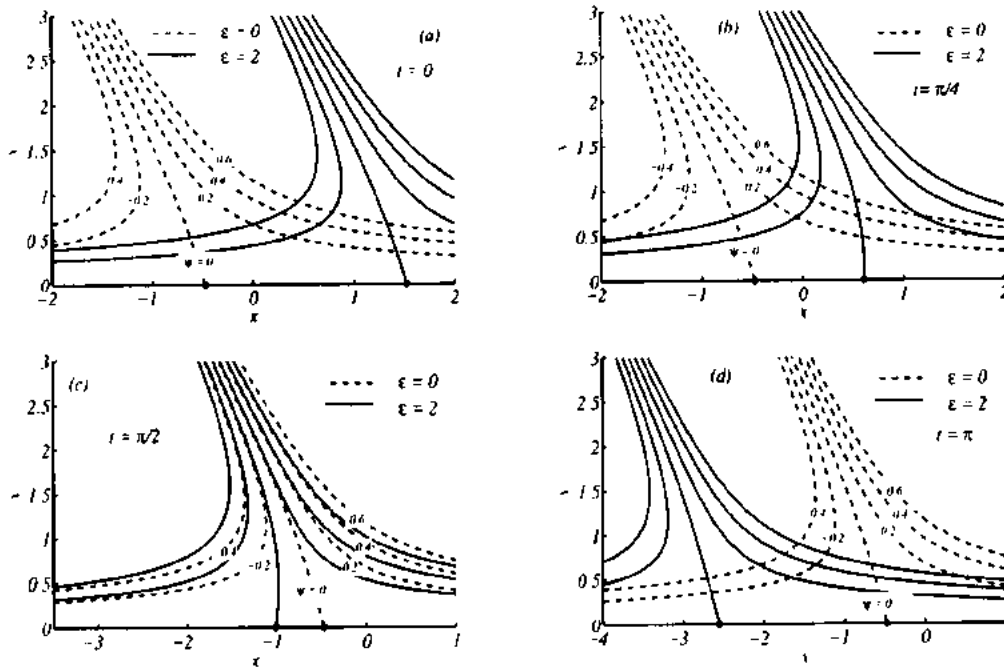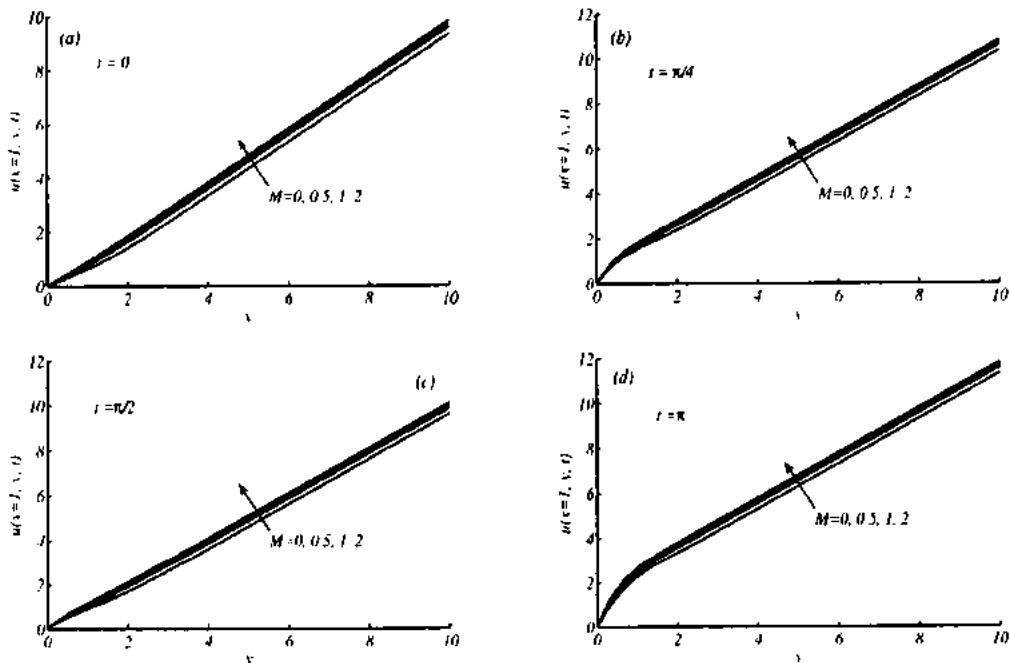

Figure 2.9: The velocity profile u for different values of M while $x = 1$, $\gamma = 1$, $\varepsilon = 1$, $\beta^* = 2$ and $Pr = 0.7$ at **(a)** $t = 0.0$, **(b)** $t = \pi/4$, **(c)** $t = \pi/2$ and **(d)** $t = \pi$.

35
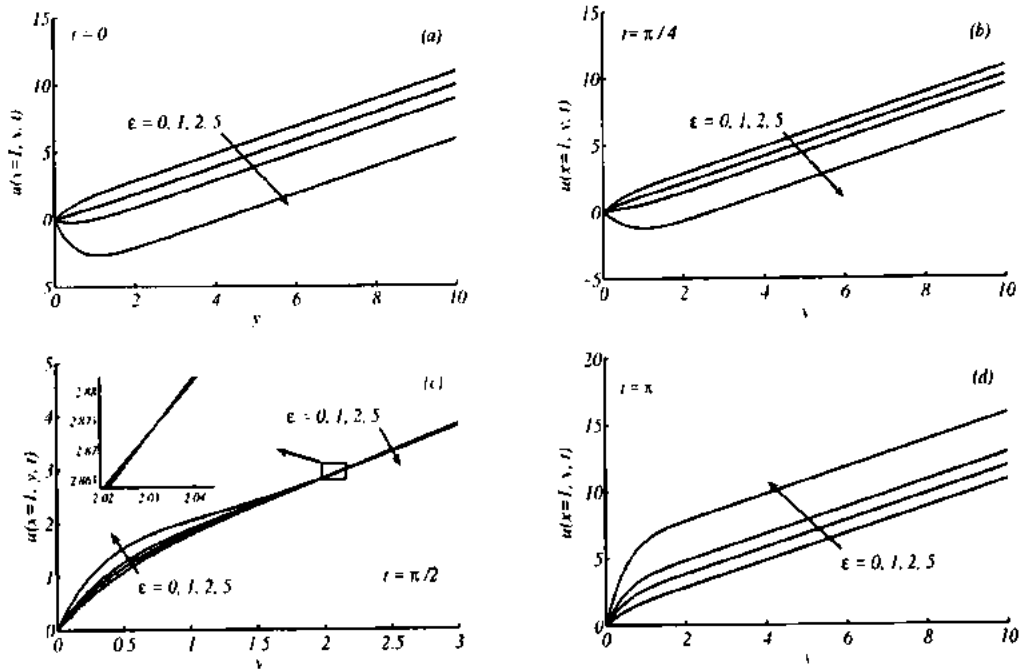
Figure 2.10: The velocity profile u for different values of ε while $x - 1, \gamma = 1, M = 2, \beta^* = 2$ and $Pr = 0.7$ at **(a)** $t = 0.0$, **(b)** $t = \pi/4$, **(c)** $t = \pi/2$ and **(d)** $t = \pi$.
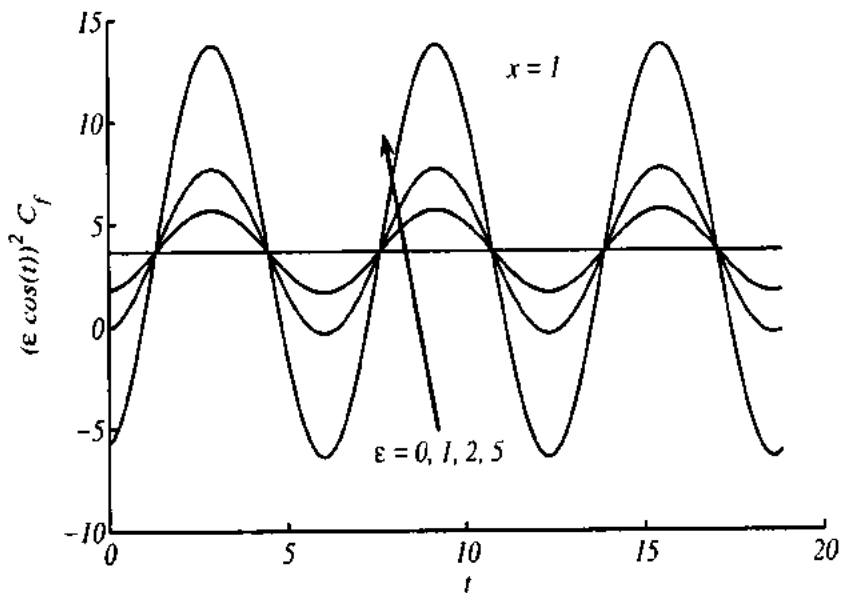
Figure 2.11: Skin friction coefficient for different values of ε at $x - 1$.
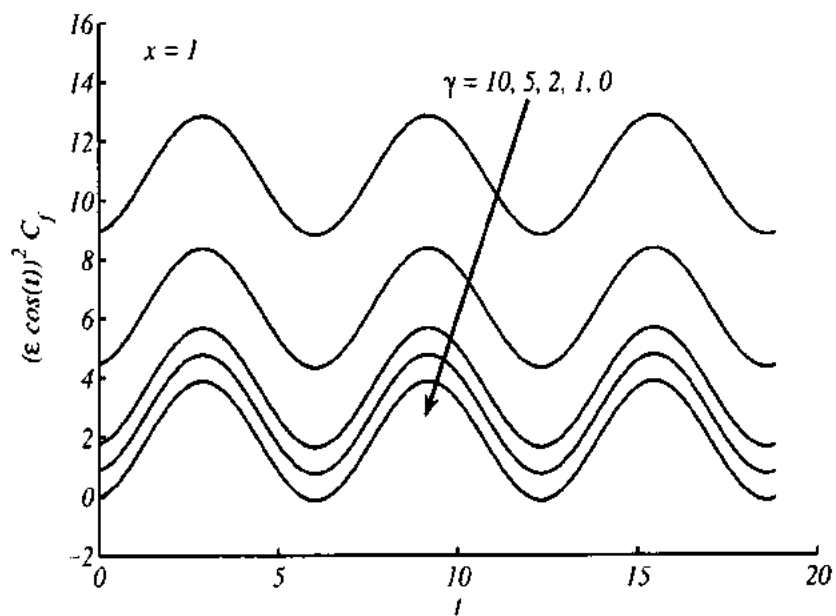
Figure 2.12: Skin friction coefficient for different values of γ at $x = 1$.
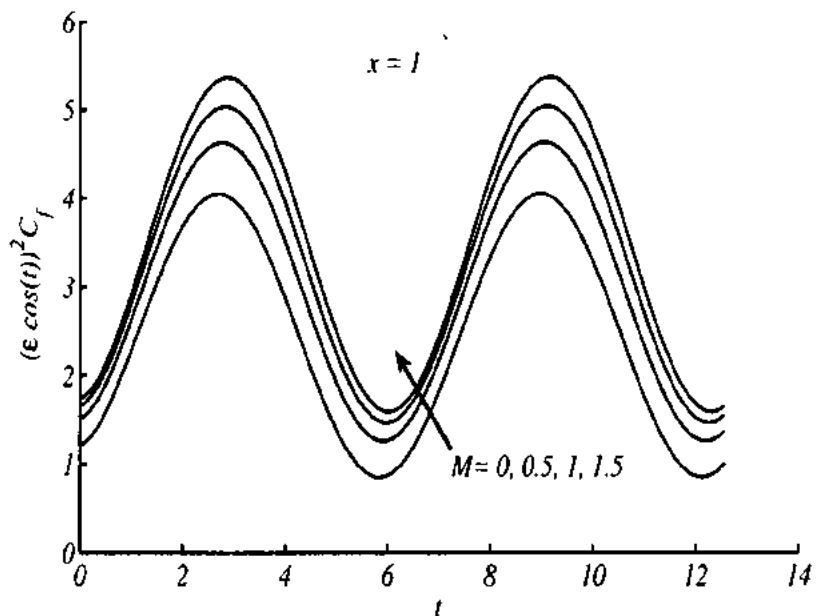
Figure 2.13: Skin friction coefficient for different values of M at $x = 1$.

37

2.4 Conclusions

Unsteady MHD oblique stagnation point flow of laminar, incompressible flow of an electrically conducting viscous fluid due to an oscillating flat plate and an oscillating free stream is presented in this chapter. The governing boundary layer equations are transformed in dimensionless form. The obtained partial differential equations are highly nonlinear and its difficult to present their exact solution. To overcome this situation, a finite difference scheme namely the Keller-box method is employed. The effects of magnetic field on the flow and heat transfer, for both cases of oscillating plate and oscillating free stream are shown through several graphs of stream functions, velocity and temperature. The present investigation helps to conclude that

- Application of magnetic field increases the velocity of the fluid but reduces the momentum and thermal boundary layer thicknesses in the stagnation point region for both cases of oscillating plate and oscillating free stream.

- Temperature of the fluid decreases by increase the magnetic parameter M.

- Magnetic field helps to increases the skin friction coefficient.

- With increase of obliqueness parameter, the skin friction coefficient can be increased.

Chapter 3

Study of non-Newtonian Maxwell fluid flow in the region of oblique stagnation point over a stretching sheet

In this chapter, a numerical study is carried out for the steady two-dimensional flow of an incompressible Maxwell fluid in the region of oblique stagnation point over a stretching sheet. The governing equations are transformed to dimensionless boundary layer equations. After some manipulation, a system of ordinary differential equations is obtained and is solved by using parallel shooting method. A comparison with the previous studies validates the accuracy of our results and analysis. The effects of involving parameters are discussed in detail and the streamlines are drawn to predict the flow pattern of the fluid. It is observed that increasing velocities ratio parameter (ratio of straining to stretching velocity) helps to decrease the boundary layer thickness. Furthermore, the velocity of fluid increases by increasing the obliqueness parameter.

The appropriate boundary conditions for oblique stagnation point flow over a stretching sheet are (see re. [81])

$$\bar{u}(\bar{x},\bar{y}) = c\bar{x}, \quad \bar{v} = 0 \quad at \ \bar{y} = 0,$$

$$\bar{u}(\bar{x},\bar{y}) = U_e(\bar{x},\bar{y}) = a\bar{x} + b\bar{y}, \quad \bar{v} = -\left(a\bar{y}+\bar{A}\right) \quad as \ \bar{y} \to \infty,$$

(3.3)

where a, b and c are positive constants of dimension $[1/T]$ and $\bar{A}$ is the constant that accounts the boundary layer displacement whose dimension is $[L/T]$. From the point of view of the boundary layer, the outer edge of the boundary layer (of thickness δ) is far from the surface. Therefore, the boundary condition for the velocity at the edge of the boundary layer is written as $\lim \bar{y} \to \infty \ \bar{u}(\bar{x},\bar{y}) = U_e(\bar{x},\bar{y})$, so for the larger value of $\bar{y}(\bar{y} \to \infty)$ i.e. at the edge of boundary layer, we get (see ref. [80,82,83]) the following

$$-\frac{1}{\rho}\frac{\partial \bar{p}}{\partial \bar{x}} - \frac{\lambda_1}{\rho}\left(\bar{u}\frac{\partial^2 \bar{p}}{\partial \bar{x}^2} + \bar{v}\frac{\partial^2 \bar{p}}{\partial \bar{x}\partial \bar{y}} - \frac{\partial \bar{u}}{\partial \bar{x}}\frac{\partial \bar{p}}{\partial \bar{x}} - \frac{\partial \bar{u}}{\partial \bar{y}}\frac{\partial \bar{p}}{\partial \bar{y}}\right) = a^2\bar{x} - b\bar{A}$$

(3.4)

and

$$-\frac{1}{\rho}\frac{\partial \bar{p}}{\partial \bar{y}} - \frac{\lambda_1}{\rho}\left(\bar{v}\frac{\partial^2 \bar{p}}{\partial \bar{y}^2} + \bar{u}\frac{\partial^2 \bar{p}}{\partial \bar{x}\partial \bar{y}} - \frac{\partial \bar{v}}{\partial \bar{x}}\frac{\partial \bar{p}}{\partial \bar{x}} - \frac{\partial \bar{v}}{\partial \bar{y}}\frac{\partial \bar{p}}{\partial \bar{y}}\right) = a(a\bar{y}+\bar{A}).$$

(3.5)

Eqs. (3.1) and (3.2) thus give

$$\bar{u}\frac{\partial \bar{u}}{\partial \bar{x}} + \bar{v}\frac{\partial \bar{u}}{\partial \bar{y}} = a^2\bar{x} - b\bar{A} + \nu\left(\frac{\partial^2 \bar{u}}{\partial \bar{x}^2} + \frac{\partial^2 \bar{u}}{\partial \bar{y}^2}\right) - \lambda_1\left(\bar{v}^2\frac{\partial^2 \bar{u}}{\partial \bar{y}^2} + 2\bar{u}\bar{v}\frac{\partial^2 \bar{u}}{\partial \bar{x}\partial \bar{y}} + \bar{u}^2\frac{\partial^2 \bar{u}}{\partial \bar{x}^2}\right),$$

(3.6)

$$\bar{u}\frac{\partial \bar{v}}{\partial \bar{x}} + \bar{v}\frac{\partial \bar{v}}{\partial \bar{y}} = a(a\bar{y}+\bar{A}) + \nu\left(\frac{\partial^2 \bar{v}}{\partial \bar{x}^2} + \frac{\partial^2 \bar{v}}{\partial \bar{y}^2}\right) - \lambda_1\left(\bar{v}^2\frac{\partial^2 \bar{v}}{\partial \bar{y}^2} + 2\bar{u}\bar{v}\frac{\partial^2 \bar{v}}{\partial \bar{x}\partial \bar{y}} + \bar{u}^2\frac{\partial^2 \bar{v}}{\partial \bar{x}^2}\right).$$

(3.7)

Incorporting the usual boundary layer assumptions (also see [80,82,83]) where $\bar{u}$, $\bar{x}$ and λ_1 are of order 1, $\bar{y}$ and $\bar{v}$ are of order δ and order of ν is δ^2. where δ represents the boundary layer thickness which is very small as compared to the length of sheet, we get

$$\bar{u}\frac{\partial \bar{u}}{\partial \bar{x}} + \bar{v}\frac{\partial \bar{u}}{\partial \bar{y}} = a^2\bar{x} - b\bar{A} + \nu\frac{\partial^2 \bar{u}}{\partial \bar{y}^2} - \lambda_1\left(\bar{v}^2\frac{\partial^2 \bar{u}}{\partial \bar{y}^2} + 2\bar{u}\bar{v}\frac{\partial^2 \bar{u}}{\partial \bar{x}\partial \bar{y}} + \bar{u}^2\frac{\partial^2 \bar{u}}{\partial \bar{x}^2}\right).$$

(3.8)

Now using the following transformation proposed by Labropulu [81]

$$x = \bar{x}\sqrt{\frac{c}{\nu}}, \ y = \bar{y}\sqrt{\frac{c}{\nu}}, \ u = \frac{1}{\sqrt{\nu c}}\bar{u}, \ v = \frac{1}{\sqrt{\nu c}}\bar{v},$$

(3.9)

41

Eq. (3.8) with boundary conditions will take the following dimensionless form

$$u\frac{\partial u}{\partial x}+v\frac{\partial u}{\partial y}=\left(\frac{a}{c}\right)^2 x-\gamma A+\frac{\partial^2 u}{\partial y^2}-\beta\left(v^2\frac{\partial^2 u}{\partial y^2}+2uv\frac{\partial^2 u}{\partial x\partial y}+u^2\frac{\partial^2 u}{\partial x^2}\right),\qquad(3.10)$$

$$u=x,\ v=0\qquad at\ y=0,$$
$$u=\frac{a}{c}x+\frac{b}{c}y,\ v=-\left(\frac{a}{c}y+A\right)\qquad as\ y\to\infty,\qquad(3.11)$$

where $\beta=\lambda_1 c$ is the dimensionless number called Deborah number, which describes the fluidity of materials, $\gamma=b/c$ is the dimensionless constant characterizing the obliqueness of oncoming flow, $A=\bar A/\sqrt{vc}$ is the dimensionless constant which accounts the boundary layer displacement (shown in Fig. 3.8), and a/c is the ratio of the straining to stretching velocity.

Now using the stream function ψ such that $u=\partial\psi/\partial y$, $v=-\partial\psi/\partial x$, the above equation can be expressed in the form of stream function as

$$\frac{\partial\psi}{\partial y}\left(\frac{\partial^2\psi}{\partial x\partial y}\right)-\frac{\partial\psi}{\partial x}\left(\frac{\partial^2\psi}{\partial y^2}\right)+\beta\left(\left(\frac{\partial\psi}{\partial x}\right)^2\frac{\partial^3\psi}{\partial y^3}-2\frac{\partial\psi}{\partial y}\frac{\partial\psi}{\partial x}\frac{\partial^3\psi}{\partial x\partial y^2}+\left(\frac{\partial\psi}{\partial y}\right)^2\frac{\partial^3\psi}{\partial x^2\partial y}\right)$$
$$=x\left(\frac{a}{c}\right)^2-A\gamma+\frac{\partial^3\psi}{\partial y^3}$$

$$(3.12)$$

and the dimensionless boundary conditions in term of stream function can be written as

$$\psi=0,\ \frac{\partial\psi}{\partial y}=x\qquad at\ y=0,$$
$$\frac{\partial\psi}{\partial y}=\frac{a}{c}x+\gamma y,\ \frac{\partial\psi}{\partial x}=\frac{a}{c}y+A\qquad as\ y\to\infty.\qquad(3.13)$$

In order to solve the Eq. (3.12) subject to the boundary conditions (3.13), we suppose the solution of is of the form

$$\psi=xf(y)+g(y),\qquad(3.14)$$

where functions $f(y)$ and $g(y)$ are normal and oblique components of the flow. Incorporating Eq. (3.14) into Eqs. (3.12) and (3.13) one gets the following equations with the boundary

42

conditions

$$f'(y)\left(xf'(y)+g'(y)\right)-f(y)\left(xf''(y)+g''(y)\right)+$$

$$\beta\left(f(y)^2\left(xf'''(y)+g'''(y)\right)-2f(y)f''(y)\left(xf'(y)+g'(y)\right)\right)=x\left(\frac{a}{c}\right)^2-A\gamma+xf'''(y)+g'''(y),$$

(3.15)

$$f(y)=0,\ f'(y)=1,\ g(y)=g'(y)=0 \quad at\ y=0,$$

(3.16)

$$f(y)=\frac{a}{c}y+A,\ f'(y)=\frac{a}{c},\ g'(y)=\gamma y \quad as\ y\to\infty,$$

where for the large values of y (at the edge of boundary layer i.e. $y\to\infty$) $f(y)=(a/c)y+A$, which means that solution of $f(y)$ is the linear function of y. In Eq. (3.16) the boundary condition $f'(y)=a/c$ is the derivative of $f(y)=(a/c)y+A$ which are identically same so we use only one of them to compute the solution. Comparing the like powers of x in Eq. (3.15) and selecting the boundary conditions, we get the following equations

$$f'''+ff''-(f')^2+\left(\frac{a}{c}\right)^2+\beta\left(2ff'f''-f^2f'''\right)=0,$$

(3.17)

$$g'''+fg''-f'g'+\beta\left(2ff''g'-f^2g'''\right)=A\gamma$$

(3.18)

and boundary conditions are (see ref. [81])

$$f(0)=0,\ f'(0)=1,\ f'(\infty)=\frac{a}{c}$$

(3.19)

$$g(0)=g'(0)=0\ g''(\infty)=\gamma,$$

(3.20)

where the prime denotes the derivative w.r.t y. For simplicity introducing a new variable $g'(y)=\gamma h(y)$, Eq. (3.18) with boundary condition (3.20) can be written as

$$h''+fh'-f'h+\beta\left(2ff''h-f^2h''\right)=A,$$

(3.21)

$$h(0)=0\ h'(\infty)=1.$$

(3.22)

For $\beta=0$, we get the Newtonian fluid case and equations (3.17) and (3.19) reduce to equations (3.4) and (3.5) as reported by Mahapatra and Gupta [24]. Dimensionless components of the

43

velocity are

$$u = \frac{\partial \psi}{\partial y} = xf'(y) + g'(y),$$ (3.23)

$$v = -\frac{\partial \psi}{\partial x} = -f(y).$$ (3.24)

In Fig. 3.1, the dividing stream line making angle α with the stretching sheet. The slope of dividing stream line can be found by setting $\psi = 0$ as was reported in reference [34]

$$\psi = \frac{a}{c} xy + \frac{1}{2} \gamma y^2 = 0, \implies y = \left(-\frac{2a}{\gamma c}\right) x,$$

which gives

$$slope - m = -\frac{2a}{\gamma c}$$

So the relationship of impinging angle α and shearing parameter γ can be written as

$$\alpha = \tan^{-1}\left(-\frac{2a}{\gamma c}\right)$$

3.2 Parallel shooting scheme

In order to solve nonlinear equations (3.17) and (3.21), subject to the boundary conditions (3.19) and (3.22) for different values of involving parameters, parallel shooting method [84] is used. To find the solution of complex rheological models different techniques are proposed as mentioned in the introduction. The main problem with these methods while discretizing the differential equations into system of algebraic equations and take much time when one increase range and number of steps to achieve the desired accuracy. Simple shooting method is also very useful to achieve the accurate solution in less time but for certain non-linear problems, the method is found much dependent upon initial guess. To cope the situation, the method of parallel shooting is introduced and is very efficient, less time consuming, stable and rapid convergent. The method is described in the following steps

Step-I: Equations (3.17) and (3.21), are reduced in the system of first order differential equations by letting $f = f_1$ and $h = f_4$

$$f_1' = f_2, \ f_2' = f_3, \ f_3' = \frac{1}{1 - \beta f_1^2} \left(-f_1 f_3 + f_2^2 - 2\beta f_1 f_2 f_3 - \left(\frac{a}{c}\right)^2 \right),$$

$$f_4' = f_5, \ f_5' = \frac{1}{1 - \beta f_1^2} \left(-f_1 f_5 + f_2 f_4 - 2\beta f_1 f_3 f_4 + A \right).$$

Step-II: To apply the boundary conditions, the physical domain $[0, \infty]$ is truncated to finite domain $[0, L]$, where L is chosen sufficiently large

$$f_1(0) = 0, \ f_2(0) = 1, \ f_2(L) = \frac{a}{c}, \ f_4(0) = 0 \ f_5(L) = 1,$$

Step-III: The domain $[0, L]$ is divided into n subintervals,

$$[0, y_1], [y_1, y_2], [y_2, y_3] \ \cdots \ [y_{n-1}, y_n = L].$$

For convergence of solution, n can be increased sufficiently.

Step-IV: The problem is solved over each subinterval such that it satisfies the boundary conditions.

Step-V: A suitable guess is supplied to integrate the problem. The solution obtained for the previous interval is considered as an initial guess for the next interval.

Algorithm is developed in MATLAB R2010a.

3.3 Results and discussion

Equations (3.17) and (3.21), subject to the boundary conditions (3.19) and (3.22) have been solved numerically for different values of pertinent parameters β, a/c and γ using the parallel shooting method as described in previous scheme. To show the efficiency and accuracy of our

results, the comparison of numerical values of $f''(0)$, $h'(0)$ is presented for both Newtonian and Maxwell fluids in Table 3.1. It is found that the results are in good agreement with the previous study given in ref. [80]. From the table, it is found that the values of $f''(0)$ are increasing with increase in values of a/c, for both Newtonian and non-Newtonian fluids. However, the values of $h'(0)$ increases up to a certain value then start decreasing. The results shown in Table 3.2 are in good agreement with those reported by Labropulu et al. [81]. In Table 3.3, the values of $\psi_{yy}(0)$ and A are presented for the different values of pertinent parameters. Fig. 3.2(a-d) demonstrates the variation of the horizontal velocity u for different values of velocities ratio parameter a/c when $x = 1$, $\beta = 0.2$ with $\gamma = 0$, 0.5, 1.0, 5.0. It can be seen from the figures that the velocity increases continuously with increase in values of γ. Fig. 3.2(a) illustrate the orthogonal flow ($\gamma = 0$) and Fig. 3.2(b-d) show the results for the non-orthogonal stagnation point flow. From the figures, it can be observed that there are two boundary layer structures appearing near the surface depending upon the ratio of straining and stretching velocities. The figures depict that when $a/c > 1$, the flow has normal boundary layer structure and when $a/c < 1$ the flow has inverted boundary layer structure which is same as reported by Mahapatra and Gupta [24]. It is also noted that the thickness of the boundary layer decreases with increase in values of a/c. Physically, it represents that when the stretching velocity cx is greater than the straning velocity ax i.e $a/c < 1$, the inverted boundary layer exits near the surface, which suggest that as the stretching velocity i.e cx decreases the boundary layer thickness increases. On the other hand, when the straining velocity ax is greater than stretching velocity cx, i.e. $a/c > 1$, the acceleration of free stream velocity increases, which leads to thinning of the boundary layer with increase in value of a/c. It can also be seen from the Fig. 3.2(a-d) that the velocity of the fluid increases with increase of constant shear parameter γ. There is no boundary layer formed when straining and stretching velocities are equal. The same behavior has been

observed for both orthogonal $(\gamma = 0)$ and oblique $(\gamma \neq 0)$ stagnation point flows. Physically it means that viscous effects vanish near the wall, when both velocities are equal. Figs. 3.3 and 3.4(a, b) depicts the behavior of the fluid flow for different values of β in orthogonal $(\gamma = 0)$ and oblique $(\gamma \neq 0)$ stagnation point flow, respectively. Two different behaviors have been observed from the figures in case of boundary layer and inverted boundary layer structures (as described above). In Fig. 3.3 bunch of curves are drawn for the different values of β and a/c. If $a/c < 1$ (inverted boundary layer case), the velocity decreases and boundary layer becomes thinner with the increase of Deborah number β. On the other hand, when $a/c > 1$, the velocity increases with the increase of Deborah number β but the boundary layer thickness decreases. Fig. 3.4 also shows that the velocity in the region of non-orthogonal stagnation point is greater than the velocity in the case of orthogonal stagnation point. Figs. 3.5, 3.6 and 3.7 show the streamlines for the flow pattern of the oblique stagnation point flows $(\gamma \neq 0)$ for different values of β, a/c and γ. Both cases i.e. $\gamma > 0$ and $\gamma < 0$ are considered for the analysis. The increase in constant shear parameter $|\gamma|$ results in more obliqueness toward the left of the orthogonal stagnation point. Figs. 3.5 and 3.6 show that as the value of $|\gamma|$ increases, the shearing motion of the fluid increases in the region of stagnation point. Fig. 3.7 reveals that with the increase in stretching velocity the streamlines are tilted more towards left but the streamlines less tilted towards left due to an increase in straining velocity. For large values of a/c, the streamlines behaves same as in case of the orthogonal stagnation point flow. In Fig. 3.8, values of $f(y)$ are plotted as solid curves against y for different values of a/c and dashed lines represent the position of the boundary layer which are the tangents to $f(y)$ at point where the curves become linear. Dots on y-axis represents the value of A, which is the intersection of dotted lines and the y-axis.

47

Table 3.1: The Numerical values of $f''(0)$, $h'(0)$ and A for the different values of β and a/c.

| | Newtonian fluid ($\beta=0$) | | Maxwell fluid ($\beta=0.2$) | | | |
| | $f''(0)$ | | $f''(0)$ | | $h'(0)$ | A |
a/c	Ref. [80] ($\lambda_2 = 0$)	present	Ref. [80] ($\lambda_2 = 0$)		Present	
0.01	-0.9981	-0.99802	-1.0499	-1.05009	-0.51368	0.89077
0.02	-0.9958	-0.99579	-1.0476	-1.04778	-0.24667	0.86890
0.05	-0.9876	-0.98758	-1.0393	-1.03939	0.07239	0.80807
0.10	-0.9694	-0.96939	-1.0207	-1.02082	0.28154	0.71976
0.20	-0.9181	-0.91811	-0.9681	-0.96823	0.49218	0.57730
0.50	-0.6673	-0.66726	-0.7078	-0.70779	0.79610	0.28885
1.00	0.0000	0.00000	0.0000	0.00000	1	0.00000
2.00	2.0175	2.01749	2.2225	2.22314	1.09213	-0.32603
3.00	4.7294	4.72924	5.3544	5.35217	0.78434	-0.52063
5.00	11.7537	11.75190	14.0144	14.00169	-2.04649	-0.75564
10.00	36.2689	36.25704	48.4866	48.335404	-2.34185	-1.03301

Table 3.2: Values of $f''(0)$, $h'(0)$ and A for the different values of a/c, for Newtonian fluid ($\beta = 0$).

| | $f''(0)$ | | $h'(0)$ | | A | |
a/c	Ref. [81]	present	Ref. [81]	present	Ref. [81]	present
0.1	-0.96938	-0.96939	0.26278	0.26338	0.79170	0.79170
0.3	-0.84942	-0.84942	0.60573	0.60633	0.51949	0.51950
0.8	-0.29938	-0.29939	0.93430	0.93473	0.11452	0.11453
1	0	0	1	1	0	0
2	2.01750	2.01749	1.16489	1.16521	-0.41040	-0.41041
3	4.72928	4.72924	1.23438	1.23464	-0.69305	-0.69305
4	8.00042	8.00036	1.27272	1.27300	-0.91650	-0.91650

Table 3.3: Values of $\psi_{yy}(0)$ and A for the different values of β, a/c and γ for fixed $x = 1$.

β	a/c	γ	$\psi_{yy}(0) = xf''(0) + \gamma h'(0)$	A
0	0	0	-1.0000	1.0000
0	0.1	0	-0.9694	0.7917
0	0.5	0	-0.6673	0.3286
0	1	0	0.0000	0.0000
0	2	0	2.0175	-0.4104
0.1	0	1	-3.4390	0.9575
0.1	0.1	1	-0.7158	0.7536
0.1	0.5	1	0.1022	0.3070
0.1	1	1	1.0000	0.0000
0.1	2	1	3.2709	-0.3609
0.2	0	2	-5.8241	0.9196
0.2	0.1	2	-0.4364	0.7199
0.2	0.5	2	0.8812	0.2889
0.2	1	2	2.0000	0.0000
0.2	2	2	2.2232	-0.3252
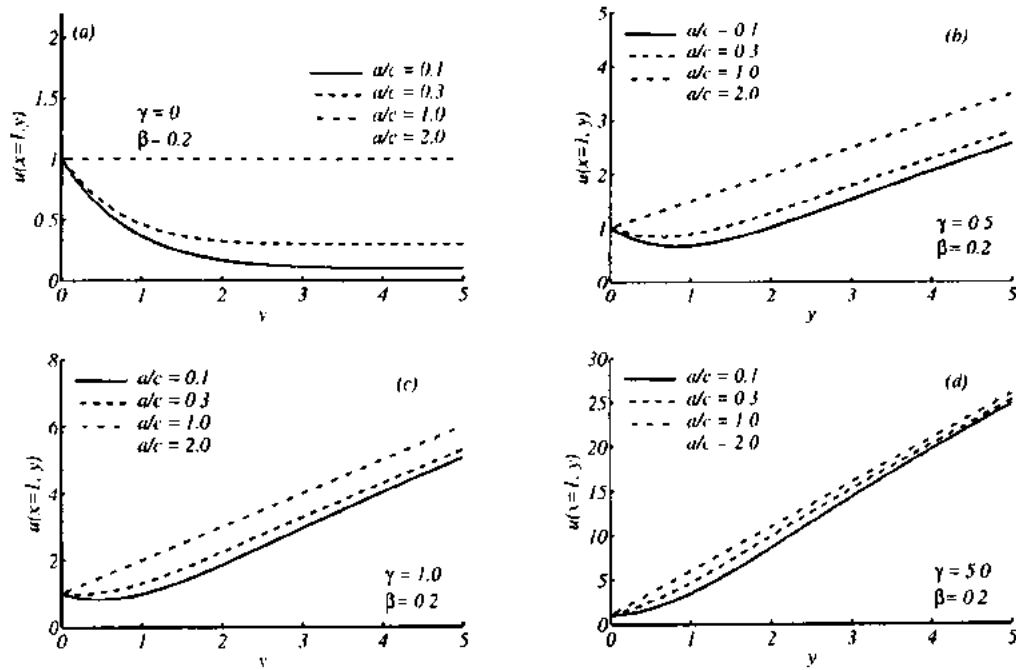
Figure 3.2: Variation in velocity u along y, for different values of a/c and (a) $\gamma = 0.5$ (b) $\gamma = 0.5$ (c) $\gamma = 0.5$ (d) $\gamma = 0.5$ at $x=1$, $\beta = 0.2$
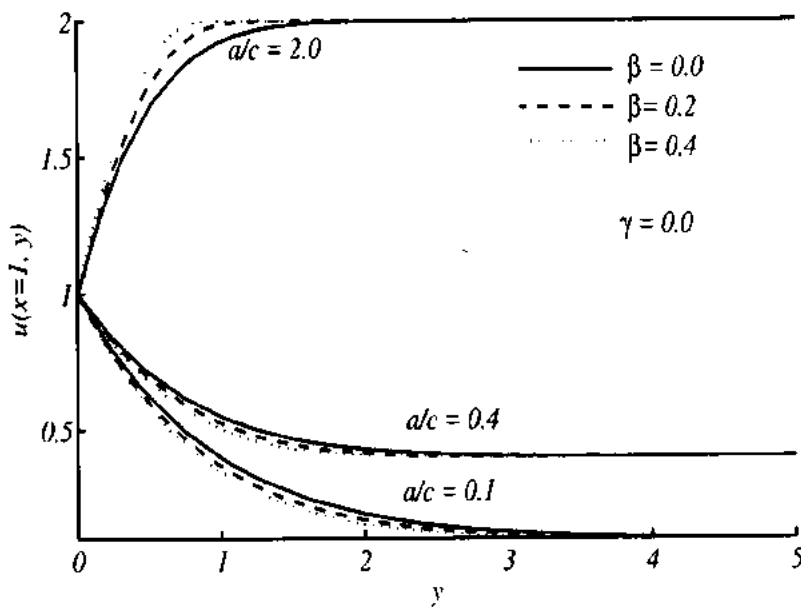
Figure 3.3: Variation in velocity u along y, for the different values of β, when $a/c = 0.1, 0.4, 2.0$ and $\gamma = 0$ (orthogonal flow).
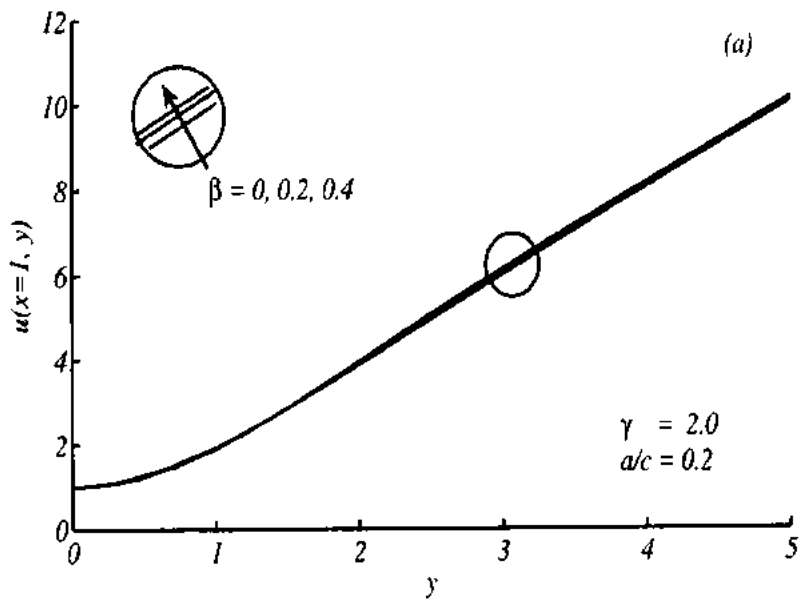
(a)
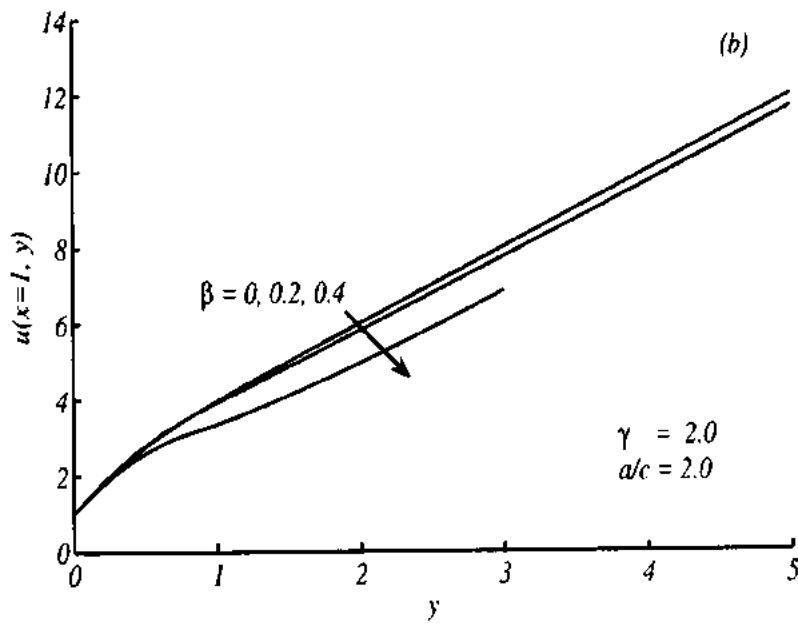
(b)

Figure 3.4: Variation in velocity u along y, for the different values of β, when (a) $a/c = 0.2$

(b) $a/c = 2.0$ and $\gamma = 2.0$ (non-orthogonal flow).

51

$\psi = 1, 0.5, 0.1, 0, -0.1, -0.5, -1$

$\gamma = 10.0$
$a/c = 0.5$
$\beta = 0.2$

(a)

$\psi = 1, 0.5, 0.1, 0, -0.1, -0.5, -1$

$\gamma = -10.0$
$a/c = 0.5$
$\beta = 0.2$

(b)
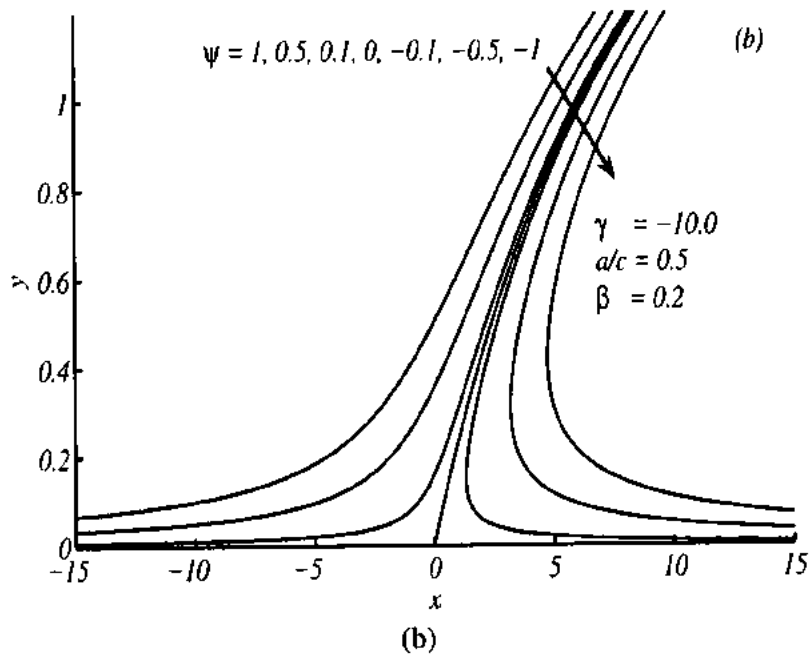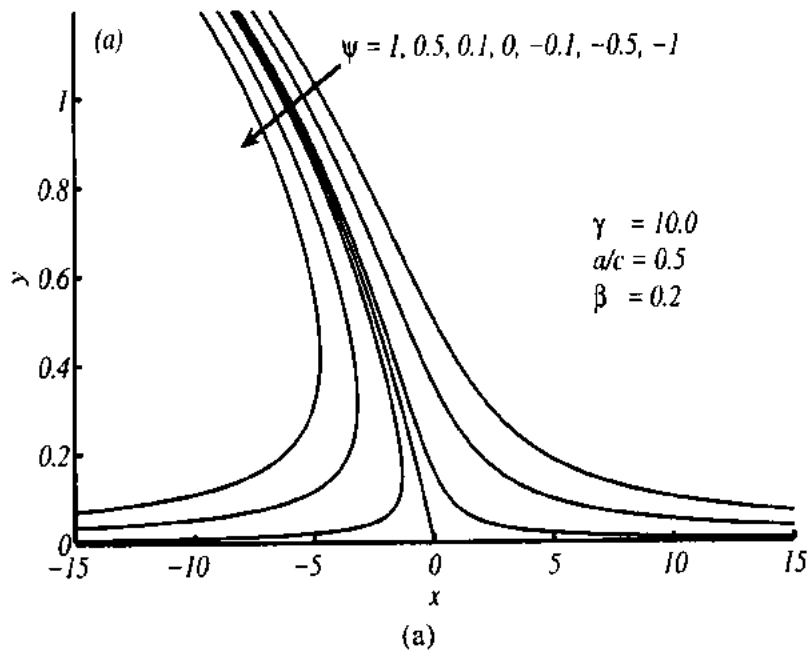
Figure 3.5: Streamlines for oblique flow, when $\beta = 0.2$, $a/c = 0.5$ and (a) $\gamma = 10$ (b) $\gamma = -10$.

52
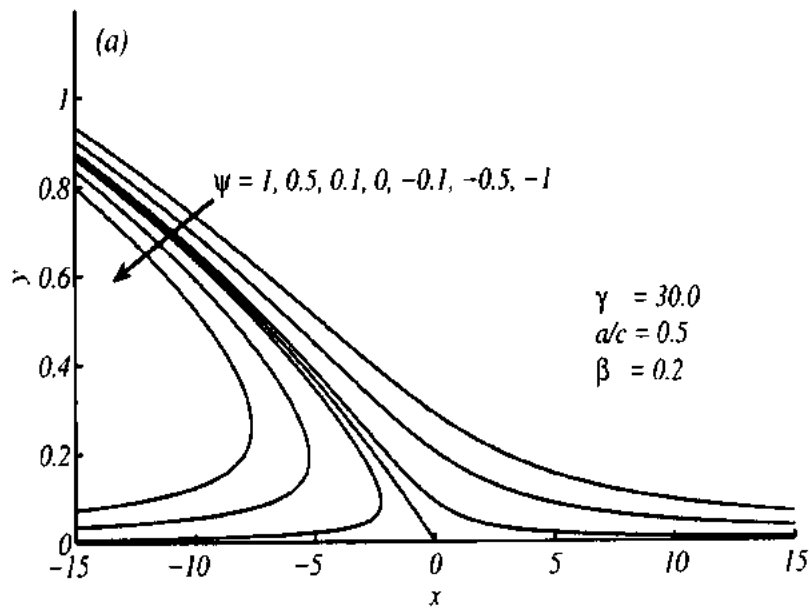
(a)
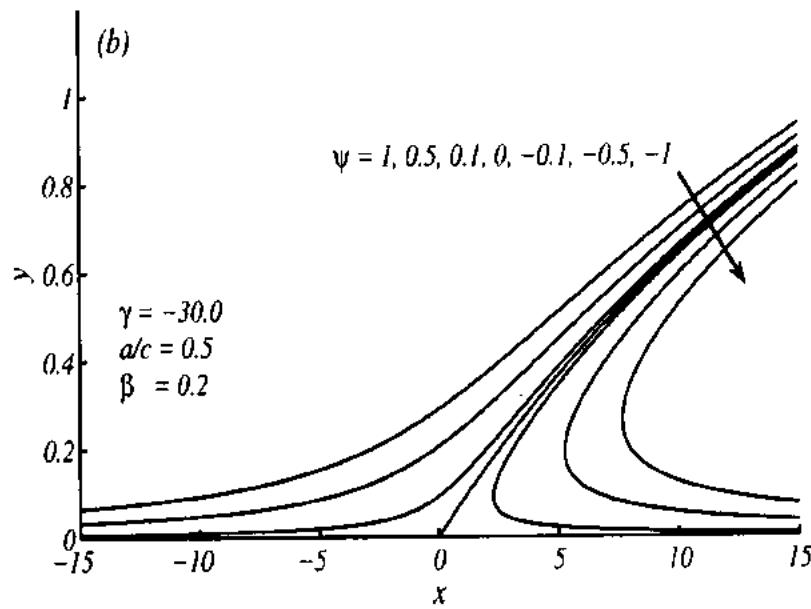
(b)

Figure 3.6: Streamlines for oblique flow, when $\beta = 0.2$, $a/c = 0.5$ and (a) $\gamma = 30$ (b) $\gamma = -30$.
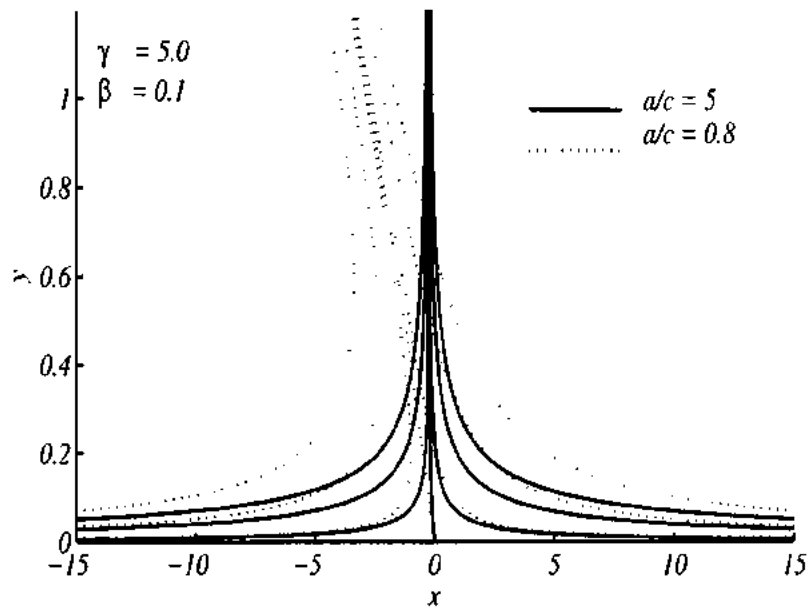
Figure 3.7: Streamlines for oblique flow, when $\beta = 0.1$ and $\gamma = 5$ for $a/c = 0.8, 5.0$.
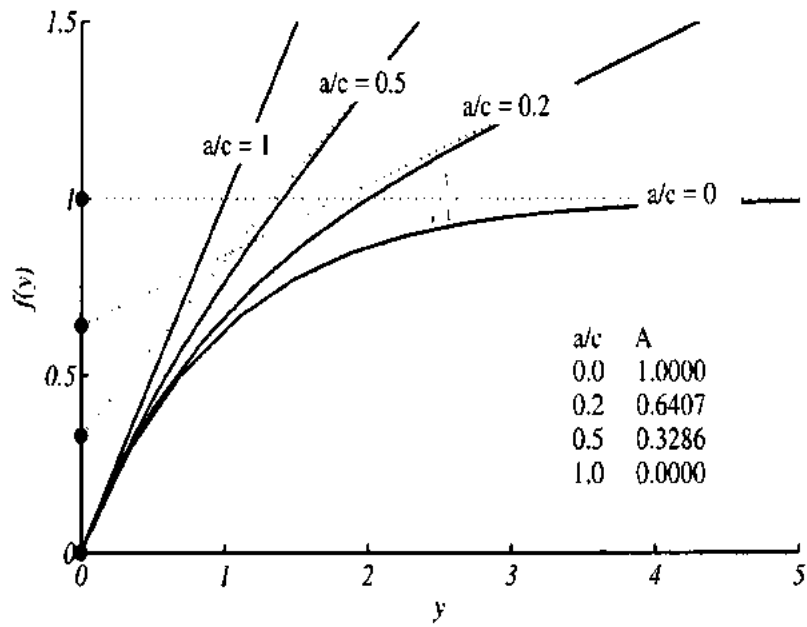
Figure 3.8: Graph of boundary layer displacement for different values of a/c

3.4   Conclusions

Numerical solution of non-Newtonian Maxwell fluid in the region of oblique stagnation point flow over a stretching sheet is presented in this article. After using the boundary layer approximation the governing equation are transformed to dimensionless form by means of some useful transformations. The obtained system of equations is solved numerically through parallel shooting method. The effects of velocity ratio parameter a/c, Deborah number and obliqueness parameter are shown through graphs. The present investigation helps to conclude that

- With the increase in value of velocities ratio parameter a/c (the ratio of straining and stretching velocity), thickness of the boundary layer decreases.

- The boundary layer vanishes when $a/c = 1$.

- In the case of oblique stagnation point flow for large values of a/c, the streamlines look like those in the case of orthogonal stagnation point flow.

- The velocity of the fluid increases with increase in values of shearing parameter .

- If $a/c < 1$ (inverted boundary layer case), the velocity decreases and the boundary layer thickness reduces the increase in Deborah number β.

- If $a/c > 1$, the velocity increases with the increase in Deborah number β. However, the boundary layer thickness decreases.

Chapter 4

Study of viscoelastic fluid flow in the region of oblique stagnation point through a porous medium with radiation

This chapter addresses the non-linear radiation effect on the two-dimensional oblique stagnation point flow through a porous medium. Constitutive equations of viscoelastic second grade fluid are employed in the mathematical development of the relevant problem. The resulting nonlinear system is solved using Chebyshev Spectral Newton Iterative Scheme (CSNIS). A comparative study of the present results with that of previous studies have been presented in the tables. Excellent agreement shows that the used numerical scheme is stable and the results are highly accurate. Impact of sundry variables on the quantities of interest are discussed. It is observed that shearing parameter γ helps to increase the fluid velocity. Thermal boundary layer thickness can be controlled due to small value of radiation parameter and surface heating parameter. It is also noted that with an increase in value of porosity parameter K, the velocity increases but the momentum boundary layer thickness decreases in the region of stagnation

point. Moreover, the streamlines are plotted to predict the flow pattern.
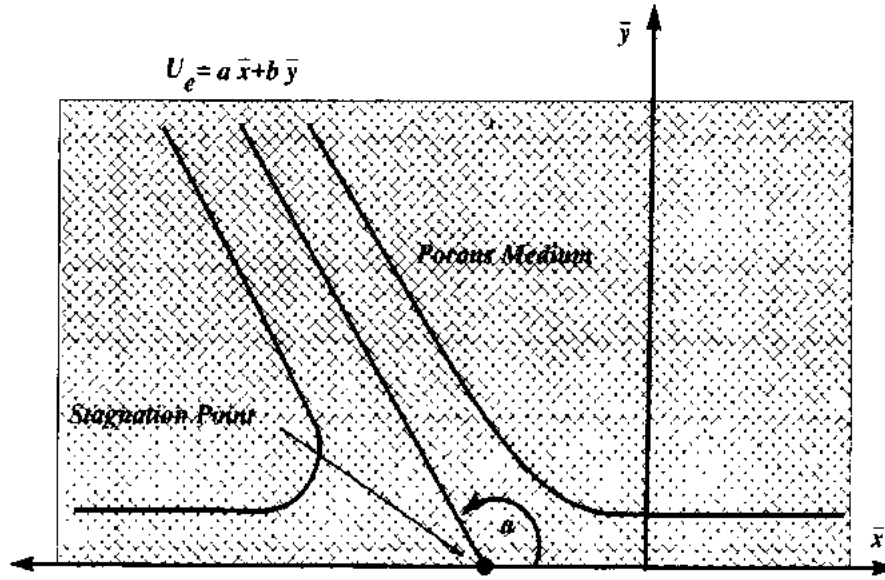
Figure 4.1: Physical Model of the problem

4.1   Problem formulation

Consider the steady, two dimensional, incompressible Darcy flow of a second grade fluid near

the oblique stagnation point over an impermeable surface. The surface is placed at $\bar{y} = 0$, and

the porous medium occupies in the region $\bar{y} > 0$. It is assumed that the fluid is transparent

to the radiation so the radiation term will only appear in energy equation of solid phase [85].

Thus the governing equations are

$$\nabla.\mathbf{V} = 0, \tag{4.1}$$

$$\rho\frac{d\mathbf{V}}{dt} = \nabla.\tau - \frac{\mu}{k_1}\mathbf{V}, \tag{4.2}$$

Energy equation for solid phase:

$$(1 - \phi)\nabla.(k_s\nabla\bar{T}_s) - \nabla.\mathbf{q}_r = 0, \tag{4.3}$$

57

Energy equation for fluid phase:

$$\phi \nabla \cdot \left(k_f \nabla \bar{T}_f \right) - \rho c_p \mathbf{V} \cdot \nabla \bar{T}_f = 0, \tag{4.4}$$

where $\bar{T}_f$ is temperature of fluid, $\bar{T}_s$ is temperature of solid, k_1 is Darcy permeability parameter, d/dt is material derivative, k_s is the thermal conductivity of solid, k_f is the thermal conductivity of fluid, c_p is specific heat at constant pressure, $(1 - \phi)$ is the ratio of area covered by solid to the total covered area of the medium and q_r is radiative heat flux. We assumed that the no net heat transfer from solid to fluid or fluid to solid so the heat transfer in parallel from both phases. For the simplification of Eqs. (4.3) and (4.4), we assumed that there is local thermal equilibrium i.e. $\bar{T}_f = \bar{T}_s = \bar{T}$, so by adding Eqs. (4.3) and (4.4), we get

$$\rho C_p \mathbf{V} \cdot \nabla \bar{T} + k_{eff} \nabla^2 \bar{T} - \nabla \cdot q_r = 0. \tag{4.5}$$

where $k_{eff} = \left(\phi k_f + (1 - \phi) k_s \right)$ is the effective thermal conductivity for both fluid and porous medium. Upon using the Rosseland approximation for radiation, one can obtain [87]

$$q_r = -\frac{4\sigma_{SB}}{3(\alpha_r + \sigma_s)} \nabla \bar{T}^4, \tag{4.6}$$

where α_r, σ_{SB} and σ_s are the Rosseland mean absorption coefficient, Stefan-Boltzmann constant and the scattering coefficient respectively. The rheological equation of second grade fluid can be expressed as

$$\tau = -\bar{p}\mathbf{I} + \mu \mathbf{A}_1 + \alpha_1 \mathbf{A}_2 + \alpha_2 \left(\mathbf{A}_1 \right)^2, \tag{4.7}$$

where $\bar{p}$ is the pressure, μ is the dynamic viscosity of the fluid, α_1 and α_2 are normal stress moduli and the tensors $\mathbf{A}_1$ and $\mathbf{A}_2$ are the first and second Rivlin-Eriksen tensors which can be calculated as

$$\mathbf{A}_1 = (\nabla \mathbf{V}) + (\nabla \mathbf{V})^{tran}, \tag{4.8}$$

$$\mathbf{A}_2 = \frac{d\mathbf{A}_1}{dt} + \mathbf{A}_1 (\nabla \mathbf{V}) + (\nabla \mathbf{V})^{tran} \mathbf{A}_1. \tag{4.9}$$

where d/dt is defined as

$$\frac{d(\bullet)}{dt} = \frac{\partial(\bullet)}{\partial t} + \mathbf{V} \cdot [\nabla(\bullet)]. \tag{4.10}$$

The thermodynamic constraints for the fluid model (Eq. (4.7)) are compatible with Clausius-Duhem inequality and it is assumed that the free energy density of the fluid be locally at rest are

$$\mu \geq 0, \quad \alpha_1 \geq 0, \quad \alpha_1 + \alpha_2 = 0. \tag{4.11}$$

If $\alpha_1 = \alpha_2 = 0$, then Eq. (4.7) reduces to Cauchy stress tensor for a Newtonian fluid. The governing equations in component form are

$$\frac{\partial \bar{u}}{\partial \bar{x}} + \frac{\partial \bar{v}}{\partial \bar{y}} = 0, \tag{4.12}$$

$$\bar{u}\frac{\partial \bar{u}}{\partial \bar{x}} + \bar{v}\frac{\partial \bar{u}}{\partial \bar{y}} = -\frac{1}{\rho}\frac{\partial \bar{p}}{\partial \bar{x}} + v\left(\frac{\partial^2 \bar{u}}{\partial \bar{x}^2} + \frac{\partial^2 \bar{u}}{\partial \bar{y}^2}\right) + \frac{\alpha_1}{\rho}\left\{\frac{\partial}{\partial \bar{x}}\left[\begin{array}{c} 2\bar{u}\frac{\partial^2 \bar{u}}{\partial \bar{x}^2} + 2\bar{v}\frac{\partial^2 \bar{u}}{\partial \bar{x}\partial \bar{y}} + \\ 4\left(\frac{\partial \bar{u}}{\partial \bar{x}}\right)^2 + 2\frac{\partial \bar{v}}{\partial \bar{x}}\left(\frac{\partial \bar{v}}{\partial \bar{x}} + \frac{\partial \bar{u}}{\partial \bar{y}}\right)\end{array}\right] + \right.$$

$$\left. \frac{\partial}{\partial \bar{y}}\left[\begin{array}{c} \left(\bar{u}\frac{\partial}{\partial \bar{x}} + \bar{v}\frac{\partial}{\partial \bar{y}}\right)\left(\frac{\partial \bar{v}}{\partial \bar{x}} + \frac{\partial \bar{u}}{\partial \bar{y}}\right) + \\ 2\frac{\partial \bar{u}}{\partial \bar{x}}\frac{\partial \bar{u}}{\partial \bar{y}} + 2\frac{\partial \bar{v}}{\partial \bar{x}}\frac{\partial \bar{v}}{\partial \bar{y}}\end{array}\right]\right\} + \frac{\alpha_2}{\rho}\frac{\partial}{\partial \bar{x}}\left[4\left(\frac{\partial \bar{u}}{\partial \bar{x}}\right)^2 + \left(\frac{\partial \bar{v}}{\partial \bar{x}} + \frac{\partial \bar{u}}{\partial \bar{y}}\right)^2\right] - \frac{v}{k_1}\bar{u}, \tag{4.13}$$

$$\bar{u}\frac{\partial \bar{v}}{\partial \bar{x}} + \bar{v}\frac{\partial \bar{v}}{\partial \bar{y}} = -\frac{1}{\rho}\frac{\partial \bar{p}}{\partial \bar{y}} + v\left(\frac{\partial^2 \bar{v}}{\partial \bar{x}^2} + \frac{\partial^2 \bar{v}}{\partial \bar{y}^2}\right) + \frac{\alpha_1}{\rho}\left\{\frac{\partial}{\partial \bar{x}}\left[\begin{array}{c} 2\frac{\partial \bar{u}}{\partial \bar{x}}\frac{\partial \bar{u}}{\partial \bar{y}} + 2\frac{\partial \bar{v}}{\partial \bar{x}}\frac{\partial \bar{v}}{\partial \bar{y}} + \\ \left(\bar{u}\frac{\partial}{\partial \bar{x}} + \bar{v}\frac{\partial}{\partial \bar{y}}\right)\left(\frac{\partial \bar{v}}{\partial \bar{x}} + \frac{\partial \bar{u}}{\partial \bar{y}}\right)\end{array}\right] + \right.$$

$$\left. \frac{\partial}{\partial \bar{y}}\left[\begin{array}{c} 2\frac{\partial \bar{u}}{\partial \bar{y}}\left(\frac{\partial \bar{v}}{\partial \bar{x}} + \frac{\partial \bar{u}}{\partial \bar{y}}\right) + 4\left(\frac{\partial \bar{v}}{\partial \bar{y}}\right)^2 \\ 2\bar{v}\frac{\partial^2 \bar{v}}{\partial \bar{y}^2} + 2\bar{u}\frac{\partial^2 \bar{v}}{\partial \bar{x}\partial \bar{y}}\end{array}\right]\right\} + \frac{\alpha_2}{\rho}\frac{\partial}{\partial \bar{y}}\left[4\left(\frac{\partial \bar{v}}{\partial \bar{y}}\right)^2 + \left(\frac{\partial \bar{v}}{\partial \bar{x}} + \frac{\partial \bar{u}}{\partial \bar{y}}\right)^2\right] - \frac{v}{k_1}\bar{v}, \tag{4.14}$$

$$\bar{u}\frac{\partial \bar{T}}{\partial \bar{x}} + \bar{v}\frac{\partial \bar{T}}{\partial \bar{y}} = \frac{1}{\rho c_p}\nabla \cdot \left(\left[k + \frac{16\sigma_{SB}\bar{T}^3}{3(\alpha_r + \sigma_s)}\right]\nabla \bar{T}\right), \tag{4.15}$$

where $\bar{u}$ and $\bar{v}$ are the velocity components in $\bar{x}$ and $\bar{y}$ directions respectively, $\bar{p}(\bar{x},\bar{y})$ is the pressure function of the fluid and v is the kinematic viscosity. Here the fluid flow is considered as potential flow, in which the flow is impinging obliquely to the flat plate and far away from the plate the fluid is moving with velocity $U_e(\bar{x},\bar{y}) = a\bar{x} + b\bar{y}$. The boundary conditions for the

59

present fluid flow are given by

$$\bar{y} = 0 \quad : \quad \bar{u} = 0, \ \bar{v} = 0, \ \bar{T} = T_w,$$

$$\bar{y} \to \infty \quad : \quad \bar{u} = a\bar{x} + b\bar{y}, \ \bar{T} = T_\infty,$$

(4.16)

where a, b are the constant having positive values with dimension inverse of time. T_∞ is the ambient temperature of the fluid away from the surface and T_w is the surface temperature. Introducing following non-dimensional variables

$$x = \bar{x}\sqrt{\frac{a}{v}}, \ y = \bar{y}\sqrt{\frac{a}{v}}, \ u = \frac{1}{\sqrt{va}}\bar{u}, \ v = \frac{1}{\sqrt{va}}\bar{v}, \ p = \frac{1}{\rho va}\bar{p}, \ T = \frac{\bar{T} - T_\infty}{T_w - T_\infty},$$

(4.17)

into equations (4.12)–(4.16), we obtained the following dimensionless form

$$\frac{\partial u}{\partial x} + \frac{\partial v}{\partial y} = 0,$$

(4.18)

$$u\frac{\partial u}{\partial x} + v\frac{\partial u}{\partial y} = -\frac{\partial p}{\partial x} + \left(\frac{\partial^2 u}{\partial x^2} + \frac{\partial^2 u}{\partial y^2}\right) + We\left\{\frac{\partial}{\partial x}\left[\begin{array}{c} 2u\frac{\partial^2 u}{\partial x^2} + 2v\frac{\partial^2 u}{\partial x\partial y} + \\ 4\left(\frac{\partial u}{\partial x}\right)^2 + 2\frac{\partial v}{\partial x}\left(\frac{\partial v}{\partial x} + \frac{\partial u}{\partial y}\right) \end{array}\right] + \right.$$

$$\left. \frac{\partial}{\partial y}\left[\begin{array}{c} \left(u\frac{\partial}{\partial x} + v\frac{\partial}{\partial y}\right)\left(\frac{\partial v}{\partial x} + \frac{\partial u}{\partial y}\right) + \\ 2\frac{\partial u}{\partial x}\frac{\partial u}{\partial y} + 2\frac{\partial v}{\partial x}\frac{\partial v}{\partial y} \end{array}\right]\right\} + \lambda\frac{\partial}{\partial x}\left[4\left(\frac{\partial u}{\partial x}\right)^2 + \left(\frac{\partial v}{\partial x} + \frac{\partial u}{\partial y}\right)^2\right] - K^2 u,$$

(4.19)

$$u\frac{\partial v}{\partial x} + v\frac{\partial v}{\partial y} = -\frac{\partial p}{\partial y} + \left(\frac{\partial^2 v}{\partial x^2} + \frac{\partial^2 v}{\partial y^2}\right) + We\left\{\frac{\partial}{\partial x}\left[\begin{array}{c} 2\frac{\partial u}{\partial x}\frac{\partial u}{\partial y} + 2\frac{\partial v}{\partial x}\frac{\partial v}{\partial y} + \\ \left(u\frac{\partial}{\partial x} + v\frac{\partial}{\partial y}\right)\left(\frac{\partial v}{\partial x} + \frac{\partial u}{\partial y}\right) \end{array}\right] + \right.$$

$$\left. \frac{\partial}{\partial y}\left[\begin{array}{c} 2\frac{\partial u}{\partial y}\left(\frac{\partial v}{\partial x} + \frac{\partial u}{\partial y}\right) + 4\left(\frac{\partial v}{\partial y}\right)^2 \\ 2v\frac{\partial^2 v}{\partial x^2} + 2u\frac{\partial^2 v}{\partial x\partial y} \end{array}\right]\right\} + \lambda\frac{\partial}{\partial y}\left[4\left(\frac{\partial v}{\partial y}\right)^2 + \left(\frac{\partial v}{\partial x} + \frac{\partial u}{\partial y}\right)^2\right] - K^2 v,$$

(4.20)

$$u\frac{\partial T}{\partial x} + v\frac{\partial T}{\partial y} = \frac{1}{Pr}\nabla\cdot\left(\left[1 + \frac{16\sigma_{SB}T_\infty^3(1 + (\theta_w - 1)T)^3}{3k(\alpha_r + \sigma_s)}\right]\nabla T\right).$$

(4.21)

The boundary conditions become

$$y = 0 \quad : \quad u = 0, \ v = 0, \ T = 1,$$

$$y \to \infty \quad : \quad u = x + \frac{b}{a}y, \ T = 0,$$

(4.22)

60

where $We = \alpha_1 a / \mu$ is Weissenberg number. $K^2 = \nu / ak_1$ is the porosity parameter, $\theta_w = T_w / T_\infty$

is surface heating parameter, $\lambda = \alpha_2 a / \mu$ and $Pr = \mu c_p / k$ is the Prandtl number. Introducing

the stream function ψ which satisfies the continuity condition such that

$$u = \frac{\partial \psi}{\partial y}, \quad v = -\frac{\partial \psi}{\partial x}. \tag{4.23}$$

By eliminating pressure terms from Eqs. (4.19, 4.20) by using $p_{xy} = p_{yx}$ and then using Eq.

(4.23), Eqs. (4.19−4.22) take the following form

$$\frac{\partial \psi}{\partial y} \frac{\partial^3 \psi}{\partial x^3} - \frac{\partial \psi}{\partial x} \frac{\partial^3 \psi}{\partial y^3} + \frac{\partial \psi}{\partial y} \frac{\partial^3 \psi}{\partial x \partial y^2} - \frac{\partial \psi}{\partial x} \frac{\partial^3 \psi}{\partial x^2 \partial y} - \frac{\partial^4 \psi}{\partial x^4} - \frac{\partial^4 \psi}{\partial y^4} - 2 \frac{\partial^4 \psi}{\partial x^2 \partial y^2} + K^2 \left(\frac{\partial^2 \psi}{\partial x^2} + \frac{\partial^2 \psi}{\partial y^2} \right)$$

$$+ We \left(\frac{\partial \psi}{\partial x} \frac{\partial^5 \psi}{\partial y^5} - \frac{\partial \psi}{\partial y} \frac{\partial^5 \psi}{\partial x \partial y^4} + 2 \frac{\partial \psi}{\partial x} \frac{\partial^5 \psi}{\partial x^2 \partial y^3} - 2 \frac{\partial \psi}{\partial y} \frac{\partial^5 \psi}{\partial x^3 \partial y^2} + \frac{\partial \psi}{\partial x} \frac{\partial^5 \psi}{\partial x^4 \partial y} - \frac{\partial \psi}{\partial y} \frac{\partial^5 \psi}{\partial x^5} \right) = 0 \tag{4.24}$$

$$\frac{\partial \psi}{\partial y} \frac{\partial T}{\partial x} - \frac{\partial \psi}{\partial x} \frac{\partial T}{\partial y} = \frac{1}{Pr} \nabla \cdot \left(\left[1 + \frac{16 \sigma_{SB} T_\infty^3 (1 + (\theta_w - 1) T)^3}{3k(\alpha_r + \sigma_s)} \right] \nabla T \right). \tag{4.25}$$

The dimensionless boundary conditions in terms of stream function ψ take the following form

$$y = 0 \quad : \quad \psi = 0, \ \frac{\partial \psi}{\partial y} = 0, \ T = 1.$$

$$y \to \infty : \quad \psi = xy + \frac{\gamma}{2} y^2, \ T = 0, \tag{4.26}$$

where $\gamma = b/a$ is non-dimensional constant characterizing the obliqueness of incoming flow.

Suppose the solution of Eqs. (4.24, 4.25) subject to the boundary conditions (4.26) is of the

form

$$\psi = xf(y) + g(y), \quad T = \theta(y), \tag{4.27}$$

where $f(y)$ and $g(y)$ are the functions representing normal and oblique flow components. Us-

ing the Eq. (4.27) in Eqs. (4.24−4.26) and comparing the coefficient of x^0 and x^1, we get

$$f^{iv} + ff''' - f'f'' - We \left(ff^v - f'f^{iv} \right) - K^2 f'' = 0, \tag{4.28}$$

$$g^{iv} + fg''' - g'f'' - We \left(fg^v - g'f^{iv} \right) - K^2 g'' = 0, \tag{4.29}$$

$$\frac{\partial}{\partial y} \left[\left\{ 1 + \frac{4}{3} Rd (1 + (\theta_w - 1) \theta)^3 \right\} \theta' \right] + Pr f \theta' = 0, \tag{4.30}$$

61

subject to boundary conditions

$$y = 0 \quad : \quad f(y) = 0, \ f'(y) = 0, \ g(y) = g'(y) = 0, \ \theta = 1,$$

$$y \to \infty \quad : \quad f'(y) = 1, \ g'(y) = \gamma y, \ \theta = 0,$$

(4.31)

where $Rd = 4\sigma_{SB}T_\infty^3/k\,(\alpha_r + \sigma_s)$, prime denotes the derivative with respect to y. Integrating

Eqs. (4.28) and (4.29), and by employing boundary conditions (4.31) at infinity, we have

$$f''' + ff'' - (f')^2 - We\left(ff^{iv} - 2f'f''' + (f'')^2\right) - K^2(f' - 1) + 1 = 0, \quad (4.32)$$

$$g''' + fg'' - g'f' - We\left(fg^{iv} - f'g''' + g''f'' - f'''g'\right) - K^2(g' - \gamma y) - A\gamma = 0, \quad (4.33)$$

where the constant A accounts the boundary layer displacement. It arises when $y \to \infty$, $f(y)$

behaves as $f(y) = y + A$. For simplicity introducing a new variable $g'(y) = \gamma h(y)$, Eq. (4.33)

with boundary conditions can be written as

$$h'' + fh' - f'h - We\left(fh''' - f'h'' + h'f'' - f'''h\right) - K^2 h = A - K^2 y, \quad (4.34)$$

$$h(0) = 0 \quad h'(\infty) = 1. \quad (4.35)$$

The values of $f''(0)$, $h'(0)$ and $\theta'(0)$ can be found from equations (4.30), (4.32) and (4.34) with

boundary conditions (4.31) and (4.35) for different values of the parameter We, K, Rd and γ.

We mention here that for $Rd=0$ and orthogonal stagnation point flow ($\gamma = 0$) equations (4.30)

and (4.32) reduce to equations (11) and (12) as reported by Attia [86]. The dimensionless

components of velocity can be obtain by using the relation of ψ given in Eq. (4.27)

$$u = \frac{\partial \psi}{\partial y} = xf'(y) + \gamma h(y), \quad (4.36)$$

$$v = -\frac{\partial \psi}{\partial x} = -f(y). \quad (4.37)$$

The physical quantities of interest are wall shear srtess and local Nusselt number can be defined as

$$\tau_w = x(1 + 3We) f''(0) + (1 + 2We) \gamma h'(0),$$ (4.38)

$$Re_x^{-1/2} Nu_x = -\left(1 + \frac{4}{3} Rd\, \theta_w^3\right) \theta'(0).$$ (4.39)

The stagnation point occurs when the streamline $\psi = 0$ meets the wall at $x = x_s$. The values of x_s can be calculated at zero skin friction ($\tau_w = 0$), which is

$$x_s = -\frac{(1 + 2We)\, \gamma h'(0)}{(1 + 3We)\, f''(0)}.$$ (4.40)

4.2 Chebyshev Spectral Newton Iterative Scheme

In order to solve nonlinear equations (4.30), (4.32) and (4.34) with boundary conditions (4.31) and (4.35) for different values of involving parameters, Chebyshev spectral Newton iterative scheme (CSNIS) is used. For $(i+1)$th iterates, we write

$$f_{i+1} = f_i + \delta f_i,$$ (4.41)

and similarly for all other dependent variables. Using Eq. (4.41) in (4.32), we obtained

$$c_{0,i}\delta f_i^{iv} + c_{1,i}\delta f_i''' + c_{2,i}\delta f_i'' + c_{3,i}\delta f_i' + c_{4,i}\delta f_i = R_i, \quad i = 1, 2, 3....N$$ (4.42)

subject to boundary conditions

$$\delta f_i(0) = -f_i(0), \quad \delta f_i'(0) = -f_i'(0), \quad \delta f_i'(\infty) = 1 - f_i'(\infty).$$ (4.43)

The coefficients $c_{j,i}$ ($j = 0, 1, 2, 3, 4$) and R_i are

$$c_{0,i} = -We f_i, \quad c_{1,i} = 1 + 2We f_i', \quad c_{2,i} = 1 - 2We f_i''.$$

$$c_{3,i} = -2f_i' + 2We f_i''' - K^2, \quad c_{4,i} = f_i'' - We f_i^{iv},$$ (4.44)

$$R_i = We\left(f_i f_i^{iv} - 2f_i' f_i''' + \left(f_i''\right)^2\right) - f_i''' - f_i f_i'' + \left(f_i'\right)^2 + K^2\left(f_i' - 1\right) - 1.$$

Eq. (4.42) is now linear and is solved using the Chebyshev spectral collocation method [88–90]. For this purpose, the physical domain $[0, \infty]$ is truncated to $[0, L]$, where L is chosen sufficiently large. The reduced domain is transformed to $[-1, 1]$ by using transformation $\xi = 2\eta/L - 1$. Nodes from -1 to 1 are defined as $\xi_k = cos(\pi k/N)$, $k=0, 1, 2, \ldots$ N, and are known Gauss-Lobatto collocation points. Chebyshev spectral collocation method is based on differentiation matrix D, which can be computed in different ways. Here we used D as suggested by Trefethen [91]. For $i=0$, Eqs. (4.41) and (4.42) become

$$f_1 = f_0 + \delta f_0,$$

$$c_{0,0}\delta f_0^{iv} + c_{1,0}\delta f_0''' + c_{2,0}\delta f_0'' + c_{3,0}\delta f_0' + c_{4,0}\delta f_0 = R_0,$$

(4.45)

f_0 is used as an initial guess and we found δf_0 for first iteration. Similarly for $i=1$, (4.41) and (4.42) become

$$f_2 = f_1 + \delta f_1,$$

$$c_{0,1}\delta f_1^{iv} + c_{1,1}\delta f_1''' + c_{2,1}\delta f_1'' + c_{3,1}\delta f_1' + c_{4,1}\delta f_1 = R_1,$$

(4.46)

In which $f_1 (=f_0 + \delta f_0)$ is known function and we found δf_1 for second iteration. We continue this procedure until $f_{i+1} - f_i \approx 0$. As the equation (4.32) subjected to the boundary, condition (4.31) has been solved and solution of f is obtained. Once the f is known, then equation (4.34) becomes linear and it is solved by using the Chebyshev spectral collocation method. However, the energy equation defined in Eq. (4.30) is still non-linear and it is solved in the same way as proposed for Eq. (4.32). MATLAB R2010a is used to develop the algorithm.

4.3 Results and discussion

Non-linear ordinary differential equations (4.30), (4.32) and (4.34) with boundary conditions (4.31) and (4.35) have been solved numerically against all physically important values of the

64

parameters We (Weissenberg number), K (Porosity parameter) Rd (Radiation parameter) and γ

(shearing flow parameter) by using the Chebyshev spectral Newton iterative scheme (CSNIS)

as described above. In Table 4.1, the comparison of numerical values of $f''(0)$ has been made

with the results obtained by CSNIS and finite difference method for the different values of

We and K. It is seen from the Table 4.1 that the results obtained by CSNIS are in excellent

agreement with the results obtained by finite difference method. CPU time is also calculated

for both techniques and it is observed that CSNIS takes less time to achieve its desired results.

In table 4.2, the values of the skin friction coefficient $(Re_x^{1/2}C_f)$ are presented to show the

validity and convergence of the results obtained by CSNIS. In this table it is observed that val-

ues of the skin friction coefficient $(Re_x^{1/2}C_f)$ converge rapidly after only 3 iterations. Table

4.2 also clearly indicates that after performing small number of iterations, the present CSNIS

results made an excellent agreement with the results of Attia [86] and Li et al. [92]. Compar-

ison of the computed values of $-\theta'(0)$ and $f''(0)$ with Attia [86] is given in Tables 4.3−4.5

for various values of We, Pr and K when $Rd=0$ and $\gamma=0$. It is found that the results are in

good agreement and hence accurate. However, small difference occurs quantitatively due to

variation in numerical technique. In Table 4.6, the values of $f''(0)$, $h'(0)$, A and $Re_x^{-1/2}Nu_x$

are given for the various values of We and K when $Pr=1$, $Rd=2$ and $\theta_w = 1.5$. From the table

it is found that the values of $f''(0)$ are increasing with the increase in porosity parameter K

but with increasing the effects of Weissenberg number (We), the values of $f''(0)$ decrease.

It is also observed that the Weissenberg number (We) helps to reduce the heat transfer rate

where the porosity parameter (K) enhances the heat transfer rate. Fig. 4.2(a-d) indicates the

influence of Weissenberg parameter We and obliqueness parameter γ on the velocity profile.

Fig. 4.2(a) represents the orthogonal stagnation point flow $(\gamma = 0)$ and Fig. 4.2(b-c) are drawn

for non-orthogonal stagnation point flow $(\gamma \neq 0)$. It can be seen from the Fig. 4.2(a-d) that

with the increase in values of We, the velocity of the fluid decreases and the boundary layer thickness increases. Further, it is observed that with increase in value of γ the velocity of the fluid increases as shown in Fig. 4.2(b-d). In Fig. 4.3(a-d) the variation of the velocity profile is shown against y for different value of K and γ. It is observed that the velocity increases but the boundary layer becomes thinner with the increase in value of K for orthogonal stagnation point flow as shown in Fig. 4.3a. On the other hand, the velocity increases rapidly against y for different values of K in oblique stagnation point flow (Fig. 4.3(b-d)). In Fig. 4.4, variation of the temperature is plotted against y for the different values of radiation parameter Rd. The solid lines show the variation in case of non-linear radiation and the dashed lines show the variation in case of linear radiation. It is observed that the temperature of the fluid enhances due to enhancement of the radiation. It is because of the reason that due to application of radiation the surface become hot. From the figure, a rapid increase in the temperature is also observed in the case of non-linear radiation as compared to the case of linear radiation. This increase is due to an extra surface heating term, which enhance the temperature rapidly. Where in linear radiation we ignored the surface heating effect. Temperature variation against y for different value of surface heating parameter θ_w is plotted in Fig. 4.5. The dotted line is plotted for $\theta_w = 1$ (linear radiation case) and solid lines are plotted for $\theta_w = 1.3, 1.5, 1.7$ (non-linear radiation case). With increase of surface heating parameter θ_w the enhancement in the temperature is observed. Figure 4.6 highlights the effects of viscoelastic parameter on temperature profile. From this figure, it is observed that the temperature is an increasing function of We. It is due to the reason that with increase of viscoelasticity of the fluid, the heat transfer rate decreases within the boundary layer, which enhances the temperature in stagnation point region. This behavior also validates the results demonstrated in Fig. 4.9. Figure 4.7 depicts the temperature variation for porosity parameter K. It is observed that temperature profile is

decreasing function of K. It is because of the reason that higher heat transfer rate results in cooling of the surface which is shown in Fig. 4.9. Variation of wall shear stress and heat transfer rate is shown through Figs. 4.8 and 4.9 respectively. Wall shear stress is observed an increasing function of viscoelastic parameter We and decreasing function of porosity parameter K. Moreover, the heat transfer rate is observed an increasing function of K and decreasing function of We. The variation of the local Nusselt number against K for the different values of Rd is plotted in Fig. 4.10. The solid lines are drawn in case of non-linear radiation and dashed lines are drawn in case of linear radiation. It is observed that heat transfer rate increases with the enhancement of radiation effects. Moreover, by increasing the porosity parameter K the enhancement in heat transfer rate is also observed. In Fig. 4.11, values of the local Nusselt number are plotted against K for different values of Pr. It is observed that with increase of Pr the heat transfer rate increases, which results in reduction of the temperature. In Fig 4.10 and 4.11 it is also observed that heat transfer rate increases in case of non-linear radiation as compared to linear radiation. Figs. 4.12 and 4.13 are plotted for streamlines, where dots indicate the position of stagnation point. In Fig. 4.12, streamlines are plotted for the various values of obliqueness parameter γ. The effect of K on streamlines is shown in Fig. 4.13. Increase in constant obliqueness parameter $|\gamma|$ and porosity parameter K helps to translate the stagnation point. It is also noted that the streamlines come closer to the plate and the boundary layer thickness gets reduces, which indicates an increase in the velocity.

Table 4.1: Variation of $f''(0)$ for different values of We and K.

We	K	Finite difference	CPU time (sec)	CSNIS	CPU time (sec)
0	0	1.2325976	4.146076	1.2325877	0.461214
	0.1	1.2366126	6.599541	1.2366026	0.450157
	0.5	1.3294170	6.494227	1.3294067	0.369675
	1	1.5853423	4.829643	1.5853307	0.343862
1	0	0.7527695	5.913931	0.7527678	0.425973
	0.1	0.7556376	5.394916	0.7556359	0.586347
	0.5	0.8215089	5.833578	0.8215072	0.547974
	1	1.0000000	5.950510	1.0000001	0.467803
5	0	0.4128861	13.02250	0.4128854	0.466235
	0.1	0.4146696	13.47708	0.4146689	0.504567
	0.5	0.4553938	11.623624	0.4553939	0.398360
	1	0.5640846	10.154764	0.5640877	0.559593

Table 4.2: Values of skin friction coefficient $(Re_x^{1/2}C_f)$ at different iterations

	Iterations ↓	$We = 0$		$We = 1$	
		$K = 0$	$K = 1$	$K = 0$	$K = 1$
	1	2.5765664	2.7620723	0.88579430	2.9997276
	2	1.2783484	1.6079020	0.75774750	1.6013812
	3	1.2329404	1.5853840	0.75277610	1.0774925
$Re_x^{1/2}C_f \rightarrow$	4	1.2325877	1.5853307	0.75276780	1.0009531
	5	1.2325877	1.5853307	0.75276780	1.0000002
	6	1.2325877	1.5853307	0.75276780	1.0000001
	7	1.2325877	1.5853307	0.75276780	1.0000001
	8	1.2325877	1.5853307	0.75276780	1.0000001
Li et al. [92] →	1.23259			0.752763	
Attia [86] →	1.2326	1.5840		0.7528	1.0000

Table 4.3: Comparison of $f''(0)$ for the various values of We and K. The results in small brackets are reported by Attia [86].

K	$We=0$	$We=0.5$	$We=1$	$We=5$	$We=10$
0	1.2326(1.2326)	0.9025(0.9025)	0.7528(0.7528)	0.4130(0.4130)	0.3031(0.3031)
0.5	1.3294(1.3283)	0.9810(0.9810)	0.8215(0.8215)	0.4554(0.4555)	0.3353(0.3355)
1	1.5853(1.5840)	1.1860(1.1860)	1.0000(1.0000)	0.5641(0.5641)	0.4180(0.4180)
1.5	1.9390(1.9374)	1.4658(1.4666)	1.2420(1.2420)	0.7092(0.7092)	0.5277(0.5277)
2	2.3467(2.3449)	1.7855(1.7854)	1.5175(1.5175)	0.8728(0.8727)	0.6510(0.6509)

Table 4.4: Comparison of $-\theta'(0)$ for the different values of We and Pr when $K = 0.1, Rd = 0$. The results in small brackets are reported by Attia [86].

| We	$Pr = 0.05$	$Pr = 0.1$	$Pr = 0.5$	$Pr = 1$	$Pr = 2$
0	0.1610(0.1667)	0.2196(0.2206)	0.4336(0.4354)	0.5708(0.5739)	0.7442(0.7496)
0.5	0.1546(0.1607)	0.2086(0.2098)	0.4025(0.4041)	0.5258(0.5285)	0.6814(0.6861)
1	0.1505(0.1569)	0.2019(0.2032)	0.3849(0.3864)	0.5007(0.5033)	0.6470(0.6513)
5	0.1354(0.1440)	0.1785(0.1806)	0.3291(0.3304)	0.4238(0.4238)	0.5432(0.5464)
10	0.1269(0.1377)	0.1661(0.1695)	0.3021(0.3039)	0.3875(0.3899)	0.4952(0.4968)

Table 4.5: Comparison values of $-\theta'(0)$ for the different values of K and Pr when $We = 1$, $Rd = 0$. The results in small brackets are reported by Attia [86].

| K	$Pr = 0.05$	$Pr = 0.1$	$Pr = 0.5$	$Pr = 1$	$Pr = 2$
0	0.1504(0.1569)	0.2019(0.2031)	0.3846(0.3861)	0.5004(0.5029)	0.6465(0.6507)
0.5	0.1516(0.1580)	0.2038(0.2050)	0.3903(0.3918)	0.5088(0.5114)	0.6587(0.6631)
1	0.1543(0.1605)	0.2084(0.2095)	0.4035(0.4051)	0.5285(0.5313)	0.6871(0.6918)
1.5	0.1572(0.1632)	0.2134(0.2134)	0.4184(0.4202)	0.5509(0.5539)	0.7197(0.7249)
2	0.1598(0.1657)	0.2179(0.2179)	0.4323(0.4342)	0.5720(0.5753)	0.7506(0.7563)

Table 4.6: The Numerical values of $f''(0)$, $h'(0)$, A and $Re_x^{-1/2}Nu_x$ for the different values of K and We when $Pr = 1$, $Rd = 2$ and $\theta_w = 1.5$.

	We	K	$f''(0)$	$h'(0)$	A	$Re_x^{1/2}Nu_x$
Newtonian case		0	1.2326	1.4065	-0.6479	1.8309
		0.1	1.2366	1.4043	-0.6465	1.8315
		0.2	1.2486	1.3977	-0.6423	1.8332
	0	0.5	1.3294	1.3569	-0.6151	1.8443
		1	1.5853	1.2617	-0.5410	1.8751
		1.5	1.9390	1.1816	-0.4618	1.9092
		2	2.3467	1.1273	-0.3936	1.9398
Non-Newtonian case		0	0.7528	1.2128	-1.2028	1.6661
		0.1	0.7556	1.2094	-1.2001	1.6669
		0.2	0.7642	1.1992	-1.1920	1.6693
	1	0.5	0.8215	1.1378	-1.1399	1.6846
		1	1.0000	1.0000	-1.0000	1.7269
		1.5	1.2420	0.8891	-0.8522	1.7740
		2	1.5175	0.8159	-0.7258	1.8167
		0	0.4129	1.0852	-2.3348	1.4560
		0.1	0.4147	1.0804	-2.3294	1.4570
		0.2	0.4200	1.0661	-2.3135	1.4599
	5	0.5	0.4554	0.9810	-2.2112	1.4787
		1	0.5641	0.7962	-1.9378	1.5305
		1.5	0.7092	0.6525	-1.6506	1.5884
		2	0.8728	0.5596	-1.4054	1.6418
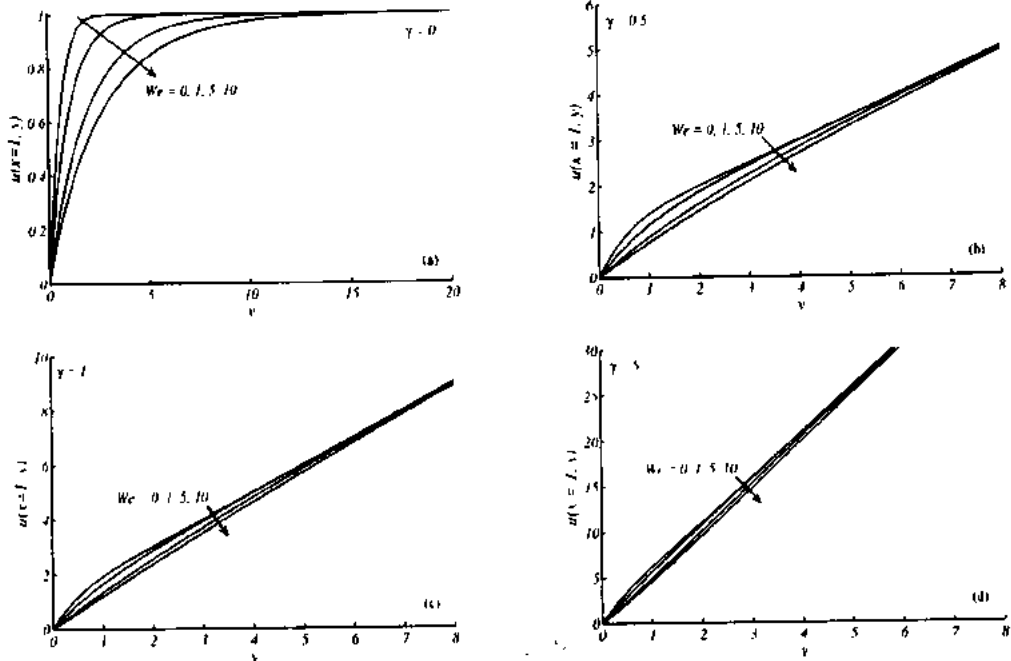
Figure 4.2: Variation of velocity profile for the different values of (a) $\gamma = 0$ (b) $\gamma = 0.5$ (c) $\gamma = 1$ (d) $\gamma = 5$ and We when $K = 1$.
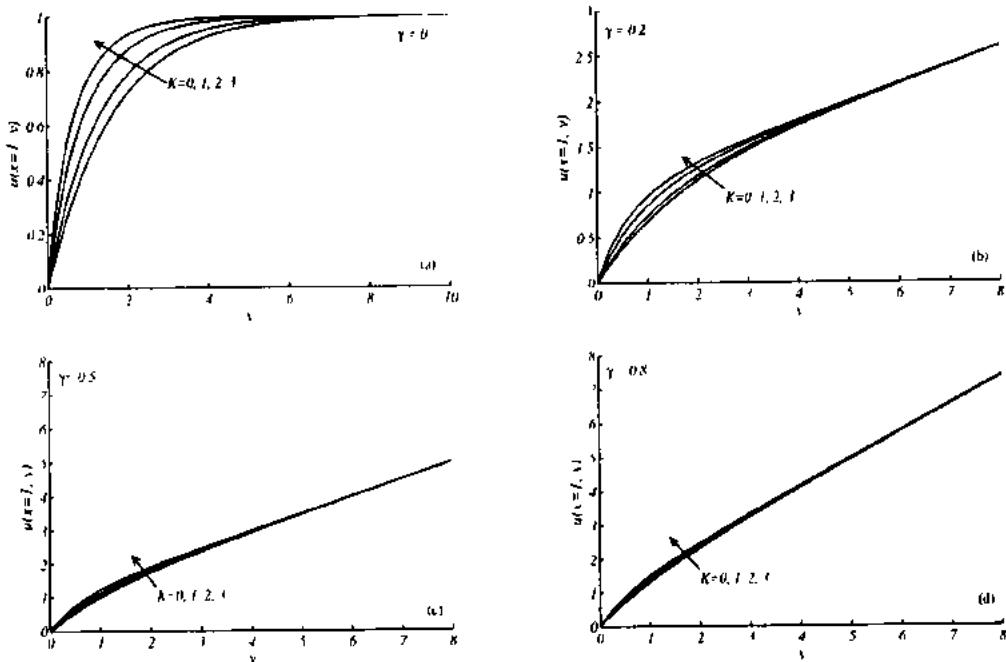
Figure 4.3: Variation of velocity profile for the different values of (a) $\gamma = 0$ (b) $\gamma = 0.2$ (c) $\gamma = 0.5$ (d) $\gamma = 0.8$ and K when $We = 2$
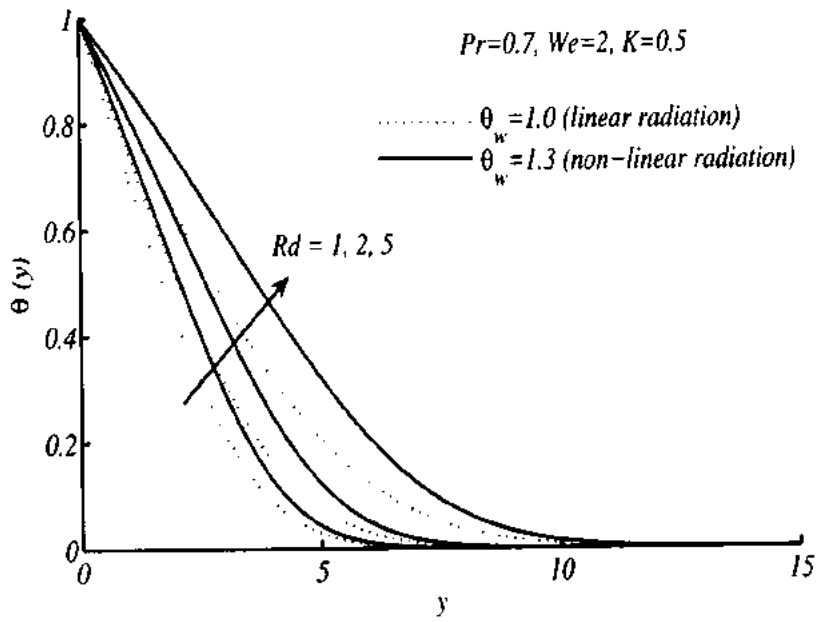
Figure 4.4: Variation of temperature profile for the different values of Rd.
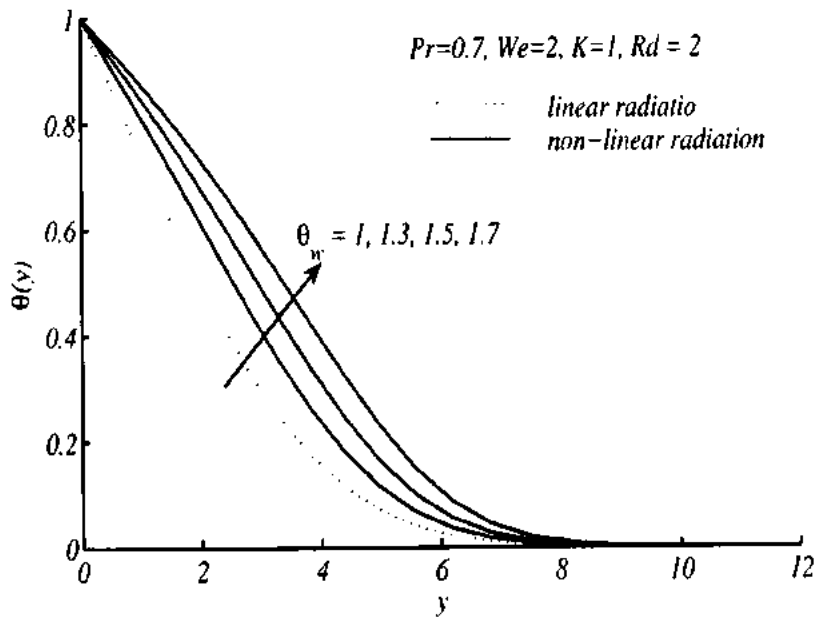
Figure 4.5: Variation of temperature profile for the different values of θ_w.

72
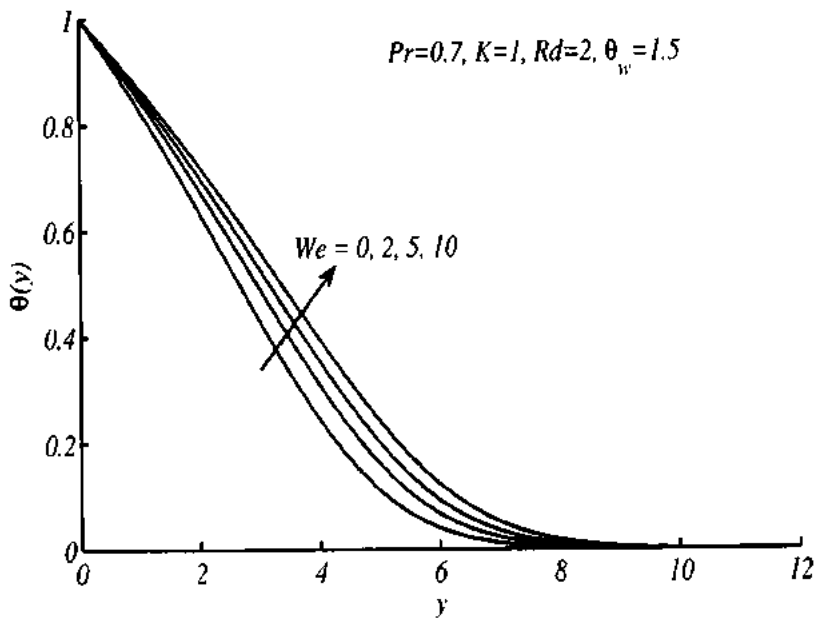
Figure 4.6: Variation of temperature profile for the different values of *We*.
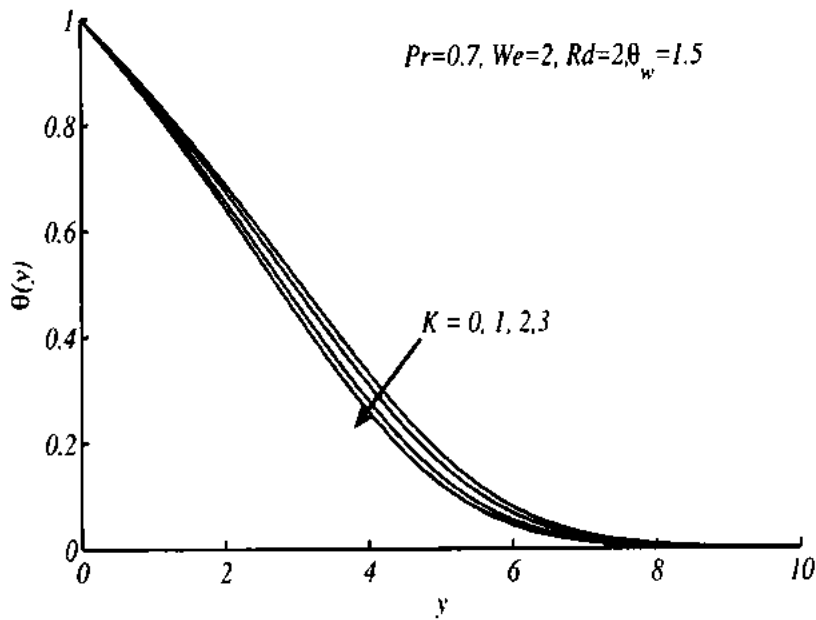
Figure 4.7: Variation of temperature profile for the different values of *K*.

73
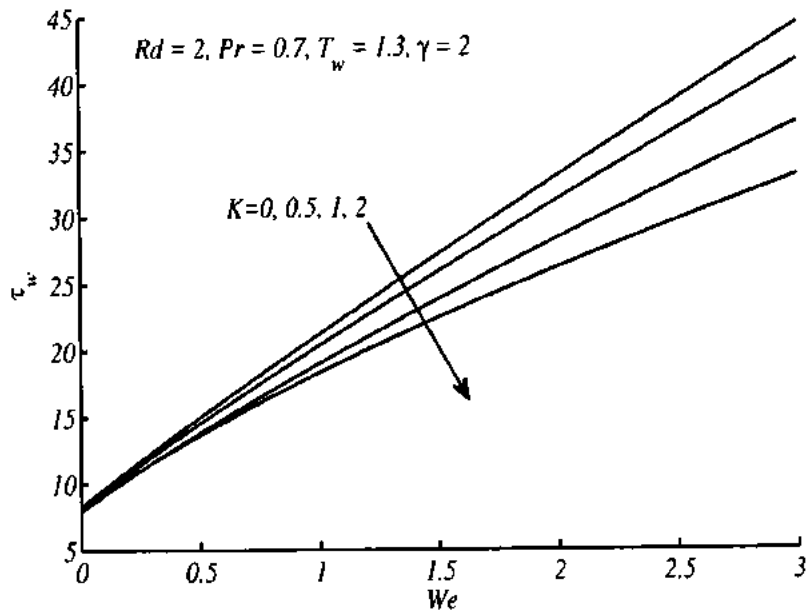
Figure 4.8: Variation of wall shear stress against We for the different values of K.
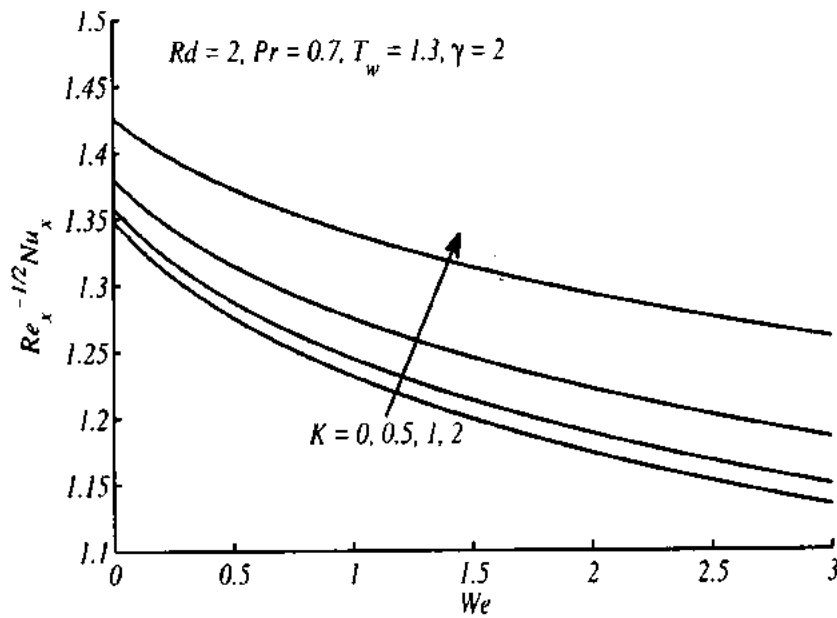
Figure 4.9: Variation of local Nusselt number against We for the different values of K.
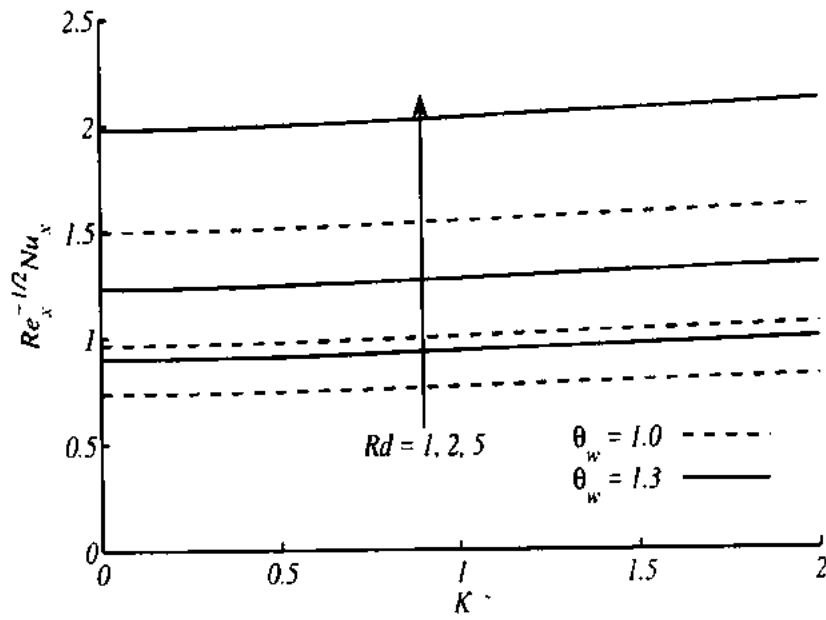
Figure 4.10: Variation of local Nusselt number against K for the different values of Rd when

$\theta_w = 1.0$ and $\theta_w = 1.3$
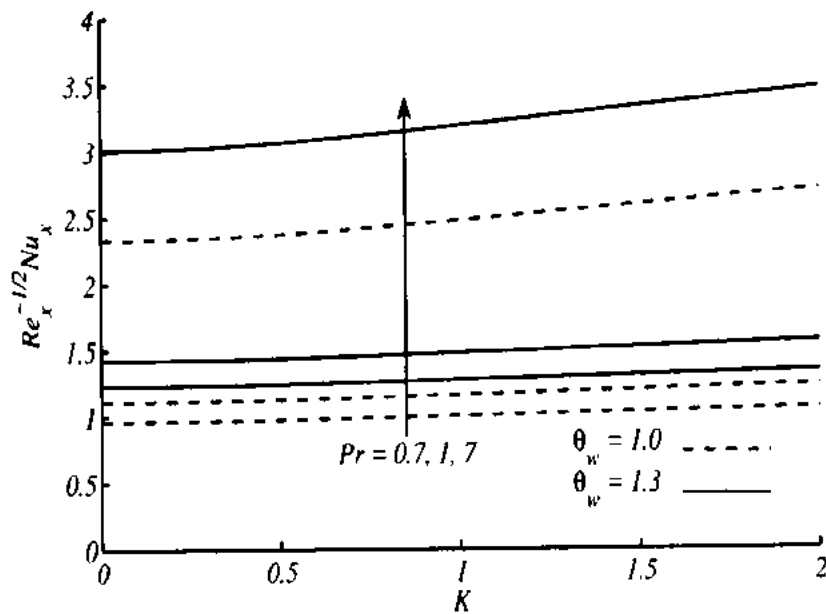
Figure 4.11: Variation of local Nusselt number against K for the different values of Pr when

$\theta_w = 1.0$ and $\theta_w = 1.3$.

$We = 1, K = 1$

$\gamma = 0$

$\gamma = 10$

$\gamma = 20$

$\gamma = 30$

$x_s = 0$

$\psi = -1.0$

1.0

-0.5

-0.1

0.5

0.1

$x_s = -7.5$

$x_s = -15.0$

$x_s = -22.5$
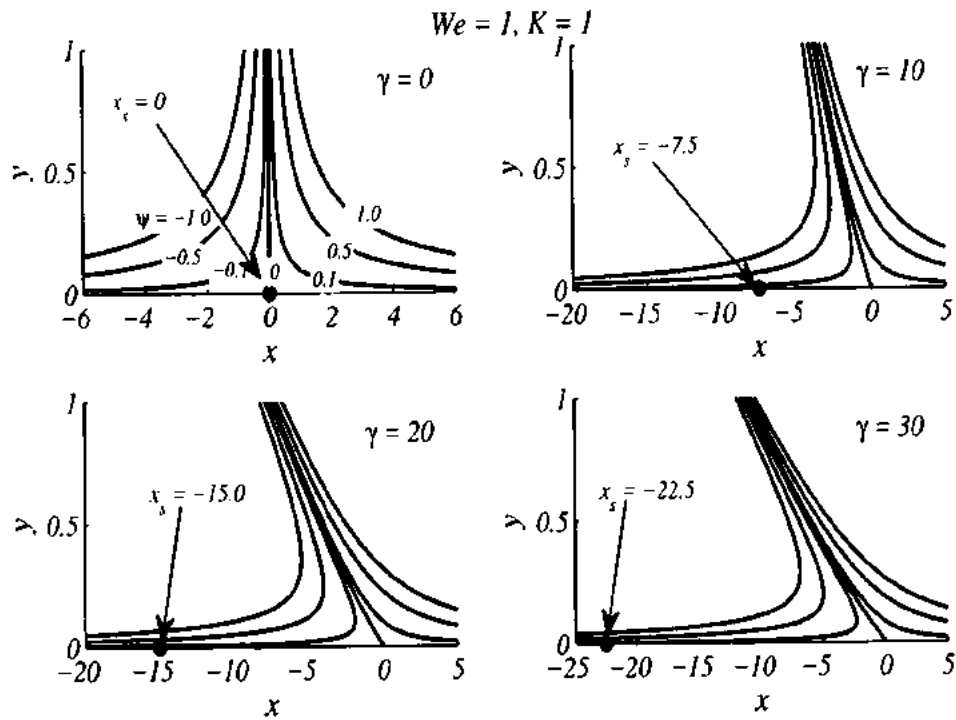
Figure 4.12: Streamlines for the different values of obliqueness parameter γ.

$We = 0, \gamma = 5$

$K = 0$

$K = 1$

$K = 2$

$K = 3$

$x_s = -6.894$

$\psi = -1.0$

1.0

-0.5

0.5

-0.1

0

0.1

$x_s = -4.041$

$x_s = -4.041$

$x_s = -1.281$
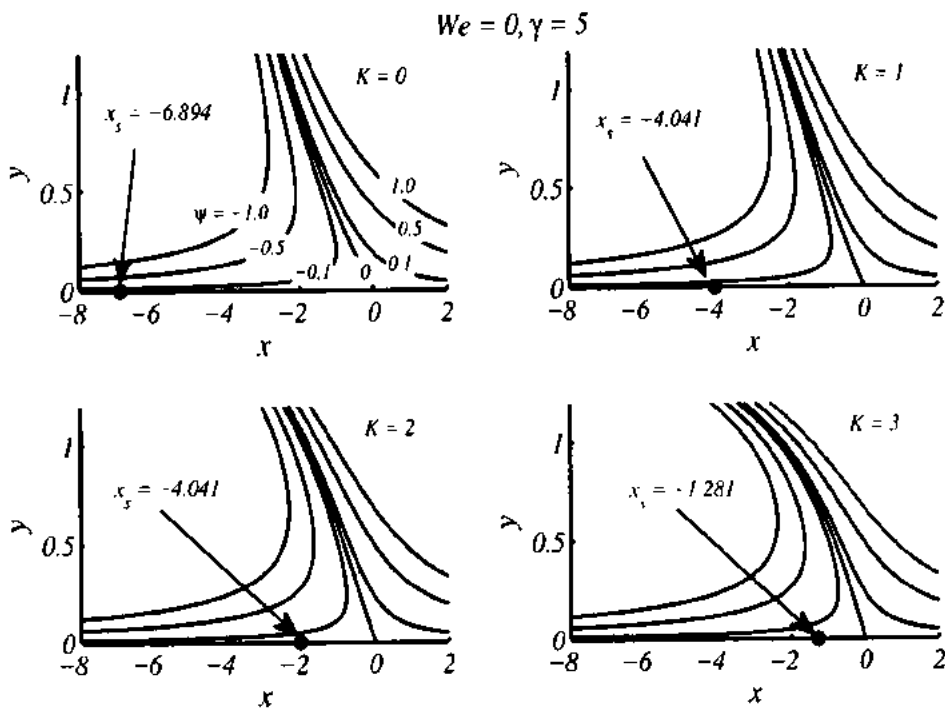
Figure 4.13: Streamlines for the different values of porosity parameter K.

4.4 Conclusions

The Chebyshev Spectral Newton Iterative Scheme (CSNIS) has been successfully applied to perform a comparative study of steady two-dimensional oblique stagnation point flow of a second grade fluid in a porous medium with non-linear radiation effects. It is observed that the CSNIS is efficient, less time consuming, stable and rapid convergent and have excellent agreement with available data in the limiting case. This study is based on a new idea of non-linear radiation effects in oblique stagnation point region through porous medium. The findings of this study may be summarized as follows

- Velocity of the fluid increases with increase in the values of shearing parameter .

- It is seen that increase of radiation and surface heating parameter, the temperature and the thermal boundary thickness increases. .

- Heat transfer rate is observed an increasing function of porosity parameter K and decreasing function of viscoelastic parameter We.

- Enhancement in the temperature is observed with increase of We, where the reduction in the temperature is due to enhancement of porosity parameter K.

Chapter 5

Study of nanofluid in the region of oblique stagnation point flow over a stretching surface with radiation

In this chapter, we discussed the enhancement of thermal conductivity of elastico-viscous fluid filled with nanoparticles, due to the implementation of radiation and convective boundary condition. The flow is considered impinging obliquely over a stretching sheet near a stagnation point. The governing partial differential equations are transformed into a system of ordinary differential equations by employing suitable similarity transformations. Solution of the resulting equations is computed numerically using Chebyshev Spectral Newton Iterative Scheme (CSNIS). An excellent agreement with the results available in the literature is achieved and is evident from tables. Effects of involving parameters on the flow and heat transfer characteristics are observed and shown through graphs. It is noted that the larger values of Biot number imply the enhancement in heat transfer, thermal and concentration boundary layer thickness.
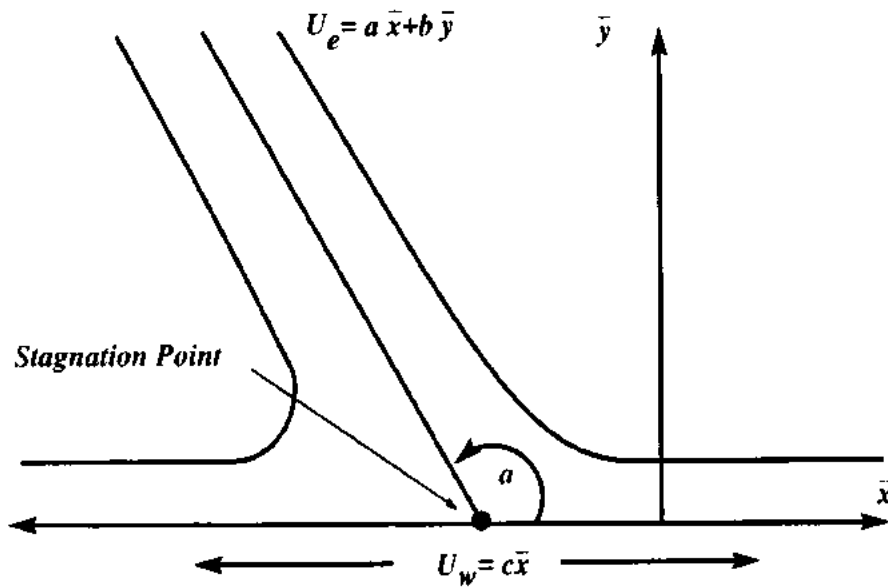
Figure 5.1: Schematic diagram of the flow geometry

5.1 Problem formulation

Consider the steady, two-dimensional, laminar flow of Walter's B nanofluid impinging obliquely on a stretching surface, at $\bar{y} = 0$. The fluid occupies the upper half space $\bar{y} > 0$ as shown in Fig. 5.1. The surface is heated convectively, by convective heating process, which is characterized by a temperature T_f and a heat transfer coefficient h_f. We neglect the viscous dissipation to estimate accurately the effect of convective boundary condition because viscous dissipation would disturb the thermal boundary conditions. The velocity of the outer flow far away from the surface is $U_e(\bar{x}, \bar{y}) = a\bar{x} + b\bar{y}$. The flow, energy and concentration equations are (see Beard and Walters [93])

$$\frac{\partial \bar{u}}{\partial \bar{x}} + \frac{\partial \bar{v}}{\partial \bar{y}} = 0, \tag{5.1}$$

$$\bar{u}\frac{\partial \bar{u}}{\partial \bar{x}} + \bar{v}\frac{\partial \bar{u}}{\partial \bar{y}} = -\frac{1}{\rho}\frac{\partial \bar{p}}{\partial \bar{x}} + v\left(\frac{\partial^2 \bar{u}}{\partial \bar{x}^2} + \frac{\partial^2 \bar{u}}{\partial \bar{y}^2}\right) + \frac{k_o}{\rho}\left\{\frac{\partial}{\partial \bar{x}}\left[2\bar{u}\frac{\partial^2 \bar{u}}{\partial \bar{x}^2} + 2\bar{v}\frac{\partial^2 \bar{u}}{\partial \bar{x}\partial \bar{y}} + 4\left(\frac{\partial \bar{u}}{\partial \bar{x}}\right)^2 + \right.\right.$$

$$\left.\left. 2\frac{\partial \bar{v}}{\partial \bar{x}}\left(\frac{\partial \bar{v}}{\partial \bar{x}} + \frac{\partial \bar{u}}{\partial \bar{y}}\right)\right] + \frac{\partial}{\partial \bar{y}}\left[\left(\bar{u}\frac{\partial}{\partial \bar{x}} + \bar{v}\frac{\partial}{\partial \bar{y}}\right)\left(\frac{\partial \bar{v}}{\partial \bar{x}} + \frac{\partial \bar{u}}{\partial \bar{y}}\right) + 2\frac{\partial \bar{u}}{\partial \bar{x}}\frac{\partial \bar{u}}{\partial \bar{y}} + 2\frac{\partial \bar{v}}{\partial \bar{x}}\frac{\partial \bar{v}}{\partial \bar{y}}\right]\right\},$$

(5.2)

$$\bar{u}\frac{\partial \bar{v}}{\partial \bar{x}} + \bar{v}\frac{\partial \bar{v}}{\partial \bar{y}} = -\frac{1}{\rho}\frac{\partial \bar{p}}{\partial \bar{y}} + v\left(\frac{\partial^2 \bar{v}}{\partial \bar{x}^2} + \frac{\partial^2 \bar{v}}{\partial \bar{y}^2}\right) + \frac{k_o}{\rho}\left\{\frac{\partial}{\partial \bar{x}}\left[2\frac{\partial \bar{u}}{\partial \bar{x}}\frac{\partial \bar{u}}{\partial \bar{y}} + 2\frac{\partial \bar{v}}{\partial \bar{x}}\frac{\partial \bar{v}}{\partial \bar{y}} + \left(\bar{u}\frac{\partial}{\partial \bar{x}} + \bar{v}\frac{\partial}{\partial \bar{y}}\right)\times\right.\right.$$

$$\left.\left. \left(\frac{\partial \bar{v}}{\partial \bar{x}} + \frac{\partial \bar{u}}{\partial \bar{y}}\right)\right] + \frac{\partial}{\partial \bar{y}}\left[2\frac{\partial \bar{u}}{\partial \bar{y}}\left(\frac{\partial \bar{v}}{\partial \bar{x}} + \frac{\partial \bar{u}}{\partial \bar{y}}\right) + 4\left(\frac{\partial \bar{v}}{\partial \bar{y}}\right)^2 + 2\bar{v}\frac{\partial^2 \bar{v}}{\partial \bar{y}^2} + 2\bar{u}\frac{\partial^2 \bar{v}}{\partial \bar{x}\partial \bar{y}}\right]\right\},$$

(5.3)

$$\bar{u}\frac{\partial \bar{T}}{\partial \bar{x}} + \bar{v}\frac{\partial \bar{T}}{\partial \bar{y}} = \frac{k}{\rho c_p}\left(\frac{\partial^2 \bar{T}}{\partial \bar{x}^2} + \frac{\partial^2 \bar{T}}{\partial \bar{y}^2}\right) - \frac{1}{\rho c_p}\frac{\partial q_r}{\partial \bar{y}} + \tau^*\left\{D_B\left(\frac{\partial \bar{C}}{\partial \bar{x}}\frac{\partial \bar{T}}{\partial \bar{x}} + \frac{\partial \bar{C}}{\partial \bar{y}}\frac{\partial \bar{T}}{\partial \bar{y}}\right) + \right.$$

$$\left. \frac{D_T}{T_\infty}\left[\left(\frac{\partial \bar{T}}{\partial \bar{x}}\right)^2 + \left(\frac{\partial \bar{T}}{\partial \bar{y}}\right)^2\right]\right\}$$

(5.4)

$$\bar{u}\frac{\partial \bar{C}}{\partial \bar{x}} + \bar{v}\frac{\partial \bar{C}}{\partial \bar{y}} = D_B\left(\frac{\partial^2 \bar{C}}{\partial \bar{x}^2} + \frac{\partial^2 \bar{C}}{\partial \bar{y}^2}\right) + \frac{D_T}{T_\infty}\left(\frac{\partial^2 \bar{T}}{\partial \bar{x}^2} + \frac{\partial^2 \bar{T}}{\partial \bar{y}^2}\right).$$

(5.5)

where $\bar{C}(\bar{x}, \bar{y})$ is the concentration, k_0 is elasticity of fluid, D_T and D_B are the Brownian motion coefficient and thermophoretic diffusion coefficient respectively. $\tau^*(= (\rho c)_p/(\rho c)_f)$ is the ratio of effective heat capacity of nanoparticles materials to heat capacity of the fluid. The boundary conditions of the problem are given by

$$\bar{y} = 0 \quad : \quad \bar{u} = c\bar{x}, \ \bar{v} = 0, \ -k\frac{\partial \bar{T}}{\partial \bar{y}} = h_f\left(T_f - \bar{T}\right), \ \bar{C} = C_w,$$

(5.6)

$$\bar{y} \to \infty \quad : \quad \bar{u} = a\bar{x} + b\bar{y}, \ \bar{T} = T_\infty, \ \bar{C} = C_\infty.$$

in which a, b and c are positive constants having the dimensions of inverse time and h_f is the heat transfer coefficient. The radiative heat flux can be modeled by using Rosseland's approximation as follows

$$q_r = -\frac{4\sigma_{SB}}{3(\alpha_r + \sigma_s)}\frac{\partial \bar{T}^4}{\partial \bar{y}},$$

(5.7)

where σ_{SB} is the Stefan-Boltzmann constant, α_r is the Rosseland mean absorption coefficient and σ_s is the scattering coefficient. Assuming that the temperature difference within the flow is sufficiently small so that $\bar{T}^4$ may be expressed as linear function $\bar{T}$ such that

$$\bar{T}^4 = 4T_\infty^3\bar{T} - 3T_\infty^4$$

(5.8)

80

thus Eq. (5.7) takes the following form

$$q_r = -\frac{16\sigma_{SB}T_\infty^3}{3(\alpha_r + \sigma_s)}\frac{\partial \bar{T}}{\partial \bar{y}}.$$ (5.9)

Upon using non-dimensional variables and stream function ψ of the form

$$x = \bar{x}\sqrt{\frac{c}{v}},\ y = \bar{y}\sqrt{\frac{c}{v}},\ u = \frac{1}{\sqrt{vc}}\bar{u},\ v = \frac{1}{\sqrt{vc}}\bar{v},\ p = \frac{1}{\rho vc}\bar{p},$$

$$T = \frac{\bar{T} - T_\infty}{T_f - T_\infty},\ C = \frac{\bar{C} - C_\infty}{C_w - C_\infty},\ u = \frac{\partial \psi}{\partial y},\ v = -\frac{\partial \psi}{\partial x}$$ (5.10)

and eliminating pressure from Eqs. (5.2), (5.3), Eqs. (5.2), (5.6) take the following form in

terms of ψ

$$\frac{\partial \left(\psi, \nabla^2 \psi\right)}{\partial (x,y)} + We\frac{\partial \left(\psi, \nabla^4 \psi\right)}{\partial (x,y)} + \nabla^4 \psi = 0,$$ (5.11)

$$\frac{\partial \psi}{\partial y}\frac{\partial T}{\partial x} - \frac{\partial \psi}{\partial x}\frac{\partial T}{\partial y} = \frac{1}{Pr}\left(\frac{\partial^2 T}{\partial x^2} + \frac{\partial^2 T}{\partial y^2} + \frac{16\sigma_{SB}T_\infty^3}{3k(\alpha_r + \sigma_s)}\frac{\partial^2 T}{\partial y^2}\right) + N_b\left(\frac{\partial C}{\partial x}\frac{\partial T}{\partial x} + \frac{\partial C}{\partial y}\frac{\partial T}{\partial y}\right)$$

$$+ N_t\left(\left(\frac{\partial T}{\partial x}\right)^2 + \left(\frac{\partial T}{\partial y}\right)^2\right).$$ (5.12)

$$Sc\left(\frac{\partial \psi}{\partial y}\frac{\partial C}{\partial x} - \frac{\partial \psi}{\partial x}\frac{\partial C}{\partial y}\right) = \left(\frac{\partial^2 C}{\partial x^2} + \frac{\partial^2 C}{\partial y^2}\right) + \frac{N_t}{N_b}\left(\frac{\partial^2 T}{\partial x^2} + \frac{\partial^2 T}{\partial y^2}\right),$$ (5.13)

$$y = 0\quad :\quad \frac{\partial \psi}{\partial y} = x,\ \psi = 0,\ \frac{\partial T}{\partial y} = -Bi(1 - T),\ C = 1,$$

$$y \to \infty :\quad \psi = \frac{a}{c}xy + \frac{\gamma}{2}y^2,\ T_\infty = 0,\ C = 0,$$ (5.14)

where $We = k_0c/\rho v$ be the Weissenberg number $Pr = \mu c_p/k$ be the Prandtl number, $Sc = v/D_B$ be the Schmidt number, $N_t = D_T\tau^*(T_f - T_\infty)/T_\infty v$ be the thermophoresis parameter, $N_b = D_B\tau^*(C_w - C_\infty)/v$ be the Brownian motion parameter, $Bi = -\left(h_f/k\right)\sqrt{v/c}$ be the Biot number and $\gamma = b/c$ represents shear in the free stream. Suppose the solution of Eqs. (5.11) and (5.14) is of the form

$$\psi = xf(y) + g(y),\quad T = \theta(y),\quad C = \phi(y),$$ (5.15)

where the functions $f(y)$ and $g(y)$ are normal and oblique components of the flow. Using Eq. (5.15) in Eqs. (5.11 − 5.14), and comparing the coefficient of like powers of x, we get

$$f^{iv} + ff''' - f'f'' + We\left(ff^v - f'f^{iv}\right) = 0, \tag{5.16}$$

$$g^{iv} + fg''' - g'f'' + We\left(fg^v - g'f^{iv}\right) = 0, \tag{5.17}$$

$$\left(1 + 4Rd/3\right)\theta'' + Pr\left[f\theta' + N_b\phi'\theta' + N_t\left(\theta'\right)^2\right] = 0, \tag{5.18}$$

$$\phi'' + Sc\,f\phi' + \left(N_t/N_b\right)\theta'' = 0, \tag{5.19}$$

$$y = 0: f(y) = 0,\ f'(y) = 1,\ g(y) = g'(y) = 0,\ \theta'(y) = -Bi\left(1 - \theta(y)\right), \phi(y) = 1,$$
$$y \to \infty: f'(y) = a/c,\ g'(y) = \gamma y,\ \theta(y) = 0,\ \phi(y) = 0, \tag{5.20}$$

where $Rd = 4\sigma_{SB}T_\infty^3/k(\alpha_r + \sigma_s)$ is the radiation parameter and prime denotes the differentiation with respect to y. Integrating Eqs. (5.16) and (5.17) employing the boundary conditions at infinity, we get

$$f''' + ff'' - (f')^2 + We\left(ff^{iv} - 2f'f''' + (f'')^2\right) + \frac{a^2}{c^2} = 0, \tag{5.21}$$

$$g''' + fg'' - g'f' + We\left(fg^{iv} - f'g''' + g''f'' - f'''g'\right) - A\gamma = 0, \tag{5.22}$$

where $A = A(a/c,\ We)$ is a constant which measures the boundary layer displacement. Constant A at free stream behave as $(a/c)y$ which also corresponds to the behavior of $f(y)$ at the free stream. For simplicity, introducing a new variable, $g'(y) = \gamma h(y)$, then Eq. (5.22) with boundary conditions is written as

$$h'' + fh' - f'h + We\left(fh''' - f'h'' + h'f'' - f'''h\right) = A, \tag{5.23}$$

$$h(0) = 0\quad h'(\infty) = 1. \tag{5.24}$$

Thus the system of boundary value problem becomes

$$f''' + ff'' - (f')^2 + We\left(ff^{iv} - 2f'f''' + (f'')^2\right) + \frac{a^2}{c^2} = 0, \tag{5.25}$$

$$h'' + fh' - f'h + We\left(fh''' - f'h'' + h'f'' - f'''h\right) = A, \tag{5.26}$$

$$(1 + 4Rd/3)\,\theta'' + \Pr\left[f\theta' + N_b\phi'\theta' + N_t\left(\theta'\right)^2\right] = 0, \tag{5.27}$$

$$\phi'' + Sc\,f\phi' + \left(N_t/N_b\right)\theta'' = 0, \tag{5.28}$$

with boundary conditions

$$y = 0 : f(y) = 0,\ f'(y) = 1,\ h(y) = 0,\ \theta'(y) = -Bi\,(1 - \theta(y)),\ \phi(y) = 1,$$
$$\tag{5.29}$$
$$y \to \infty : f'(y) = a/c,\ h'(y) = 1,\ \theta(y) = 0,\ \phi(y) = 0.$$

To solve the fourth order ordinary differential equations (5.25) and (5.26), augmented boundary conditions [94, 95] $f''(y) = 0$ and $h''(y) = 0$ as $y \to \infty$ are utilized.

$$u = \frac{\partial \psi}{\partial y} = xf'(y) + g'(y),\ v = -\frac{\partial \psi}{\partial x} = -f(y). \tag{5.30}$$

The quantities of physical interest are the skin friction coefficients C_f, the local Nusselt number Nu_x and the local Sherwood number Sh_x are

$$C_f = \frac{\tau_w}{\rho u_w^2};\quad Nu_x = \frac{\bar{x}(q_w + q_r)}{k(T_f - T_\infty)};\quad Sh_x = \frac{\bar{x}q_m}{D_B(C_w - C_\infty)}, \tag{5.31}$$

where τ_w is shear stress at the wall, q_r is the radiative heat flux, q_w and q_m represents local heat flux, and local mass diffusion flux at the wall are

$$\tau_w = \mu\left(\bar{u}_{\bar{y}} + \bar{v}_{\bar{x}}\right) - 2k_0\left(\begin{array}{c} -\bar{u}_{\bar{y}}\bar{v}_{\bar{y}} - \bar{u}_{\bar{x}}\bar{v}_{\bar{x}} - \frac{1}{2}\bar{v}_{\bar{y}}\left(\bar{u}_{\bar{y}} + \bar{v}_{\bar{x}}\right) - \frac{1}{2}\bar{u}_{\bar{x}}\left(\bar{u}_{\bar{y}} + \bar{v}_{\bar{x}}\right) + \\ \frac{1}{2}\bar{v}\left(\bar{u}_{\bar{y}\bar{y}} + \bar{v}_{\bar{x}\bar{y}}\right) + \frac{1}{2}\bar{u}\left(\bar{u}_{\bar{x}\bar{y}} + \bar{v}_{\bar{x}\bar{x}}\right) \end{array} \right)\Bigg|_{\bar{y}=0}, \tag{5.32}$$

$$q_w = -k\left(\frac{\partial \bar{T}}{\partial \bar{y}}\right)\Bigg|_{\bar{y}=0},\quad q_m = -D_B\left(\frac{\partial \bar{C}}{\partial \bar{y}}\right)\Bigg|_{\bar{y}=0}, q_r = -\frac{4\sigma_{SB}}{3(\alpha_r + \sigma_s)}\frac{\partial \bar{T}^4}{\partial \bar{y}}.$$

In terms of dimensionless variables the skin friction coefficients C_f, the local Nusselt number Nu_x and the local Sherwood number Sh_x takes the following form

$$Re_x C_f = x(1 - 3We)\,f''(0) + (1 - 2We)\gamma h'(0),$$
$$\tag{5.33}$$
$$Re_x^{-1/2} Nu_x = -\left(1 + \frac{4}{3}Rd\right)\theta'(0),\quad Re_x^{-1/2} Sh_x = -\phi'(0).$$

83

where $Re_x = u_w x / \nu$.

5.2   Chebyshev Spectral Newton Iterative Scheme

Exact solutions of the nonlinear differential equations (5.25— 5.28) subject to the boundary conditions (5.29) are difficult to obtaine. Some authors have used analytical and semi-analytical techniques to solve these equations [70,96]. In the present study, we implemented a numerical technique namely Chebyshev Spectral Newton Iterative Scheme (CSNIS). The detailed information regarding to this scheme is provided in chapter 4, however discretization of the equations (5.25— 5.29) is given in this section. In this scheme, we first convert the system of nonlinear differential equation into a linear form by using Newton iterative scheme. For $(i+1)th$ iterates, we write

$$f_{i+1} = f_i + \delta f_i, \quad \theta_{i+1} = \theta_i + \delta \theta_i, \quad \phi_{i+1} = \phi_i + \delta \phi_i, \tag{5.34}$$

for all dependent variables, where δf_i, $\delta \theta_i$ and $\delta \phi_i$, represents a very small change in f_i, θ_i and ϕ_i respectively. The equations (5.25— 5.28) in linearized form are

$$a_{0,i} \delta f_i^{iv} + a_{1,i} \delta f_i''' + a_{2,i} \delta f_i'' + a_{3,i} \delta f_i' + a_{4,i} \delta f_i = R_{1,i},$$

$$b_{0,i} \delta f_i''' + b_{1,i} \delta f_i'' + b_{2,i} \delta f_i' + b_{3,i} \delta f + b_{4,i} \delta h_i''' + b_{5,i} \delta h_i'' + b_{6,i} \delta h_i' + b_{7,i} \delta h_i = R_{2,i},$$

$$c_{0,i} \delta f + c_{1,i} \delta \theta_i'' + c_{2,i} \delta \theta_i' + c_{3,i} \delta \phi_i' = R_{3,i},$$

$$d_{0,i} \delta f + d_{1,i} \delta \theta_i'' + d_{2,i} \delta \phi_i'' + d_{3,i} \delta \phi_i' = R_{4,i}, \tag{5.35}$$

together with the boundary conditions

$$\delta f_i(0) = -f_i(0), \; \delta f_i'(0) = a/c - f_i'(0), \; \delta f_i'(\infty) = 1 - f_i'(\infty), \; \delta f_i''(\infty) = -f_i''(\infty),$$

$$\delta h_i(0) = -h_i(0), \; \delta h_i'(\infty) = 1 - h_i'(\infty), \; \delta h_i''(\infty) = -h_i''(\infty), \tag{5.36}$$

$$\delta \theta_i'(0) - Bi \delta \theta_i(0) = -\theta_i'(0) - Bi(1 - \theta_i(0)), \; \delta \theta_i(\infty) = -\theta_i(\infty),$$

84

The coefficients $a_{j,i}$, $b_{j,i}$, $c_{j,i}$, $d_{j,i}$ and $R_{j,i}(j = 0, 1, 2, 3...)$ are

$$a_{0,i} = We f_i, \quad a_{1,i} = 1 - 2We f_i', \quad a_{2,i} = f_i - 2We f_i'',$$

$$a_{3,i} = -2f_i' - 2We f_i''', \quad a_{4,i} = f_i'' + We f_i^{iv}, b_{0,i} = -We h_i, \quad b_{1,i} = We h_i',$$

$$b_{2,i} = -h_i - We h_i'', b_{3,i} = h_i' + We h_i''', \quad b_{4,i} = We f_i, \quad b_{5,i} = 1 - We f_i',$$

$$b_{6,i} = f_i + We f_i'', b_{7,i} = -f_i' - We f_i''', \quad c_{0,i} - \text{Pr}\, \theta_i', c_{1,i} = (1 + 4Rd/3),$$

$$c_{3,i} = \text{Pr}\left(N_b \theta_i'\right), c_{2,i} = \text{Pr}\left(f_i + N_b \phi_i' + 2N_i \theta_i'\right), \quad d_{0,i} = Sc\, \phi_i',$$

(5.37)

$$d_{1,i} \quad \left(N_i/N_b\right), d_{2,i} = 1, d_{3,i} - Sc f_i$$

$$R_{1,i} = -We\left(f_i f_i^{iv} - 2f_i' f_i''' + \left(f_i''\right)^2\right) - f_i''' - f_i f_i'' + \left(f_i'\right)^2 - a^2/c^2,$$

$$R_{2,i} = -We\left(f_i h_i''' - f_i' h_i'' + f_i'' h_i' - f_i''' h_i\right) - h_i'' - f_i h_i' + f_i' h_i + A,$$

$$R_{3,i} = -(1 + 4Rd/3)\, \theta_i'' - \text{Pr}\left(f_i \theta_i' + N_b \phi_i' \theta_i' + N_i \left(\theta_i'\right)^2\right),$$

$$R_{4,i} = -\phi_i'' - Sc f_i \phi_i' - \left(N_i/N_b\right) \theta_i''.$$

The system of linear Eqs. (5.35) subject to boundary conditions (5.36) is solved using the Chebyshev spectral collocation method [88–90]. After applying collocation method to Eqs. (5.35, 5.36), the following matrix is obtained

$$\begin{bmatrix} A_{11} & A_{12} & A_{13} & A_{14} \\ A_{21} & A_{22} & A_{23} & A_{24} \\ A_{31} & A_{32} & A_{33} & A_{34} \\ A_{41} & A_{42} & A_{43} & A_{44} \end{bmatrix} \begin{bmatrix} \delta f_i \\ \delta h_i \\ \delta \theta_i \\ \delta \phi_i \end{bmatrix} = \begin{bmatrix} R_{1,i} \\ R_{2,i} \\ R_{3,i} \\ R_{4,i} \end{bmatrix},$$

(5.38)

where

$$A_{11} = a_{0,i}D^4 + a_{1,i}D^3 + a_{2,i}D^2 + a_{3,i}D + a_{4,i}I, A_{12} = 0, A_{13} = 0, A_{14} - 0,$$

$$A_{21} = b_{0,i}D^3 + b_{1,i}D^2 + b_{2,i}D + b_{3,i}I, A_{22} = b_{4,i}D^3 + b_{5,i}D^2 + b_{6,i}D + b_{7,i}I,$$

(5.39)

$$A_{23} = 0, A_{24} = 0, A_{31} = c_{0,i}I, A_{32} = 0, A_{33} = c_{1,i}D^2 + c_{2,i}D, A_{34} = c_{3,i}D,$$

$$A_{41} = d_{0,i}I, A_{42} = 0, A_{43} = d_{1,i}D^2, A_{44} = d_{2,i}D^2 + d_{3,i}D,$$

I is identity matrix, $a_{j,i}$, $b_{j,i}$, $c_{j,i}$, $d_{j,i}$ and $R_{j,i}(j = 0, 1, 2, 3...)$ are given in (5.37).

5.3 Results and discussion

The non-linear differential equations (5.25) – (5.28) subject to the boundary conditions (5.29) are solved numerically for different values of dimensionless parameters namely Weissenberg number (We), velocities ratio parameter a/c, radiation (Rd), thermophoresis (N_t), Brownian motion (N_b), Prandtl number (Pr), Schmidt number (Sc) and Biot number (Bi). The values of $f''(0)$, $-\theta'(0)$ and $-\phi'(0)$ are shown in the limiting case through Tables 5.1 and 5.2. It is found that the present results are in excellent agreement with previous investigations available in the literature. Moreover, Numerical values of A, $Re_x^{-1/2}Sh_x$ and $Re_x^{-1/2}Sh_x$ for various values of different parameters are shown in Tables 5.3 and 5.4. The results in terms of velocity profile, temperature profile, concentration profile, $f''(0)$, $-\theta'(0)$ and $-\phi'(0)$ for sundry parameters are shown through graphs. In most cases, the values of the parameters are taken as $Pr = 6.8, Sc = 1.5, Bi = 0.5, We = 0.1, N_t = N_b = 0.3, a/c = 0.3, 1.2$ and $Rd = 1$ or otherwise mentioned. The variation of $f''(0)$, $-\theta'(0)$ and $-\phi'(0)$ against We for $a/c = 0.8, 1.0, 1.1$, and 1.2 is shown in Figs. 5.2 – 5.4 respectively. From these Figs., it is observed that the similarity equations (5.25) – (5.28) subject to the boundary conditions (5.29) have dual solutions for some range of the parameter We. There exist unique solution for a particular range of the parameter We and there exist a region where the solution does not exist. The solid lines show the stable solutions and dashed lines show the unstable solutions. For $a/c > 1$, the range of solution enhances due to increase in a/c and for $a/c < 1$ the range of unstable solution become larger than the stable solution. There exist a unique solution at critical value $We = We_c$, dual solution exist between the range $0 \leq We < We_c$ and no solution exists for $We < 0$ and $We > We_c$. The critical values are $We_{c1} = 0.3149$, $We_{c2} = 0.3642$, $We_{c3} = 0.528$ and $We_{c4} = 0.33$ for different values of a/c as shown in figures. It is observed that unstable solutions have higher values of $f''(0)$, $-\theta'(0)$ and $-\phi'(0)$ than that of the stable solutions for

86

given values of *We*. It is further noted that in stable solutions (first solution) heat and mass transfer rate increase with increase in the values of a/c, where as a reverse behavior has been observed for unstable solution (second solution). The stability analysis of multiple solutions has been discussed by many researcher see [97–99]. They found that first solution is applicable physically while the second solution is not. In Figure 5.5 the velocity profile is plotted against y for the different values of *We*, *a/c* and γ. Here $\gamma = 0$ and $\gamma = 0.2$ correspond to the cases for orthogonal and non-orthogonal stagnation point flow respectively. It is noted that the velocity of the fluid increases with increase in the values of *We* when $a/c > 1$. An opposite behavior is observed for the case when $a/c < 1$. It is also seen that with increase in the values of γ the velocity of the fluid increases. In Figs. 5.6 and 5.7, local Nusselt $(Re_x^{-1/2} Nu_x)$ and local Sherwood $(Re_x^{-1/2} Sh_x)$ numbers are plotted against thermophoresis parameter N_t for different values of R_d and a/c. It is clear from Fig. 5.6 that with an increase in the values of N_t, a very slight decrease in local Nusselt number is observed for both the cases of $a/c (a/c > 1, a/c < 1)$. Consequently, the temperature and thermal boundary layer thickness increase with an increase in thermophoresis parameter N_t near the wall. Fig. 5.7 elucidates that the local Sherwood number decreases with increase of N_t, as a consequence the concentration and the concentration boundary layer increases with increase of N_t. From Figs. 5.6 and 5.7, an increase in the local Nusselt and local Sherwood numbers is observed due to enhancement of radiation. In Figs. 5.8 and 5.9, the values of the local Nusselt $(Re_x^{-1/2} Nu_x)$ and the local Sherwood $(Re_x^{-1/2} Sh_x)$ numbers are plotted against Brownian motion parameter (N_b) for different values of R_d and a/c. It is seen that with increase in Brownian motion the local Nusselt number decreases but the local Sherwood number increases. This increase in the local Sherwood number is very rapid in the range $0 < N_b < 0.2$. This phenomenon increases the temperature and the thermal boundary layer thickness but decreases the concentration. In Figs. 5.10 and 5.11, the variation

of the local Nusselt ($\mathrm{Re}_x^{-1/2}\mathrm{Nu}_x$) and local Sherwood ($\mathrm{Re}_x^{-1/2}\mathrm{Sh}_x$) numbers is plotted against

Biot number Bi (depending on the heat transfer coefficient) for different values of R_d and a/c.

It is seen that the local Nusselt number increases and the local Sherwood number decreases

for initial values of Bi and for the larger values of Bi both quantities become constant. Due

to the larger values of Biot number Bi ($Bi \rightarrow \infty$), the surface become heated and heat transfer

rate increases. In fact, the larger values of Biot number imply the strong surface convection

result in high surface temperature; therefore, increase in Biot number enhances the tempera-

ture and the thermal boundary layer thickness. This behavior can be predicted from Fig. 5.12.

In Fig. 5.13, concentration is plotted against y for different values of Bi when $R_d = 2$ and

$a/c = 0.3$. Concentration increases with increase in the values of Bi because concentration

distribution depends upon the temperature field hence the lager Biot number helps to increase

the concentration of nanoparticles in the fluid. In Figs. 5.14 and 5.15 the temperature and the

concentration profiles are plotted for the different values of We and a/c when $R_d = 1$, $Bi = 0.1$.

For $a/c < 1$, it is observed that the temperature and the concentration are increasing functions

of We but for $a/c > 1$ an opposite behavior is noted. In Figs. 5.16 and 5.17, the temperature

and the concentration profiles are plotted for the different values of R_d when $Bi = 0.1$ and

$a/c = 0.3$. With an increase in the values of radiation parameter, temperature of the fluid

increases where as the concentration decreases near the wall but away from the surface, it

increases with increase in the values of radiation parameter.

Table 5.1: Comparison of $-\theta'(0)$ for the various values of a/c and Pr in the absence Thermophoresis effects and Brownian motion of nanoparticles when $We = 0, Rd = 0$ and $Bi \to \infty$

	$Pr = 1$		$Pr = 10$		$Pr = 20$	
a/c	Present work	[81]	Present work	[81]	Present work	[81]
0.1	0.60215	0.60281	2.31693	2.31684	3.36196	3.36172
0.3	0.64728	0.64732	2.34841	2.34841	3.39149	3.39148
0.8	0.75710	0.75709	2.46778	2.46778	3.51054	3.51054
1.0	0.79788	0.79788	2.52313	2.52313	3.56825	3.56825
2.0	0.97873	0.97872	2.81389	2.81389	3.88689	3.88689
3.0	1.13209	1.13209	3.09751	3.09751	4.21307	4.21307
4.0	1.26733	1.26733	3.36440	3.36441	4.52808	4.52810

Table 5.2: Comparison of $-\theta'(0)$ and $-\phi'(0)$ for the various values of N_t and N_b when $We = 0, a/c = 0, Rd = 0, Pr = 10, Sc - 10$, and $Bi = 0.1$. The results in small brackets are reported by Makinde and Aziz [61].

	$N_b = 0.1$		$N_b = 0.3$		$N_b = 0.5$	
N_t	$-\theta'(0)$	$-\phi'(0)$	$-\theta'(0)$	$-\phi'(0)$	$-\theta'(0)$	$-\phi'(0)$
0.1	(0.0929)	(2.2774)	(0.0769)	(2.3299)	(0.0383)	(2.3560)
	0.09291	2.27741	0.07688	2.32994	0.03833	2.35603
0.3	(0.0925)	(2.2228)	(0.0729)	(2.3900)	(0.0269)	(2.4576)
	0.09255	2.22281	0.07292	2.38996	0.02690	2.45762
0.5	(0.0921)	(2.1783)	(0.0700)	(2.4792)	(0.0180)	(2.5435)
	0.09212	2.17834	0.06697	2.47923	0.01800	2.54352

Table 5.3: Numerical values of A for various values of We and a/c.

a/c	We			
	0	0.05	0.1	0.2
0.0	1.0000	0.9747	0.9487	0.8944
0.1	0.7917	0.7663	0.7402	0.6854
0.2	0.6407	0.6161	0.5906	0.5369
0.3	0.5195	0.4962	0.4720	0.4205
0.4	0.4173	0.3959	0.3735	0.3254
0.5	0.3286	0.3096	0.2896	0.2459
0.6	0.2499	0.2338	0.2167	0.1789
0.7	0.1791	0.1664	0.1527	0.1220
0.8	0.1145	0.1056	0.0960	0.0738
0.9	0.0551	0.0505	0.0454	0.0334
1.0	0.0000	0.0000	0.0000	0.0000

Table 5.4: Numerical values of $Re_x^{-1/2}Nu_x$ and $Re_x^{-1/2}Sh_x$ for wider range of Pr.

We	a/c	Rd	N_t	N_b	Bi	Sc	Pr	$Re_x^{-1/2}Nu_x$	$Re_x^{-1/2}Sh_x$
0.10	0.10	1	0.1	0.1	0.1	1	0.7	0.1681	0.5539
							1	0.1786	0.5489
							10	0.2164	0.5225
							50	0.2250	0.5107
							100	0.2268	0.5075
0.20	0.50	2	0.3	0.3	1	5	0.7	0.7404	1.5984
							1	0.8434	1.5899
							10	1.3282	1.5803
							50	0.4836	1.9263
							100	0.0776	2.0450
0.3	1.0	5	0.5	0.5	∞	10	0.7	1.7315	2.5104
							1	2.0139	2.5078
							10	3.0888	2.6083
							50	0.5032	2.9136
							100	-0.0194	2.9281

90
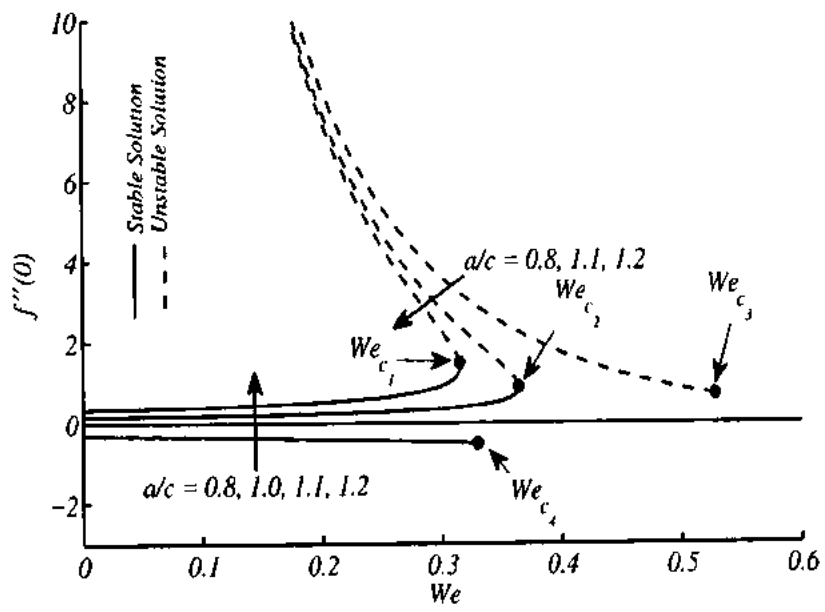
Figure 5.2: Variation of $f''(0)$ against We for the different values of a/c.
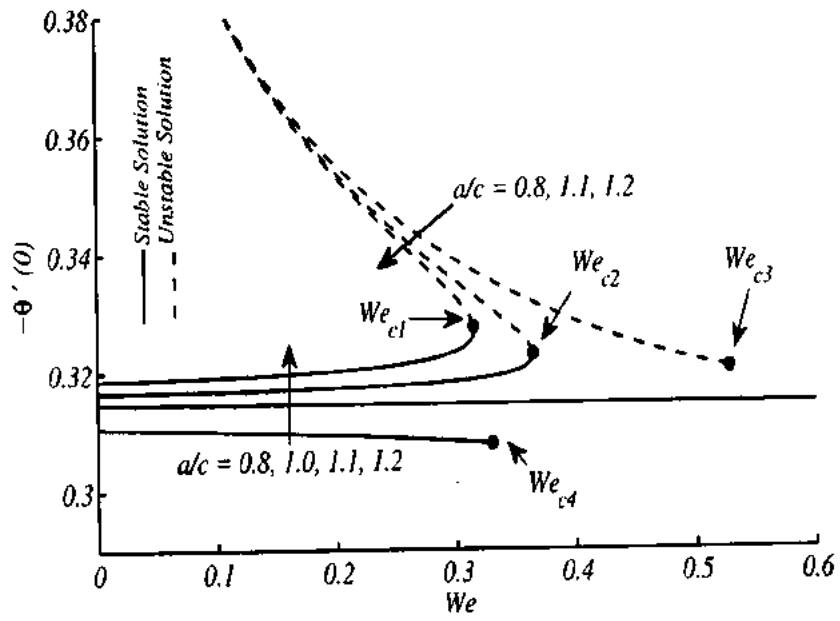
Figure 5.3: Variation of $-\theta'(0)$ against We for the different values of a/c

91
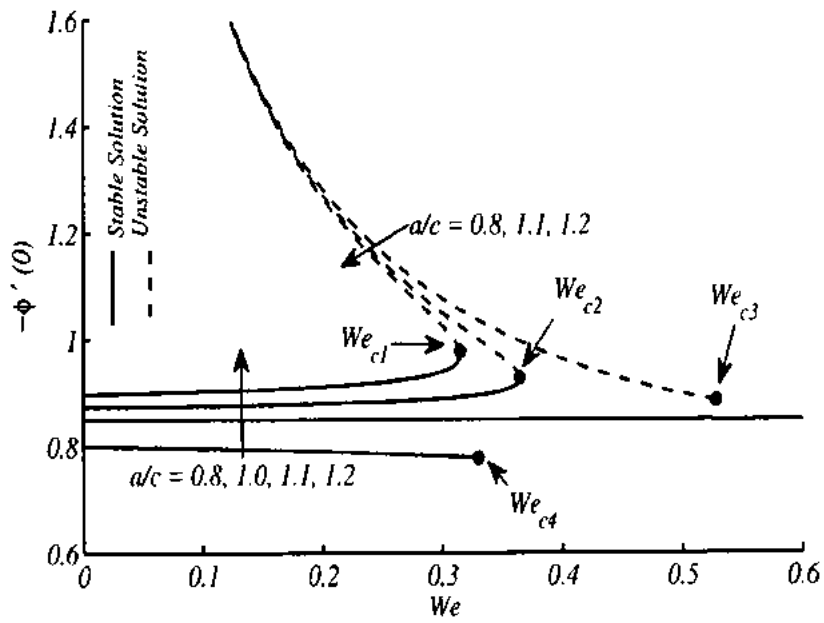
Figure 5.4: Variation of $-\phi'(0)$ against We for the different values of a/c.
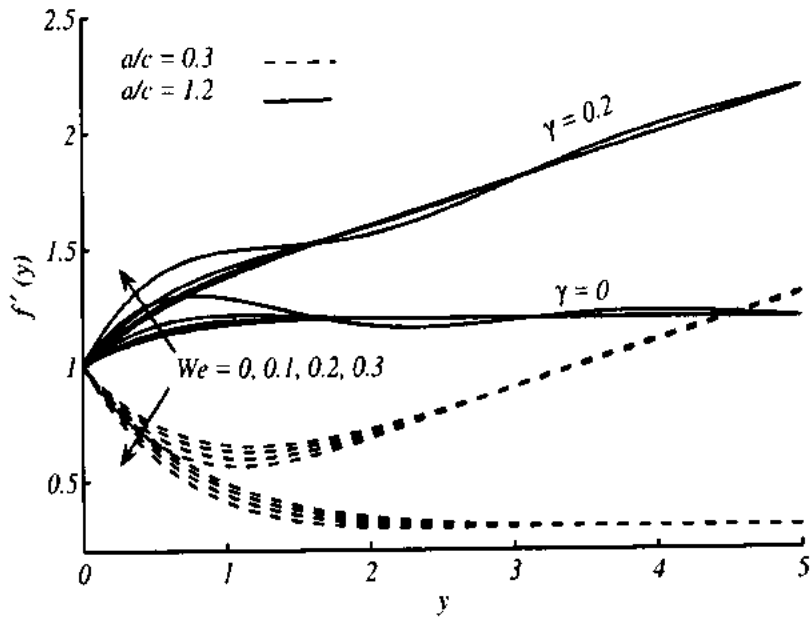
Figure 5.5: Velocity profile against y for the different values of We, a/c and γ.

92
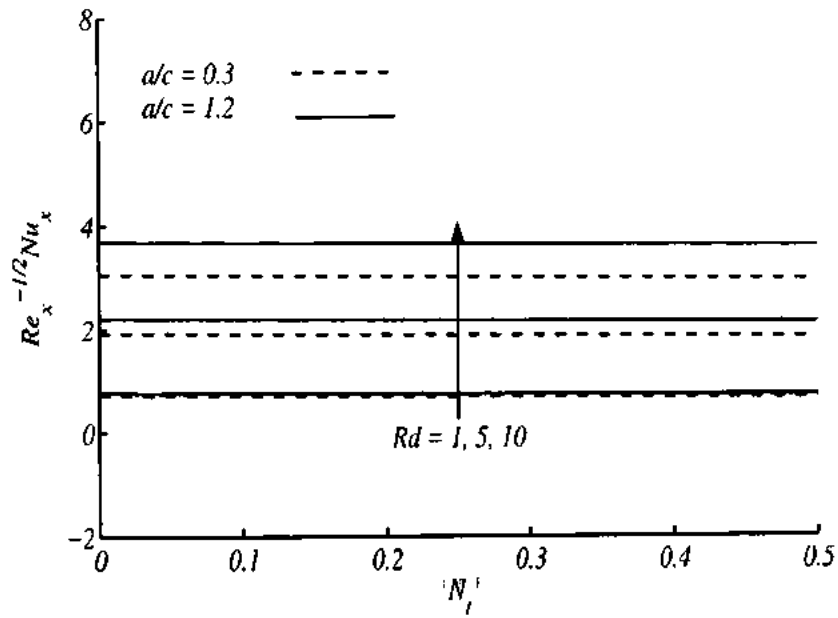
Figure 5.6: Variation of Nusselt number against N_t for the different values of Rd and a/c.
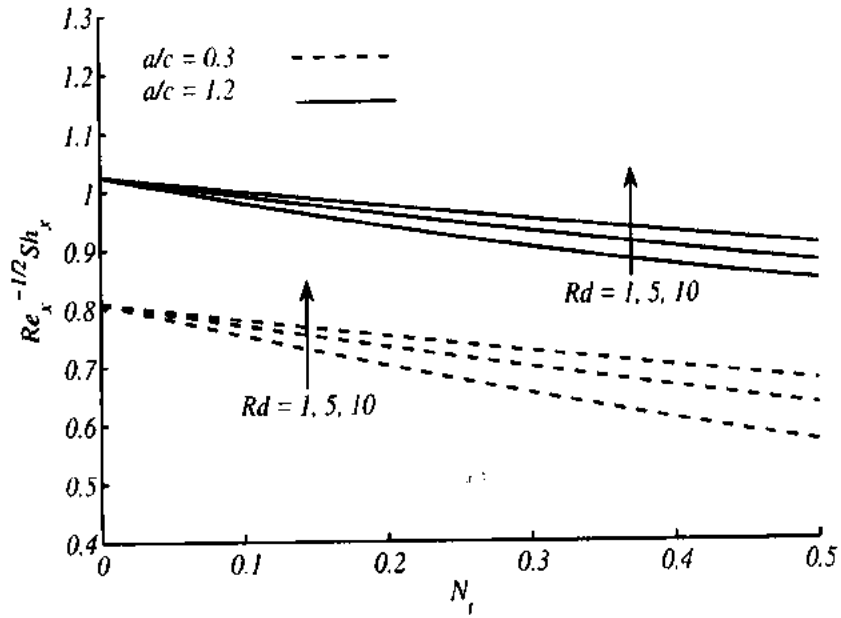
Figure 5.7: Variation of Sherwood number against N_t for the different values of Rd and a/c.
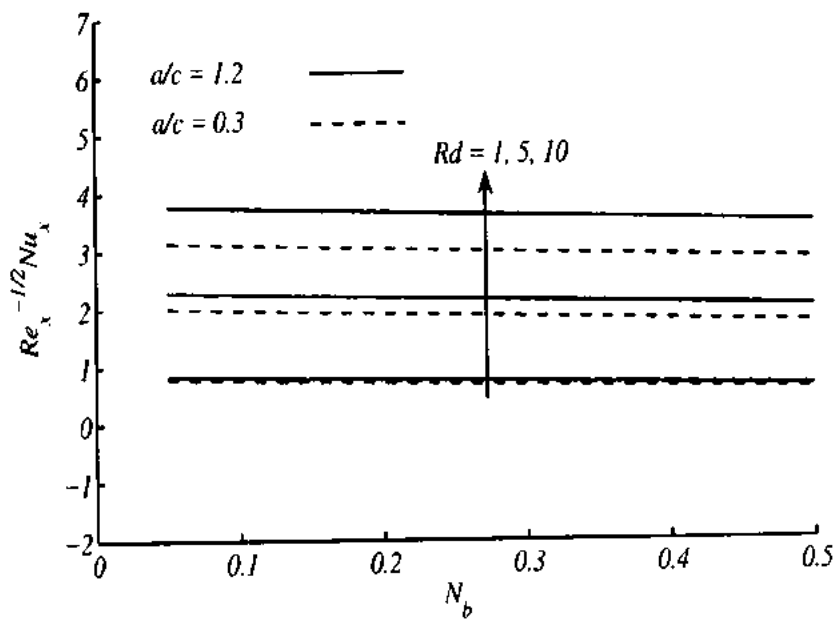
Figure 5.8: Variation of Nusselt number against N_b for the different values of Rd and a/c.
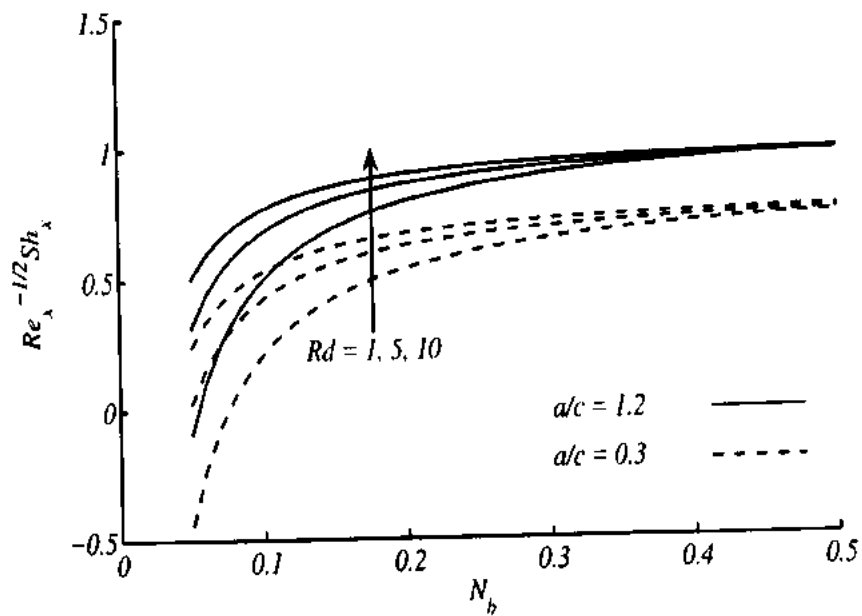
Figure 5.9: Variation of Sherwood number against N_b for the different values of Rd and a/c.
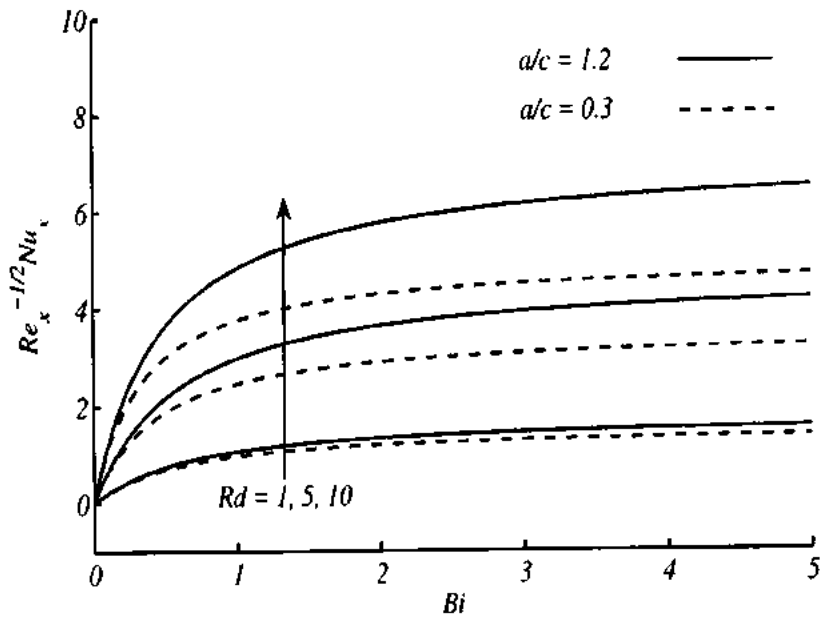
Figure 5.10: Variation of Nusselt number against Bi for the different values of Rd and a/c.
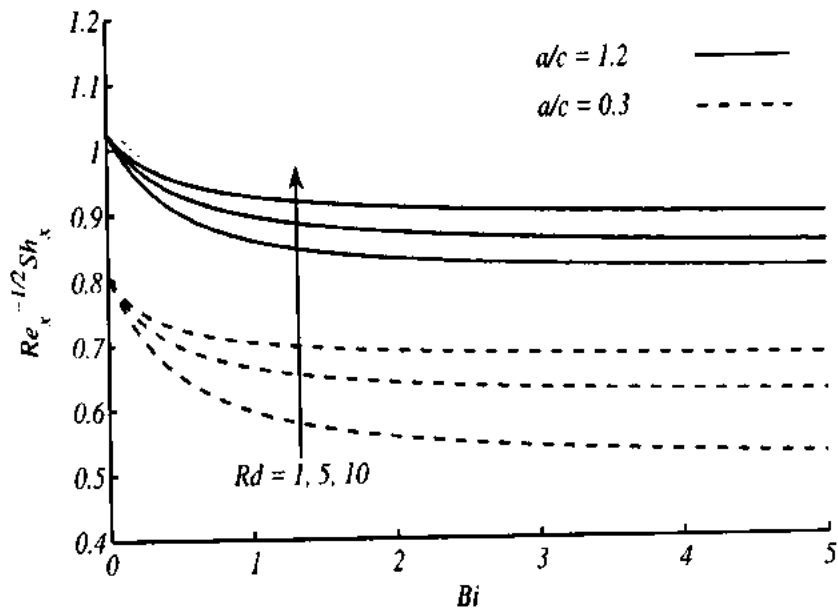
Figure 5.11: Variation of Sherwood number against Bi for the different values of Rd and a/c.

95
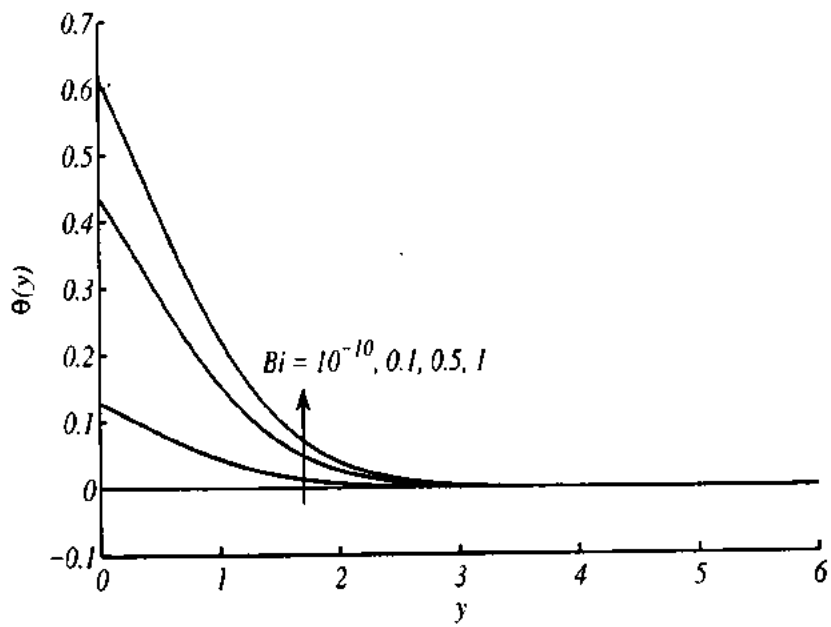
Figure 5.12: Temperature profile against y for the different values of Bi
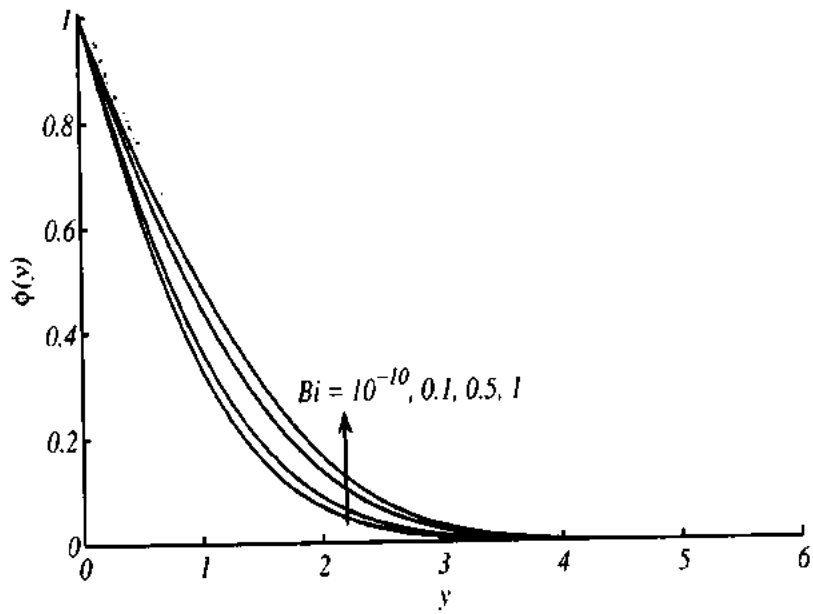
Figure 5.13: Concentration profile against y for the different values of Bi.

96
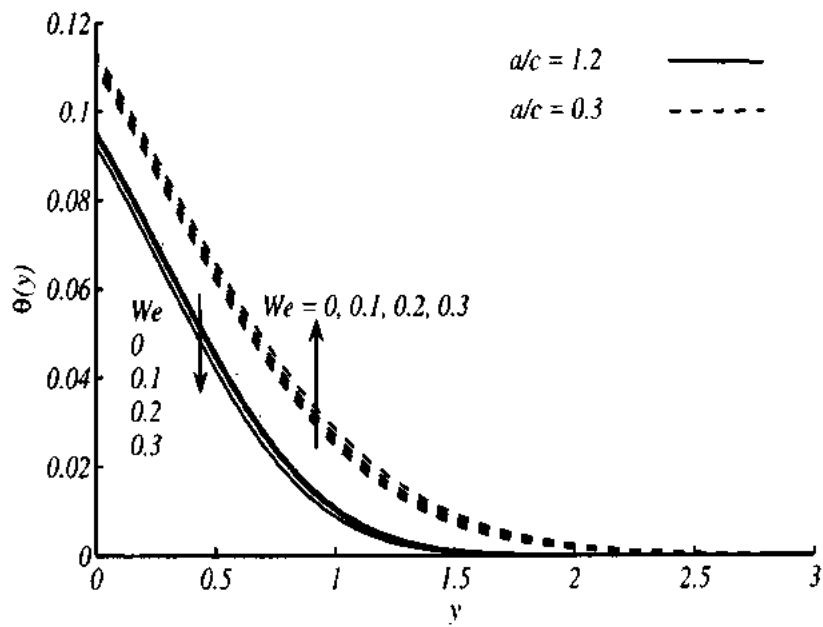
Figure 5.14: Temperature profile against y for the different values of We and a/c.
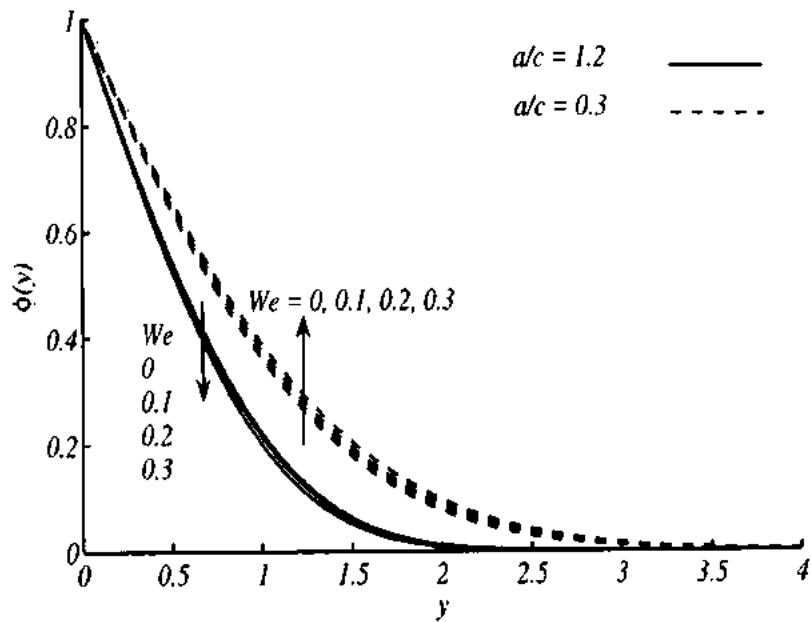
Figure 5.15: Concentration profile against y for the different values of We and a/c.

97
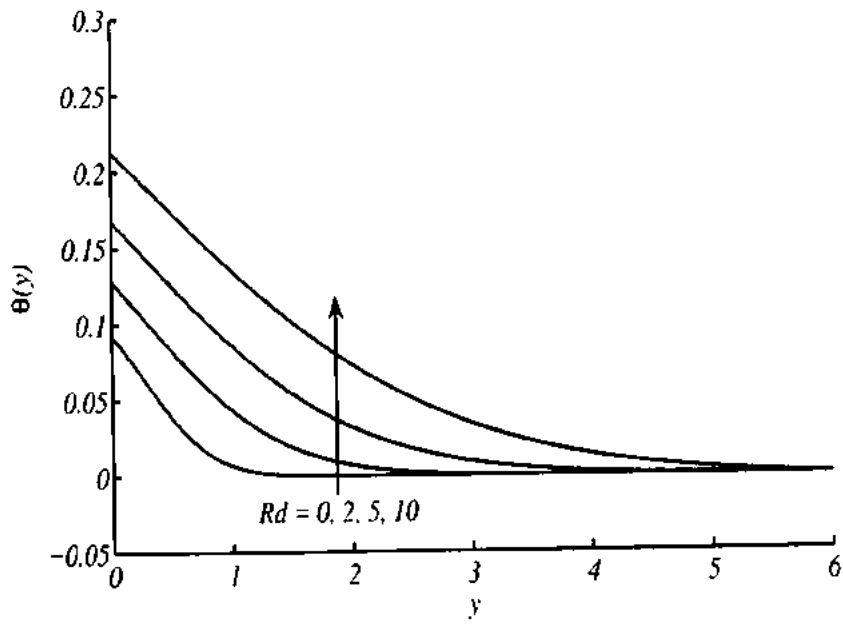
Figure 5.16: Temperature profile against y for the different values of Rd.
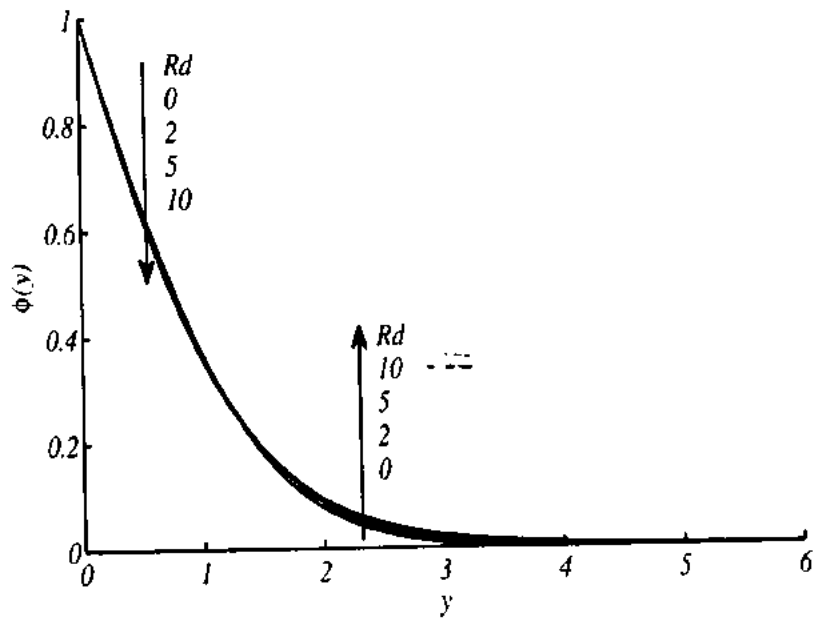
Figure 5.17: Concentration profile against y for the different values of Rd.

98

5.4 Conclusions

The combined effects of radiation and convective boundary condition in the region of oblique stagnation point flow of elastico-viscous fluid saturated with nanoparticles are considered. The governing partial differential equations are reduced into dimensionless ordinary differential equations and then solved numerically by using Chebyshev Spectral Newton Iterative Scheme (CSNIS). The present numerical results are in excellent agreement with the previously available results. It is observed that the equations (5.25)-(5.28) subject to the boundary conditions (5.29) have unique solution, dual solution and no solution in different regions of the parameter We. For $a/c > 1$, the range of existence of solution increases due to increase in a/c and for $a/c < 1$, the range of unstable solution become larger than that of the stable solution. It is also concluded that

- The velocity of the fluid intensifies due to increase in We when $a/c > 1$ but an opposite behavior is observed for $a/c < 1$.

- The velocity of the fluid is found an increasing function of γ.

- Temperature and the thermal boundary layer thickness enhance due to increase in the values thermophoresis parameter (Nt) and radiation parameter (Rd).

- Concentration and the concentration boundary layer thickness increases with increase of Nt and Biot number Bi.

- Brownian motion enhanced the thermal boundary layer thickness.

- Brownian motion decreases the concentration boundary layer thickness.

- The larger values of Biot number imply the enhancement in heat transfer and the thermal boundary layer thickness.

Chapter 6

Study of Mixed convection Walter's B fluid flow towards stagnation point over a vertical surface

In this chapter, the influence of radiation in a mixed convection flow of Walter's B fluid in the neighborhood of nonaligned stagnation point over a vertical oscillating flat plate has been investigated. The plate is assumed heated with sinusoidal surface temperature. It is further assumed that the plate is stretched linearly along the vertical x-axis. The governing partial differential equations are transformed into dimensionless form. These dimensionless partial differential equations are solved numerically using Chebyshev Spectral Newton Iterative Scheme (CSNIS). The obtained results are in excellent agreement with the previous studies. The effects of involving parameters on the fluid flow and heat transfer phenomenon are shown through tables and graphs. It is observed that, in assisting flow region, high value of effective Prandtl number reduces the velocity whereas in opposed flow region, it invigorate the velocity. It is also noted that with increase of effective Prandtl number, the skin friction coefficient decreases

100

and heat transfer rate augmented.
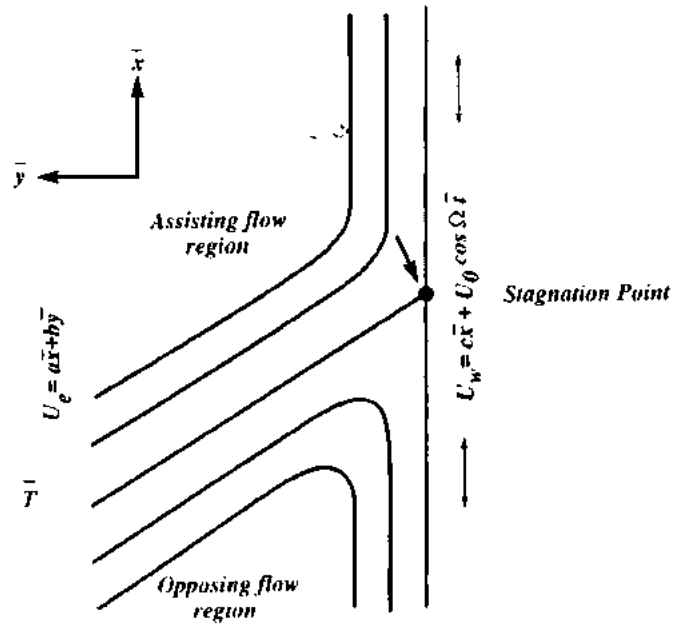
Figure 6.1: Geometry of the problem

6.1 Problem formulation

Lets us consider the flow of Walter's B fluid towards a vertical flat plate obliquely as shown

in Fig. 6.1. The plate is oscillating about its means position at $\bar{y} = 0$ with velocity $U_0 \cos \Omega \bar{t}$

and subjected to a linear stretching with velocity $c\bar{x}$ in vertical direction. It is also assumed

that plate is heated with sinusoidal surface temperature, which oscillates about the mean value

T_w, which is higher than the ambient temperature T_∞ of the surroundings. The flow and energy

equations are (see refs. [93, 100])

$$\frac{\partial \bar{u}}{\partial \bar{x}} + \frac{\partial \bar{v}}{\partial \bar{y}} = 0, \tag{6.1}$$

$$\frac{\partial \bar{u}}{\partial \bar{t}} + \bar{u}\frac{\partial \bar{u}}{\partial \bar{x}} + \bar{v}\frac{\partial \bar{u}}{\partial \bar{y}} = -\frac{1}{\rho}\frac{\partial \bar{p}}{\partial \bar{x}} + \nu \nabla^2 \bar{u} - \frac{k_0}{\rho}\left[\frac{\partial}{\partial \bar{t}}(\nabla^2 \bar{u}) + \left(\bar{u}\frac{\partial}{\partial \bar{x}} + \bar{v}\frac{\partial}{\partial \bar{y}}\right)\nabla^2 \bar{u} - \frac{\partial \bar{u}}{\partial \bar{x}}\nabla^2 \bar{u} - \right.$$

$$\left. \frac{\partial \bar{u}}{\partial \bar{y}}\nabla^2 \bar{v} - 2\left\{\frac{\partial \bar{u}}{\partial \bar{x}}\frac{\partial^2 \bar{u}}{\partial \bar{x}^2} + \frac{\partial \bar{v}}{\partial \bar{y}}\frac{\partial^2 \bar{u}}{\partial \bar{y}^2} + \left(\frac{\partial \bar{u}}{\partial \bar{y}} + \frac{\partial \bar{v}}{\partial \bar{x}}\right)\frac{\partial^2 \bar{u}}{\partial \bar{x}\partial \bar{y}}\right\}\right] \pm g\beta_T(\bar{T} - T_\infty),$$

(6.2)

$$\frac{\partial \bar{v}}{\partial \bar{t}} + \bar{u}\frac{\partial \bar{v}}{\partial \bar{x}} + \bar{v}\frac{\partial \bar{v}}{\partial \bar{y}} = -\frac{1}{\rho}\frac{\partial \bar{p}}{\partial \bar{y}} + \nu \nabla^2 \bar{v} - \frac{k_0}{\rho}\left[\frac{\partial}{\partial \bar{t}}(\nabla^2 \bar{v}) + \left(\bar{u}\frac{\partial}{\partial \bar{x}} + \bar{v}\frac{\partial}{\partial \bar{y}}\right)\nabla^2 \bar{v} - \frac{\partial \bar{v}}{\partial \bar{x}}\nabla^2 \bar{u} - \right.$$

$$\left. \frac{\partial \bar{v}}{\partial \bar{y}}\nabla^2 \bar{v} - 2\left\{\frac{\partial \bar{u}}{\partial \bar{x}}\frac{\partial^2 \bar{v}}{\partial \bar{x}^2} + \frac{\partial \bar{v}}{\partial \bar{y}}\frac{\partial^2 \bar{v}}{\partial \bar{y}^2} + \left(\frac{\partial \bar{u}}{\partial \bar{y}} + \frac{\partial \bar{v}}{\partial \bar{x}}\right)\frac{\partial^2 \bar{v}}{\partial \bar{x}\partial \bar{y}}\right\}\right],$$

(6.3)

$$\frac{\partial \bar{T}}{\partial \bar{t}} + \bar{u}\frac{\partial \bar{T}}{\partial \bar{x}} + \bar{v}\frac{\partial \bar{T}}{\partial \bar{y}} = \frac{k}{\rho c_p}\left(\frac{\partial^2 \bar{T}}{\partial \bar{x}^2} + \frac{\partial^2 \bar{T}}{\partial \bar{y}^2}\right) - \frac{1}{\rho c_p}\frac{\partial q_r}{\partial \bar{y}}.$$

(6.4)

In above equations g is the gravitational acceleration, β_T is the coefficient of thermal expansion and $q_r = -\left(16\sigma_{SB}\bar{T}^3/3a_R\right)\partial \bar{T}/\partial \bar{y}$ is the radiative heat flux. The term α_r is the Rosseland mean absorption coefficient and σ_{SB} is the Stefan-Boltzmann constant. In Eq. (6.2) the $+$ and $-$ signs represent the buoyancy assisting and buoyancy opposing flow case respectively. The relevant boundary conditions can be defined as

$$\bar{y} = 0 \quad : \quad \bar{u} = U_w = c\bar{x} + U_0\cos\Omega\bar{t}, \quad \bar{v} = 0, \quad \bar{T} = T_\infty + \Delta T(\sqrt{\frac{c}{\nu}}\bar{x} + \varepsilon_1 \sin\Omega\bar{t}),$$

(6.5)

$$\bar{y} \to \infty \quad : \quad \bar{u} = U_e = a\bar{x} + b\bar{y}, \quad \bar{T} = T_\infty,$$

where $\Delta T = T_w - T_\infty$ is the difference of mean surface temperature to the ambient temperature, $U_w = c\bar{x} + U_0\cos\Omega\bar{t}$ is the velocity of the plate, $U_e = a\bar{x} + b\bar{y}$ is the free stream velocity, ε_1 is the amplitude of the imposed temperature oscillation and Ω is the frequency of the oscillation. Using $q_r = -\left(16\sigma_{SB}\bar{T}^3/3\alpha_r\right)\partial \bar{T}/\partial \bar{y}$ in Eq. (6.4), we get

$$\frac{\partial \bar{T}}{\partial \bar{t}} + \bar{u}\frac{\partial \bar{T}}{\partial \bar{x}} + \bar{v}\frac{\partial \bar{T}}{\partial \bar{y}} = \frac{k}{\rho c_p}\frac{\partial^2 \bar{T}}{\partial \bar{x}^2} + \frac{1}{\rho c_p}\frac{\partial}{\partial \bar{y}}\left\{\left(k + \frac{16\sigma_{SB}\bar{T}^3}{3\alpha_r}\right)\frac{\partial \bar{T}}{\partial \bar{y}}\right\}.$$

(6.6)

To get the simplified form of Eq. (6.6) thermal conductivity k is consider as constant and it assumed that the temperature gradient with in flow is very small. Linearizing the radiative heat flux q_r about the ambient temperature T_∞, the Eq. (6.6) reduces to the following form

$$\frac{\partial \bar{T}}{\partial \bar{t}} + \bar{u}\frac{\partial \bar{T}}{\partial \bar{x}} + \bar{v}\frac{\partial \bar{T}}{\partial \bar{y}} = \frac{k}{\rho c_p}\frac{\partial^2 \bar{T}}{\partial \bar{x}^2} + \frac{k}{\rho c_p}\left(1 + \frac{16\sigma_{SB}T_\infty^3}{3k\alpha_r}\right)\frac{\partial^2 \bar{T}}{\partial \bar{y}^2}.$$

(6.7)

Introducing the non-dimensional variables

$$x = \bar{x}\sqrt{\frac{c}{v}}, \quad y = \bar{y}\sqrt{\frac{c}{v}}, \quad t = \Omega \bar{t}, \quad u = \frac{1}{\sqrt{vc}}\bar{u}, \quad v = \frac{1}{\sqrt{vc}}\bar{v}, \quad p = \frac{1}{\rho vc}\bar{p}, \quad T = \frac{\bar{T} - T_\infty}{T_w - T_\infty}, \quad (6.8)$$

in Eqs. (6.1)–(6.3), (6.5) and (6.7), we get the following form

$$\frac{\partial u}{\partial x} + \frac{\partial v}{\partial y} = 0, \tag{6.9}$$

$$\frac{\Omega}{c}\frac{\partial u}{\partial t} + u\frac{\partial u}{\partial x} + v\frac{\partial u}{\partial y} = -\frac{\partial p}{\partial x} + v\nabla^2 u - \frac{k_0 c}{\rho v}\left[\frac{\Omega}{c}\frac{\partial}{\partial t}(\nabla^2 u) + \left(u\frac{\partial}{\partial x} + v\frac{\partial}{\partial y}\right)\nabla^2 u - \frac{\partial u}{\partial x}\nabla^2 u - \right.$$

$$\left. \frac{\partial u}{\partial y}\nabla^2 v - 2\left\{\frac{\partial u}{\partial x}\frac{\partial^2 u}{\partial x^2} + \frac{\partial v}{\partial y}\frac{\partial^2 u}{\partial y^2} + \left(\frac{\partial u}{\partial y} + \frac{\partial v}{\partial x}\right)\frac{\partial^2 u}{\partial x \partial y}\right\}\right] \pm \frac{g\beta_T(T_w - T_\infty)}{c\sqrt{cv}}T, \tag{6.10}$$

$$\frac{\Omega}{c}\frac{\partial v}{\partial t} + u\frac{\partial v}{\partial x} + v\frac{\partial v}{\partial y} = -\frac{\partial p}{\partial y} + v\nabla^2 v - \frac{k_0 c}{\rho v}\left[\frac{\partial}{\partial t}(\nabla^2 v) + \left(u\frac{\partial}{\partial x} + v\frac{\partial}{\partial y}\right)\nabla^2 v - \frac{\partial v}{\partial x}\nabla^2 u - \right.$$

$$\left. \frac{\partial v}{\partial y}\nabla^2 v - 2\left\{\frac{\partial u}{\partial x}\frac{\partial^2 v}{\partial x^2} + \frac{\partial v}{\partial y}\frac{\partial^2 v}{\partial y^2} + \left(\frac{\partial u}{\partial y} + \frac{\partial v}{\partial x}\right)\frac{\partial^2 v}{\partial x \partial y}\right\}\right], \tag{6.11}$$

$$\frac{\Omega}{c}\frac{\partial T}{\partial t} + u\frac{\partial T}{\partial x} + v\frac{\partial T}{\partial y} = \frac{k}{\rho v c_p}\frac{\partial^2 T}{\partial x^2} + \frac{k}{\rho v c_p}\left(1 + \frac{16\sigma_{SB}T_\infty^3}{3k\alpha_r}\right)\frac{\partial^2 T}{\partial y^2}, \tag{6.12}$$

$$y = 0 \quad : \quad u = x + \varepsilon\cos t, \quad v = 0, \quad T = x + \varepsilon_1\sin t,$$

$$y \to \infty \quad : \quad u = \frac{a}{c}x + \frac{b}{c}y, \quad T = 0. \tag{6.13}$$

In which $\varepsilon = U_0/\sqrt{vc}$ is the dimensionless constant, which describe the amplitude of the plate oscillation. Introducing the stream function ψ, as proposed by Takemitsu and Matunobu [76], we write the velocity components as

$$u = \frac{\partial \psi}{\partial y}, \quad v = -\frac{\partial \psi}{\partial x}. \tag{6.14}$$

In terms of stream function, Eqs. (6.9) – (6.13) after eliminating the pressure take the following form

$$\beta^*\frac{\partial(\nabla^2\psi)}{\partial t} + We\beta^*\frac{\partial(\nabla^4\psi)}{\partial t} - \frac{\partial(\psi, \nabla^2\psi)}{\partial(x,y)} - We\frac{\partial(\psi, \nabla^4\psi)}{\partial(x,y)} - \nabla^4\psi \mp \lambda\frac{\partial T}{\partial y} = 0, \quad (6.15)$$

$$\beta^*\frac{\partial T}{\partial t} + u\frac{\partial T}{\partial x} + v\frac{\partial T}{\partial y} = \frac{1}{\Pr}\frac{\partial^2 T}{\partial x^2} + \frac{(1 + N_r)}{\Pr}\frac{\partial^2 T}{\partial y^2}, \tag{6.16}$$

$$y = 0 \quad : \quad \frac{\partial \psi}{\partial y} = x + \varepsilon \cos t, \quad \psi = 0, \quad T = x + \varepsilon_1 \sin t,$$

$$\text{(6.17)}$$

$$y \to \infty \quad : \quad \psi = \frac{a}{c} xy + \frac{\gamma}{2} y^2, \quad T = 0,$$

where $\beta^* = \Omega/c$ is dimensionless unsteady parameter, $\lambda = \dfrac{g \beta_T (T_w - T_\infty)}{c \sqrt{cv}}$ is the mixed convection parameter and $N_r = 16 \sigma_{SB} T_\infty^3 / 3k\alpha_r$ is the radiation parameter. Let us suppose that the solution of Eqs. (6.15) and (6.16) subject to boundary conditions (6.17) is of the form

$$\psi = xf(y) + h(y,t), \quad T = x\theta_1(y) + \theta_2(y,t),$$

$$\text{(6.18)}$$

where the functions $f(y)$ and $h(y,t)$ are normal and oblique components of the flow and $\theta_1(y)$, $\theta_2(y,t)$ represents the dimensionless temperature profiles. Using the Eq. (6.18) in Eqs. (6.15 – 6.17), and then after comparing the like powers of x, we get

$$f^{iv} + ff''' - f'f'' + We\left(ff^v - f'f^{iv}\right) \pm \lambda \theta_1' = 0,$$

$$\text{(6.19)}$$

$$\frac{\partial^4 h}{\partial y^4} + f \frac{\partial^3 h}{\partial y^3} - f'' \frac{\partial h}{\partial y} + We\left(f \frac{\partial^5 h}{\partial y^5} - f^{iv} \frac{\partial h}{\partial y}\right) - \beta^* \frac{\partial^3 h}{\partial t \partial y^2} - We\beta^* \frac{\partial^5 h}{\partial t \partial y^4} \pm \lambda \frac{\partial \theta_2}{\partial y} = 0, \quad \text{(6.20)}$$

$$\frac{1}{Pr_{eff}} \theta_1'' + f\theta_1' - f'\theta_1 = 0,$$

$$\text{(6.21)}$$

$$\frac{1}{Pr_{eff}} \theta_2'' + f\theta_2' - g'\theta_1 - \beta^* \frac{\partial \theta_2}{\partial t} = 0,$$

$$\text{(6.22)}$$

$$y = 0 : f(y) = 0, \; f'(y) = 1, \; h(y,t) = 0, \; \frac{\partial h(y,t)}{\partial y} = \varepsilon \cos t, \; \theta_1(y) = 1, \; \theta_2(y,t) = \varepsilon_1 \sin t,$$

$$y \to \infty : \quad f'(y) = a/c, \quad \frac{\partial^2 h(y,t)}{\partial y^2} = \gamma, \quad \theta_1(y) = 0, \quad \theta_2(y,t) = 0.$$

$$\text{(6.23)}$$

Where $Pr_{eff} = Pr / (1 + N_r)$ is effective Prandtl number, which is the combination of Prandtl number and radiation parameter as proposed by Magyari and Pantokratoras [101]. The effect of radiation can be incorporated for the smaller value of Pr_{eff}. In Eqs. (6.19 – 6.23) prime signs denote the differentiation with respect to y. Integrating Eqs. (6.19) and (6.20) with respect to y and the resulting constants of integration are evaluated by employing the boundary

conditions at infinity. Thus the Eqs. (6.19 – 6.23) reduce to

$$f''' + ff'' - (f')^2 + We\left(ff^{iv} - 2f'f''' + (f'')^2\right) + \left(\frac{a}{c}\right)^2 \pm \lambda\theta_1 = 0, \qquad (6.24)$$

$$\frac{\partial^3 h}{\partial y^3} + f\frac{\partial^2 h}{\partial y^2} - f'\frac{\partial h}{\partial y} + We\left(f\frac{\partial^4 h}{\partial y^4} - f'\frac{\partial^3 h}{\partial y^3} + f''\frac{\partial^2 h}{\partial y^2} - f'''\frac{\partial h}{\partial y}\right)$$
$$- \beta^*\frac{\partial^2 h}{\partial t\partial y} - We\beta^*\frac{\partial^4 h}{\partial t\partial y^3} - A\gamma \pm \lambda\theta_2 = 0, \qquad (6.25)$$

$$\frac{1}{Pr_{eff}}\theta_1'' + f\theta_1' - f'\theta_1 = 0, \qquad (6.26)$$

$$\frac{1}{Pr_{eff}}\theta_2'' + f\theta_2' - g'\theta_1 - \beta^*\frac{\partial\theta_2}{\partial t} = 0. \qquad (6.27)$$

$$y = 0 : f(y) = 0, \ f'(y) = 1, \ h(y,t) = 0, \ \frac{\partial h(y,t)}{\partial y} = \varepsilon\cos t, \ \theta_1(y) = 1, \ \theta_2(y,t) = \varepsilon_1\sin t,$$

$$y \to \infty : \quad f'(y) = a/c, \ \frac{\partial^2 h(y,t)}{\partial y^2} = \gamma, \ \theta_1(y) = 0, \ \theta_2(y,t) = 0.$$
$$(6.28)$$

In which A is a constant, which measures the boundary layer displacement. It arises when

$y \to \infty$, $f(v)$ behaves as $f(y) = (a/c)y + A$. The dimensionless components of velocities are

$$u = \frac{\partial\psi}{\partial y} = xf'(y) + \frac{\partial h(y,t)}{\partial y}, \qquad (6.29)$$

$$v = -\frac{\partial\psi}{\partial x} = -f(y). \qquad (6.30)$$

The quantities of physical interest are the skin friction coefficients C_f and the local Nusselt

number Nu_x, can be expressed as

$$C_f = \frac{\tau_w}{\rho u_w^2}, \quad Nu_x = \frac{\bar{x}q_{eff}}{k_{eff}(T_w - T_\infty)}, \qquad (6.31)$$

where τ_w is shear stress at the wall and q_{eff} is the effective conduction-radiation flux at the

wall. These are defined in dimensionless form as

$$\tau_w = \mu c\left(u_y + v_x\right) - 2c^2 k_0 \left(\begin{array}{c} -u_y v_y - u_x v_x - \frac{1}{2}v_y\left(u_y + v_x\right) - \frac{1}{2}u_x\left(u_y + v_x\right) \\ +\frac{1}{2}\left(u_{yt} + v_{xt}\right) + \frac{1}{2}v\left(u_{yy} + v_{xy}\right) + \frac{1}{2}u\left(u_{xy} + v_{xx}\right) \end{array}\right)\Bigg|_{y=0}, \quad (6.32)$$

$$q_{eff} = -k_{eff}\left(T_w - T_\infty\right)\sqrt{\frac{c}{v}}\left(\frac{\partial T}{\partial y}\right)\Bigg|_{y=0}. \qquad (6.33)$$

Upon using Eqs. (6.14) and (6.18), the skin friction coefficients and the local Nusselt number take the following form

$$Re_x C_f = x(1 - 3We - \varepsilon We) f''(0) + (1 - 2We)\frac{\partial^2 h(0,t)}{\partial y^2} - \beta^* We \frac{\partial^3 h(0,t)}{\partial t \partial y^2},$$

$$Re_x^{-1/2} Nu = -\left(x\theta_1'(0) + \frac{\partial \theta_2(0,t)}{\partial y}\right).$$

(6.34)

where $Re_x = c\bar{x}^2/v = x^2$. The dividing stream line $\psi = 0$ and $u = \partial \psi / \partial y = 0$ intersect the plate at the stagnation point. The location of stagnation point x_s can be find at zero skin friction or shear stress from Eq. (6.34) as follows

$$x_s = \frac{-(1 - 2We)\frac{\partial^2 g(0,t)}{\partial y^2} + \beta^* We \frac{\partial^3 g(0,t)}{\partial t \partial y^2}}{(1 - 3We - \varepsilon We) f''(0)}.$$

(6.35)

6.2 Chebyshev Spectral Newton Iterative Scheme

The nonlinear time dependent partial differential equations (6.24)–(6.27) subject to the boundary conditions (6.28) are solved numerically using Chebyshev Spectral Newton Iterative Scheme (CSNIS). Initially for the case of steady solution at $t=0$, the governing Eqs. (6.24–6.27) reduce to the following ordinary differential equations

$$f''' + ff'' - (f')^2 + We\left(ff^{iv} - 2f'f''' + (f'')^2\right) + \left(\frac{a}{c}\right)^2 \pm \lambda \theta_1 = 0,$$

(6.36)

$$h''' + fh'' - f'h' + We\left(fh^{iv} - f'h''' + f''h'' - f'''h'\right) - A\gamma \pm \lambda \theta_2 = 0,$$

(6.37)

$$\frac{1}{Pr_{eff}}\theta_1'' + f\theta_1' - f'\theta_1 = 0,$$

(6.38)

$$\frac{1}{Pr_{eff}}\theta_2'' + f\theta_2' - g'\theta_1 = 0,$$

(6.39)

and boundary conditions are

$$y = 0 \quad : \quad f(y) = 0,\ f'(y) = 1,\ h(y,0) = 0,\ h'(y,0) = \varepsilon,\ \theta_1(y) = 1,\ \theta_2(y,0) = 0,$$

$$y \to \infty \quad : \quad f'(y) - a/c,\ h''(y,0) - \gamma,\ \theta_1(y) = 0\ \theta_2(y,0) = 0.$$

(6.40)

106

To find the solution of Eqs. (6.36–6.40), first we convert the Eq. (6.36) into a linear form by using Newton's linearization process. For $(i+1)th$ iterates, we write

$$f_{i+1} = f_i + \delta f_i,$$
(6.41)

and similarly for all other dependent variables, where δf_i represents a very small change in f_i. Using Eq. (6.41) in (6.36) and dropping the quadratic and higher order terms in δf_i, one obtains

$$c_{0,i}\delta f_i^{iv} + c_{1,i}\delta f_i''' + c_{2,i}\delta f_i'' + c_{3,i}\delta f_i' + c_{4,i}\delta f_i = R_i,$$
(6.42)

subject to boundary conditions

$$\delta f_i(0) = -f_i(0), \quad \delta f_i'(0) = a/c - f_i'(0), \quad \delta f_i'(\infty) = 1 - f_i'(\infty).$$
(6.43)

The coefficients $c_{j,i}$ (j=0, 1, 2, 3, 4) and R_i are

$$c_{0,i} = We f_i, \quad c_{1,i} = 1 - 2We f_i', \quad c_{2,i} = f_i + 2We f_i'', \quad c_{3,i} = -2f_i' - 2We f_i''', \quad c_{4,i} = f_i'' + We f_i^{iv},$$

$$R_i = -We\left(f_i f_i^{iv} - 2f_i'f_i''' + (f_i'')^2\right) - f_i''' - f_i f_i'' + (f_i')^2 - (a/c)^2 \mp \lambda \theta_1.$$
(6.44)

The obtained Eq. (6.42) with boundary conditions (6.43) is now linear and is solved using the Chebyshev spectral collocation method as described in chapter 4. Once the solution of Eqs. (6.36–6.40) has been obtained for steady case ($t = 0$), we proceeded further to next time steps by taking step size $\Delta t = k_1 = \pi/90$. The time derivative in Eqs. (6.24–6.28) is replaced by backward finite difference scheme $\left(\text{e.g. } \frac{\partial}{\partial t}()_n = \frac{1}{k_1}(()_n - ()_{n-1})\right)$. The Eqs. (6.24–6.28) take the following form

$$(f''')_n + (f)_n(f'')_n - (f'^2)_n + We((f)_n(f^{iv})_n - 2(f')_n(f''')_n + (f''^2)_n) + (a/c)^2 \pm \lambda(\theta_1)_n = 0,$$
(6.45)

$$\left(\frac{\partial^3 h}{\partial y^3}\right)_n + (f)_n\left(\frac{\partial^2 h}{\partial y^2}\right)_n - (f')_n\left(\frac{\partial h}{\partial y}\right)_n + We\left((f)_n\left(\frac{\partial^4 h}{\partial y^4}\right)_n - (f')_n\left(\frac{\partial^3 h}{\partial y^3}\right)_n + (f'')_n\left(\frac{\partial^2 h}{\partial y^2}\right)_n\right)$$
$$- (f''')_n\left(\frac{\partial h}{\partial y}\right)_n - \frac{\beta^*}{k_1}\left(\left(\frac{\partial h}{\partial y}\right)_n - \left(\frac{\partial h}{\partial y}\right)_{n-1}\right) - \frac{We\beta^*}{k_1}\left(\left(\frac{\partial^3 h}{\partial y^3}\right)_n - \left(\frac{\partial^3 h}{\partial y^3}\right)_{n-1}\right) - A\gamma \pm \lambda(\theta_2)_n = 0,$$
(6.46)

$$\frac{1}{Pr_{eff}}\left(\theta_1''\right)_n + (f)_n (\theta_1)_n - \left(f'\right)_n (\theta_1)_n = 0, \tag{6.47}$$

$$\left(\frac{\partial^2 \theta_2}{\partial y^2}\right)_n + Pr_{eff}\left((f)_n \left(\frac{\partial \theta_2}{\partial y}\right)_n - \left(g'\right)_n (\theta_1)_n - \frac{\beta^*}{k_1}\left((\theta_2)_n - (\theta_2)_{n-1}\right)\right) = 0, \tag{6.48}$$

$$y = 0: (f)_n = 0, \; \left(f'\right)_n = 1, \; (h)_n = 0, \; \left(\frac{\partial h}{\partial y}\right)_n = \varepsilon \cos(nk), \; (\theta_1)_n = 1, \; (\theta_2)_n = \varepsilon_1 \sin(nk),$$

$$y \to \infty: \left(f'\right)_n = a/c, \; \left(\frac{\partial^2 h}{\partial y^2}\right)_n = \gamma, \; (\theta_1)_n = 0, \; (\theta_2)_n = 0, \; t_n = nk \text{ where } n = 1, 2, 3... \,. \tag{6.49}$$

Now the equations Eq. (6.45-6.49) can be solved for each time step up to required range of t.

For the computation purpose, a numerical code is developed in MATLAB 2010a and used.

6.3 Results and discussion

The solution of non-linear partial differential equations (6.24) - (6.27) subject to the boundary conditions (6.28) is obtained numerically for all dimensionless parameter namely Wiessenberg number We, velocities ratio parameter a/c, obliqueness parameter γ, unsteady parameter β^*, Mixed convection parameter λ, Prandtl number Pr, amplitude of oscillating plate ε and amplitude of imposed temperature oscillation ε_1, against required range of t. The present results in the limiting case are verified through numerical values with the previous studies, which are given in the Table 6.1. It is shown that our results are convergent and highly accurate. The interesting results are also plotted in terms of the velocity profile, temperature profile, the skin friction coefficient and the Nusselt number in Figs. 6.2–6.7. In Figs 6.2–6.7, the values of the parameters are kept fixed at $\varepsilon = 1, \varepsilon_1 = 1, \gamma = 2, \beta^* = 0.2, We = 0.1, Pr_{eff} = 7$. The values of the parameters, which are used for solution of the problem other than mentioned above, are given in the figures. In Fig. 6.2, variation of the velocity is shown for various values of velocities ratio parameter $a/c = 0.1, 0.5, 1, 1.5$. In the figure, the curves are drawn at $t = \pi/4$ for both assisting and opposing flow cases. It is noted from the figure that the velocity of the

fluid increases with increase of *a/c*. Further, the velocity in opposed flow region reduces as compare to the assisted flow region. Which is due to the fact that in opposed flow region, the buoyant force retard the flow having opposite direction, where as in assisted flow region it helps to enhance the fluid velocity having the same direction as of the flow field. It is also observed that for *a/c>1*, the velocity of the fluid along *y* oscillate due to viscoelastic behavior of the fluid. In Fig. 6.3, the temperature is plotted against *y* at $t = \pi/4$ for various values of velocities ratio parameter *a/c = 0.1, 0.5, 1.0, 1.5* for both assisting and opposing flow case. It is found that the temperature is a decreasing function of velocities ratio parameter *a/c* which is due to the reason that stagnation point encounters the highest heat transfer rate and therefore the temperature reduces with increase of free stream velocity within the boundary layer. It is also noted that temperature is higher in opposing region as compare to assisting region. In Fig. 6.4, the velocity profile is plotted at $t = \pi/4$ for the various values of *We= 0, 0.1, 0.2*. In this figure, both cases of boundary layer structure (*a/c>1*) and inverted boundary layer structure (*a/c<1*) are discussed. It is observed that in case of boundary layer structure, the velocity of the fluid increases with increase of viscoelastic parameter *We*. On the other hand, for inverted boundary layer case, the velocity of the fluid decreases with increase of viscoelastic parameter *We*. Similarly in Fig. 6.5, the temperature is plotted at $t = \pi/4$ for various values of *We= 0, 0.1, 0.2* for both cases of *a/c<1* and *a/c>1*. In case of boundary layer structure (*a/c>1*) the temperature of the fluid falls due to increase of viscoelastic parameter *We*, on the other hand for *a/c<1*, temperature enhances with the increase in the value of viscoelastic parameter. In Fig. 6.6 and 6.7, variation in the skin friction coefficient and the Nusselt number is shown against *t* for various values of mixed convection parameter *λ* for assisted and opposed flow regions. It is seen that for assisting flow case skin friction is increasing function of *λ* in upward direction while it is decreasing function of *λ* in downward direction. In opposing flow case an opposite

behavior is seen. Similarly, in assisting flow case, Nusselt number is increasing in downward direction while it is decreasing in upward direction and an opposite behavior is observed in opposing flow case.

Table 6.1: Comparison of $f''(0)$ and $\theta'(0)$ with Mahapatra and Gupta [24] and Nazar et al. [25], while other parameters are $We = \varepsilon = \varepsilon_1 = \gamma = \beta^* = \lambda = 0$ and $Pr = 1.5$.

	$f''(0)$			$\theta'(0)$	
a/c	Present	Ref. [24]	Ref. [25]	Present	Ref. [24]
0.1	−0.96939	−0.9694	−0.9694	−0.77680	−0.777
0.2	−0.91810	−0.9181	−0.9181	−0.79712	−0.797
0.5	−0.66726	−0.6673	−0.6673	−0.86479	−0.863
2.0	2.01750	2.0175	2.0176	−1.17810	−1.171
3.0	4.72928	4.7293	4.7296	−1.35194	−1.341
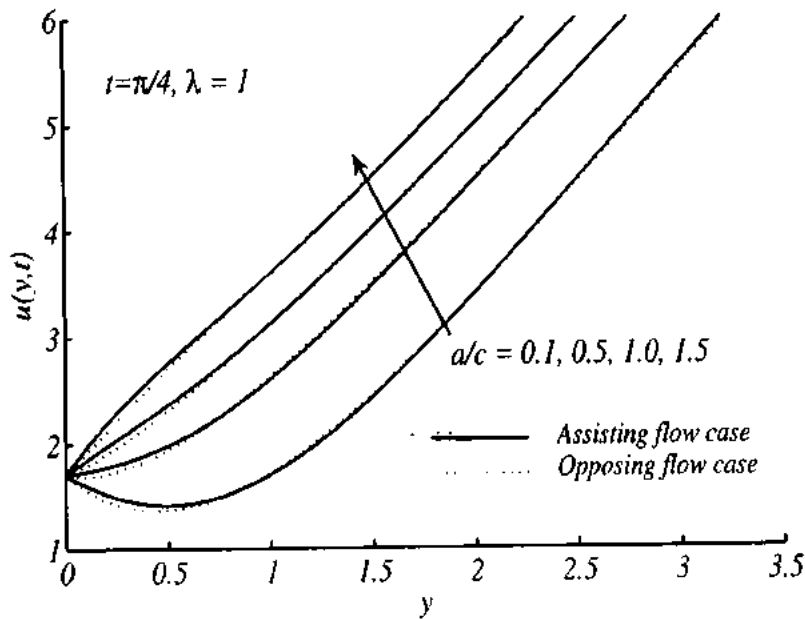
Figure 6.2: Velocity profile $u(y,t)$ against y at $t = \pi/4$ and a/c = 0.1, 0.5, 1.0, 1.5 for both assisting and opposing flow case.

110
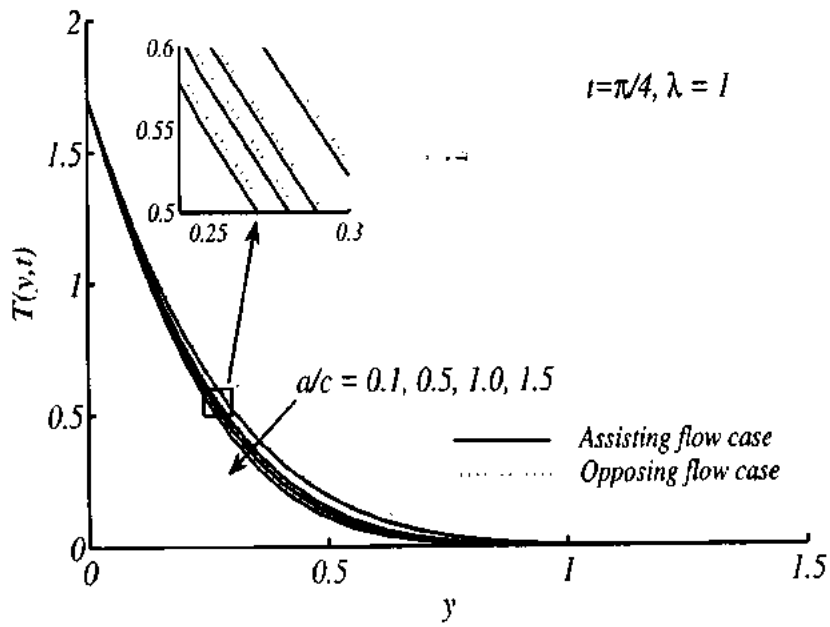
Figure 6.3: Temperature profile $T(y,t)$ against y at $t = \pi/4$ and a/c = 0.1, 0.5, 1.0, 1.5 for both assisting and opposing flow case.
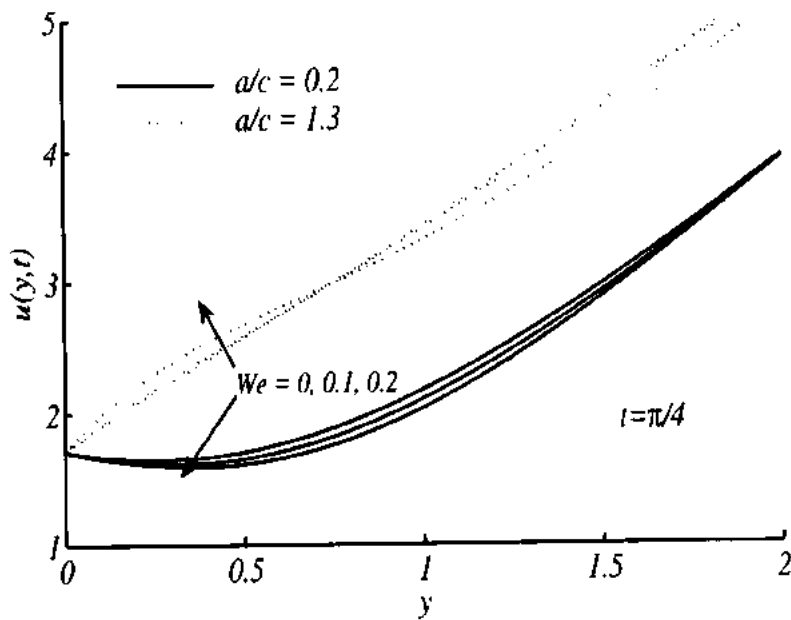
Figure 6.4: Velocity profile $u(y,t)$ against y at $t = \pi/4$ and $We = 0, 0.1, 0.2$ for both $a/c < 1$ and $a/c > 1$.
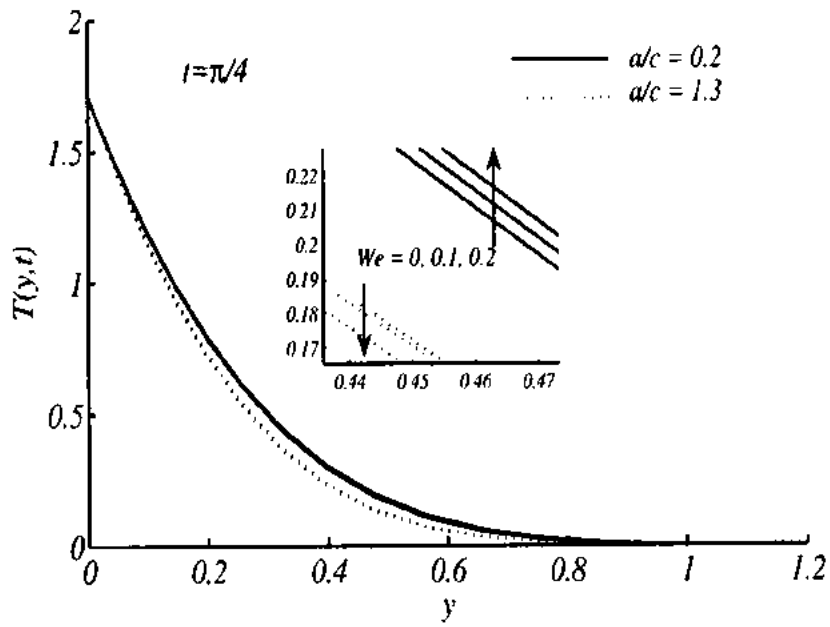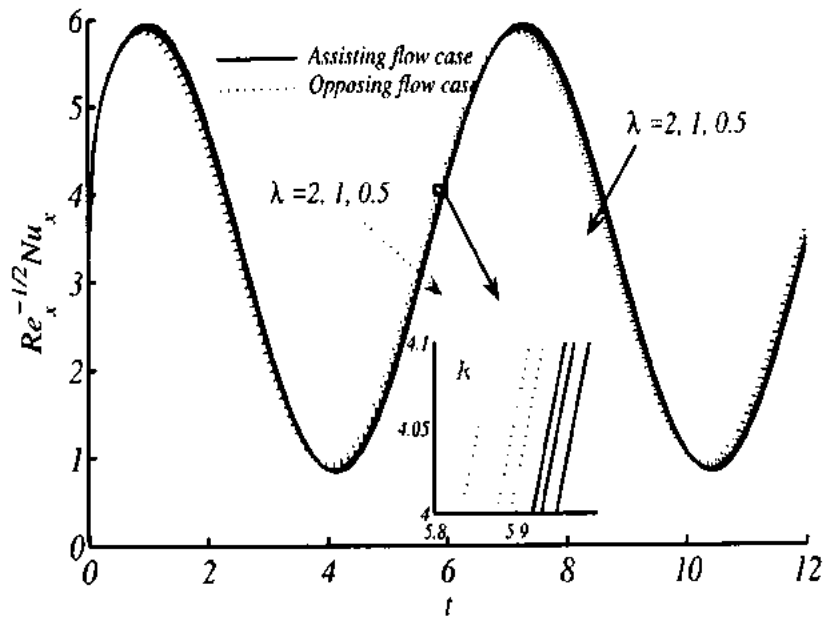
Figure 6.5: Temperature profile $T(y,t)$ against y at $t = \pi/4$ and $We = 0,0.1,0.2$ for both

$a/c < 1$ and $a/c > 1$.
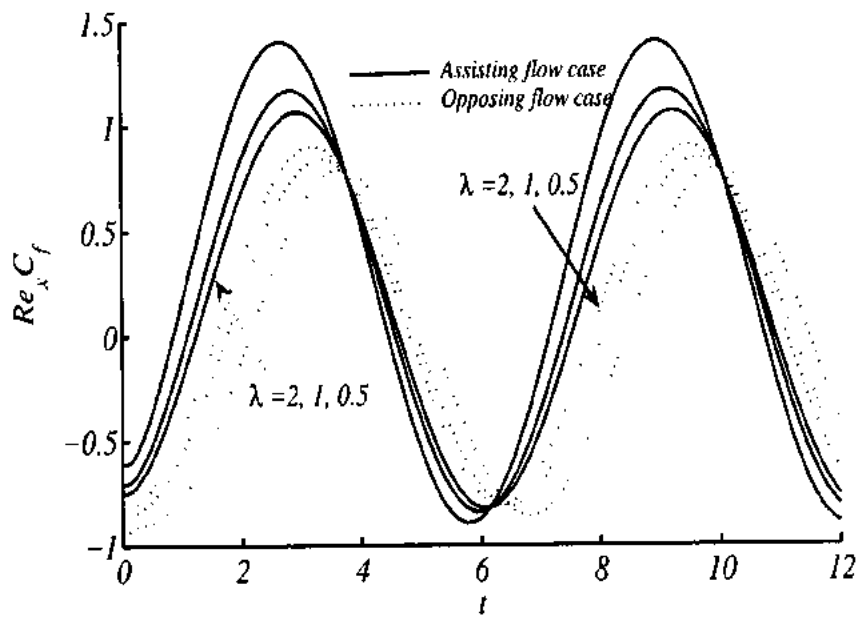
Figure 6.6: Variation in skin friction coefficient Re_xC_f against t for different values of λ for

both assisting and Opposing flow cases

Figure 6.7: Variation in Nusselt number $Re_x^{-1/2}Nu_x$ against t for different values of λ for both assisting and Opposing flow cases

6.4 Conclusions

In this chapter, the influence of thermal radiation and conduction in the region of oblique stagnation point flow is investigated subjected to the sinusoidal surface temperature of the vertical flat plate. The obtained dimensionless partial differential equations are solved numerically by using Chebyshev Spectral Newton Iterative Scheme (CSNIS). To check the validity of our results, the numerical values are verified with the existing studied as a special case. Furthermore, the results for sundry parameters are given graphically and in tabular form. It is observed that the skin friction coefficient, the local Nusselt number, stagnation point and streamlines oscillate periodically due to sinusoidal nature of the plate oscillations and surface temperature in both assisted and opposed flow regions. It is also concluded that

• The velocity is found as an increasing function of a/c, where an opposite behavior is

113

observed for the temperature.

- For large straining velocity ($a/c > 1$), the velocity of the fluid increases while the temperature falls due to increase of viscoelastic parameter We.

- For large stretching velocity ($a/c < 1$), the velocity of fluid decreases while the temperature enhances due to increment of viscoelastic parameter We.

- Velocity increases in assisting flow case as compare to opposing flow case while the temperature has opposite behavior.

Chapter 7

Heat transfer analysis of unsteady oblique stagnation point flow of viscoelastic fluid due to sinusoidal wall temperature over an oscillating-stretching surface

In this chapter, heat transfer analysis of an unsteady oblique stagnation point flow of elastico-viscous fluid over an oscillating-stretching surface which is also heated due to sinusoidal temperature is presented. The governing partial differential equations are transformed into dimensionless form. The solution of obtained partial differential equations is computed numerically using Chebyshev Spectral Newton Iterative Scheme (CSNIS). The computed results are highly accurate and compared with previous studies in limiting sense. The effects of involving parameters on the fluid flow and heat transfer are shown through tables and graphs. It is importantly noted that the amplitude of the local Nusselt number and skin friction coefficient enhances due to increase in the values of unsteady parameter. The heat transfer rate increases with increase

115

in the values of Prandtl number. In non-Newtonian fluid, the heat transfer rate is maximum decreases as compare to that of Newtonian fluid case. The variation of skin friction coefficient and local Nusselt number are discussed for the wide range of time and various pertinent parameters.
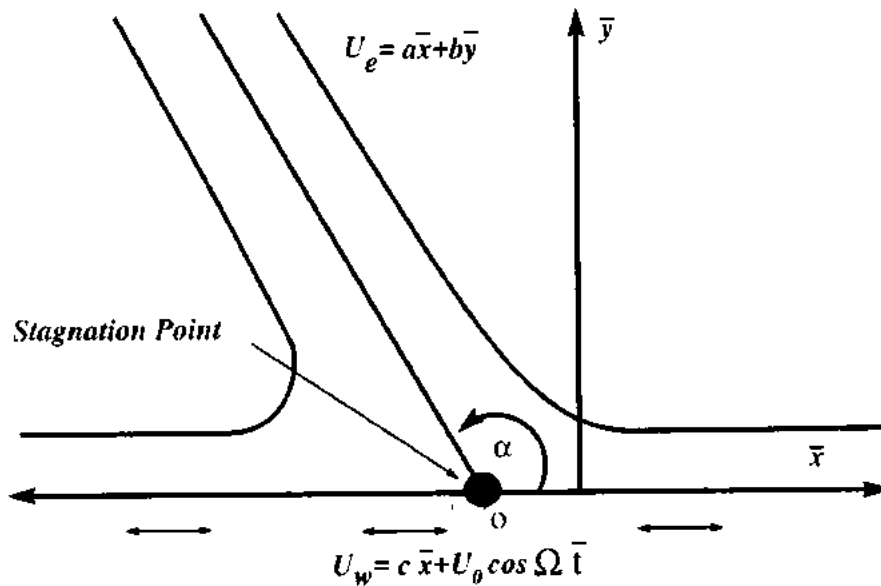
Figure 7.1: Physical Model of the problem

7.1 Problem formulation

We have considered the unsteady two-dimensional flow of elastico-viscous fluid impinging obliquely over an oscillating-stretching surface at $\bar{y} = 0$ as shown in Fig. 7.1. The elasticity of the fluid is assumed constant throughout the flow regime. The temperature of surface is taken as sinusoidal, oscillating about the mean value T_w, which is higher than the ambient temperature T_∞ of the surroundings. The flow and energy equations are (see ref. [93, 100])

$$\frac{\partial \bar{u}}{\partial \bar{x}} + \frac{\partial \bar{v}}{\partial \bar{y}} = 0, \qquad (7.1)$$

116

$$\frac{\partial \bar{u}}{\partial \bar{t}} + \bar{u}\frac{\partial \bar{u}}{\partial \bar{x}} + \bar{v}\frac{\partial \bar{u}}{\partial \bar{y}} = -\frac{1}{\rho}\frac{\partial \bar{p}}{\partial \bar{x}} + \nu \nabla^2 \bar{u} - \frac{k_0}{\rho}\left[\frac{\partial}{\partial \bar{t}}\left(\nabla^2 \bar{u}\right) + \left(\bar{u}\frac{\partial}{\partial \bar{x}} + \bar{v}\frac{\partial}{\partial \bar{y}}\right)\nabla^2 \bar{u} - \frac{\partial \bar{u}}{\partial \bar{x}}\nabla^2 \bar{u} - \frac{\partial \bar{u}}{\partial \bar{y}}\nabla^2 \bar{v}\right.$$
$$\left. -2\left\{\frac{\partial \bar{u}}{\partial \bar{x}}\frac{\partial^2 \bar{u}}{\partial \bar{x}^2} + \frac{\partial \bar{v}}{\partial \bar{y}}\frac{\partial^2 \bar{u}}{\partial \bar{y}^2} + \left(\frac{\partial \bar{u}}{\partial \bar{y}} + \frac{\partial \bar{v}}{\partial \bar{x}}\right)\frac{\partial^2 \bar{u}}{\partial \bar{x}\partial \bar{y}}\right\}\right],$$

$$(7.2)$$

$$\frac{\partial \bar{v}}{\partial \bar{t}} + \bar{u}\frac{\partial \bar{v}}{\partial \bar{x}} + \bar{v}\frac{\partial \bar{v}}{\partial \bar{y}} = -\frac{1}{\rho}\frac{\partial \bar{p}}{\partial \bar{y}} + \nu \nabla^2 \bar{v} - \frac{k_0}{\rho}\left[\frac{\partial}{\partial \bar{t}}\left(\nabla^2 \bar{v}\right) + \left(\bar{u}\frac{\partial}{\partial \bar{x}} + \bar{v}\frac{\partial}{\partial \bar{y}}\right)\nabla^2 \bar{v} - \frac{\partial \bar{v}}{\partial \bar{x}}\nabla^2 \bar{u} - \frac{\partial \bar{v}}{\partial \bar{y}}\nabla^2 \bar{v}\right.$$
$$\left. -2\left\{\frac{\partial \bar{u}}{\partial \bar{x}}\frac{\partial^2 \bar{v}}{\partial \bar{x}^2} + \frac{\partial \bar{v}}{\partial \bar{y}}\frac{\partial^2 \bar{v}}{\partial \bar{y}^2} + \left(\frac{\partial \bar{u}}{\partial \bar{y}} + \frac{\partial \bar{v}}{\partial \bar{x}}\right)\frac{\partial^2 \bar{v}}{\partial \bar{x}\partial \bar{y}}\right\}\right],$$

$$(7.3)$$

$$\frac{\partial \bar{T}}{\partial \bar{t}} + \bar{u}\frac{\partial \bar{T}}{\partial \bar{x}} + \bar{v}\frac{\partial \bar{T}}{\partial \bar{y}} = \frac{k}{\rho c_p}\left(\frac{\partial^2 \bar{T}}{\partial \bar{x}^2} + \frac{\partial^2 \bar{T}}{\partial \bar{y}^2}\right). \qquad (7.4)$$

In the above equations, $\bar{u}(\bar{x},\bar{y})$ and $\bar{v}(\bar{x},\bar{y})$ are the velocity components in $\bar{x}$ and $\bar{y}$-directions,

$\bar{T}(\bar{x},\bar{y})$ is the temperature, $\bar{p}(\bar{x},\bar{y})$ is the pressure, ν is the kinematic viscosity, ρ is the density,

k_0 is elasticity, C_p is the specific heat and k is thermal conductivity of the fluid. The boundary

conditions of the problem can be defined as

$$\bar{y} = 0: \qquad \bar{u} = c\bar{x} + U_0\cos\Omega\bar{t}, \ \bar{v} = 0, \ \bar{T} = T_\infty + \Delta T(1 + \varepsilon_1 \sin\Omega\bar{t}),$$

$$(7.5)$$

$$\bar{y} \to \infty: \qquad \bar{u} = a\bar{x} + b\bar{y}, \ \bar{T} = T_\infty,$$

where a, b and c are positive constant of dimension $1/T$, T_∞ is the ambient temperature and

$\Delta T = T_w - T_\infty$ is some temperature scale, ε_1 is the amplitude of the imposed temperature

oscillation, Ω is the frequency of the oscillation. Upon using the following non-dimensional

variable

$$x = \bar{x}\sqrt{\frac{c}{\nu}}, \ y = \bar{y}\sqrt{\frac{c}{\nu}}, \ t = \Omega\bar{t}, \ u = \frac{1}{\sqrt{\nu c}}\bar{u}, \ v = \frac{1}{\sqrt{\nu c}}\bar{v}, \ p = \frac{1}{\rho\nu c}\bar{p}, \ T = \frac{\bar{T} - T_\infty}{T_w - T_\infty} \qquad (7.6)$$

in Eqs.(7.1−7.5), we get the following form

$$\frac{\partial u}{\partial x} + \frac{\partial v}{\partial y} = 0, \qquad (7.7)$$

$$\frac{\Omega}{c}\frac{\partial u}{\partial t} + u\frac{\partial u}{\partial x} + v\frac{\partial u}{\partial y} = -\frac{\partial p}{\partial x} + \nu \nabla^2 u - \frac{k_0 c}{\rho \nu}\left[\frac{\Omega}{c}\frac{\partial}{\partial t}\left(\nabla^2 u\right) + \left(u\frac{\partial}{\partial x} + v\frac{\partial}{\partial y}\right)\nabla^2 u - \frac{\partial u}{\partial x}\nabla^2 u - \right.$$
$$\left. \frac{\partial u}{\partial y}\nabla^2 v - 2\left\{\frac{\partial u}{\partial x}\frac{\partial^2 u}{\partial x^2} + \frac{\partial v}{\partial y}\frac{\partial^2 u}{\partial y^2} + \left(\frac{\partial u}{\partial y} + \frac{\partial v}{\partial x}\right)\frac{\partial^2 u}{\partial x\partial y}\right\}\right],$$

$$(7.8)$$

117

$$\frac{\Omega}{c}\frac{\partial v}{\partial t}+u\frac{\partial v}{\partial x}+v\frac{\partial v}{\partial y}=-\frac{\partial p}{\partial y}+v\nabla^2 v-\frac{k_0 c}{\rho v}\left[\frac{\partial}{\partial t}\left(\nabla^2 v\right)+\left(u\frac{\partial}{\partial x}+v\frac{\partial}{\partial y}\right)\nabla^2 v-\frac{\partial v}{\partial x}\nabla^2 u-\right.$$
$$\left.\frac{\partial v}{\partial y}\nabla^2 v-2\left\{\frac{\partial u}{\partial x}\frac{\partial^2 v}{\partial x^2}+\frac{\partial v}{\partial y}\frac{\partial^2 v}{\partial y^2}+\left(\frac{\partial u}{\partial y}+\frac{\partial v}{\partial x}\right)\frac{\partial^2 v}{\partial x\partial y}\right\}\right],$$

(7.9)

$$\frac{\Omega}{c}\frac{\partial T}{\partial t}+u\frac{\partial T}{\partial x}+v\frac{\partial T}{\partial y}=\frac{k}{\rho v c_p}\left(\frac{\partial^2 T}{\partial x^2}+\frac{\partial^2 T}{\partial y^2}\right),$$

(7.10)

$$y=0: \qquad u=x+\varepsilon\cos t, \quad v=0, \quad T=1+\varepsilon_1\sin t,$$

$$y\to\infty: \qquad u=\frac{a}{c}x+\frac{b}{c}y, \quad T=0.$$

(7.11)

In which $\varepsilon=U_0/\sqrt{vc}$ is the dimensionless constant which describe the amplitude of the plate oscillation. Introducing the stream function ψ, which satisfies the continuity equation identically, we write the velocity components as

$$u=\frac{\partial\psi}{\partial y}, \quad v=-\frac{\partial\psi}{\partial x}.$$

(7.12)

After eliminating pressure from Eqs. (7.8) and (7.9) and then upon using Eq. (7.12), Eqs. (7.7–7.11) take the following form

$$\beta^*\frac{\partial\left(\nabla^2\psi\right)}{\partial t}+We\beta^*\frac{\partial\left(\nabla^4\psi\right)}{\partial t}-\frac{\partial\left(\psi,\nabla^2\psi\right)}{\partial(x,y)}-We\frac{\partial\left(\psi,\nabla^4\psi\right)}{\partial(x,y)}-\nabla^4\psi=0,$$

(7.13)

$$\beta^*\frac{\partial T}{\partial t}+\frac{\partial\psi}{\partial y}\frac{\partial T}{\partial x}-\frac{\partial\psi}{\partial x}\frac{\partial T}{\partial y}=\frac{1}{\text{Pr}}\left(\frac{\partial^2 T}{\partial x^2}+\frac{\partial^2 T}{\partial y^2}\right),$$

(7.14)

$$y=0: \qquad \frac{\partial\psi}{\partial y}=x+\varepsilon\cos t, \quad \psi=0, \quad T=1+\varepsilon_1\sin t,$$

$$y\to\infty: \qquad \psi=\frac{a}{c}xy+\frac{\gamma}{2}y^2, \quad T=0,$$

(7.15)

where $\gamma=b/c$ represents shear in the stream, $\beta^*=\Omega/c$ is dimensionless unsteady parameter, $We=k_0c/\rho v$ be the Wiessenberg number and $Pr=\mu c_p/k$ be the Prandtl number. Suppose the solution of Eqs. (7.13, 7.14) subject to boundary conditions (7.15) is of the form

$$\psi=xf(y)+g(y,t), \quad T=\theta(y,t),$$

(7.16)

118

where the functions $f(y)$ and $g(y)$ are normal and oblique component of the flows. Using the Eq. (7.16) in Eqs. (7.13 − 7.15), and then after comparing the the like powers of x, we get

$$f^{iv} + ff''' - f'f'' + We\left(ff^v - f'f^{iv}\right) = 0,$$ (7.17)

$$\frac{\partial^4 g}{\partial y^4} + f\frac{\partial^3 g}{\partial y^3} - f''\frac{\partial g}{\partial y} + We\left(f\frac{\partial^5 g}{\partial y^5} - f^{iv}\frac{\partial g}{\partial y}\right) - \beta^*\frac{\partial^3 g}{\partial t\partial y^2} - We\beta^*\frac{\partial^5 g}{\partial t\partial y^4} = 0,$$ (7.18)

$$\frac{\partial^2 \theta}{\partial y^2} + \Pr\left(f\frac{\partial \theta}{\partial y} - \beta^*\frac{\partial \theta}{\partial t}\right) = 0,$$ (7.19)

$$y = 0: \quad f(y) = 0, \ f'(y) = 1, \ g(y,t) = 0, \ \frac{\partial g(y,t)}{\partial y} = \varepsilon \cos t, \ \theta(y,t) = 1 + \varepsilon_1 \sin t,$$

$$y \to \infty: \quad f'(y) = a/c, \ \frac{\partial^2 g(y,t)}{\partial y^2} = \gamma, \ \theta(y,t) = 0.$$ (7.20)

The prime sign denotes the differentiation with respect to y. Integrating Eqs. (7.17) and (7.18) with respect to y and the resulting constants of integration are evaluated by employing the boundary conditions at infinity and we get

$$f''' + ff'' - (f')^2 + We\left(ff^{iv} - 2f'f''' + (f'')^2\right) + \left(\frac{a}{c}\right)^2 = 0,$$ (7.21)

$$\frac{\partial^3 g}{\partial y^3} + f\frac{\partial^2 g}{\partial y^2} - f'\frac{\partial g}{\partial y} + We\left(f\frac{\partial^4 g}{\partial y^4} - f'\frac{\partial^3 g}{\partial y^3} + f''\frac{\partial^2 g}{\partial y^2} - f'''\frac{\partial g}{\partial y}\right),$$

$$-\beta^*\frac{\partial^2 g}{\partial t\partial y} - We\beta^*\frac{\partial^4 g}{\partial t\partial y^3} - A\gamma = 0,$$ (7.22)

$$\frac{\partial^2 \theta}{\partial y^2} + \Pr\left(f\frac{\partial \theta}{\partial y} - \beta^*\frac{\partial \theta}{\partial t}\right) = 0,$$ (7.23)

$$y = 0: \quad f(y) = 0, \ f'(y) = 1, \ g(y,t) = 0, \ \frac{\partial g(y,t)}{\partial y} = \varepsilon \cos t, \ \theta(y,t) = 1 + \varepsilon_1 \sin t,$$

$$y \to \infty: \quad f'(y) = a/c, \ \frac{\partial^2 g(y,t)}{\partial y^2} = \gamma, \ \theta(y,t) = 0.$$ (7.24)

Where A is a constant which measure the boundary layer displacement. It arises when $y \to \infty$, $f(y)$ behaves as $f(y) = (a/c)y + A$. The dimensionless components of velocities are

$$u = \frac{\partial \psi}{\partial y} = xf'(y) + g'(y),$$ (7.25)

$$v = -\frac{\partial \psi}{\partial x} = -f(y).$$ (7.26)

119

The quantities of physical interest are the skin friction coefficients C_f and the local Nusselt number Nu_x, can be expressed as

$$C_f = \frac{\tau_w}{\rho u_w^2}, \quad Nu_x = \frac{\bar{x} q_w}{k(T_w - T_\infty)}, \tag{7.27}$$

where τ_w is shear stress at the wall and q_w is the local heat flux at the wall which are defined in dimensionless form as as

$$\tau_w = \mu c\,(u_y + v_x) - 2c^2 k_0 \left(-u_y v_y - u_x v_x - \frac{1}{2} v_y\,(u_y + v_x) - \frac{1}{2} u_x\,(u_y + v_x) + \frac{1}{2}\,(u_{yt} + v_{xt}) + \right.$$

$$\left. \frac{1}{2} v\,(u_{yy} + v_{xy}) + \frac{1}{2} u\,(u_{xy} + v_{xx}) \right)\Bigg|_{y=0},$$

$$q_w = -k\,(T_w - T_\infty)\sqrt{\frac{c}{v}}\left(\frac{\partial T}{\partial y}\right)\Bigg|_{y=0} \tag{7.28}$$

Using Eqs. (7.12) and (7.16), the skin friction coefficients and the local Nusselt number take the following form

$$Re_x C_f = x\,(1 - 3We - \varepsilon We)\,f''(0) + (1 - 2We)\frac{\partial^2 g(0,t)}{\partial y^2} - \beta^* We\frac{\partial^3 g(0,t)}{\partial t \partial y^2}, \tag{7.29}$$

$$Re_x^{1/2} Nu_x = -\theta'(0,t).$$

where $Re_x = c\bar{x}^2/v = x^2$.

7.2 Chebyshev Spectral Newton Iterative Scheme

The nonlinear time dependent partial differential equations (7.21)–(7.23) subject to the boundary conditions (7.24) are solved numerically by using Chebyshev Spectral Newton Iterative Scheme [90]. This method has advantages over other numerical techniques such as shooting method, parallel shooting method, and finite difference method. In this method, we transform our domain - 1 to 1 and for very small number of points we get accurate solution while in other method we discretize our domain in thousands of points to get accuracy. This numerical

120

scheme is also repaid convergent. On the other hand, present method have make a comparison

with other studies as Tables 7.1 and 7.2, and obtained good agreement with their study results.

For the initial steady solution at $t = 0$, the governing Eqs. (7.21)–(7.24) reduce to the follow-

ing ordinary differential equations

$$f''' + ff'' - (f')^2 + We\left(ff^{iv} - 2f'f''' + (f'')^2\right) + \left(\frac{a}{c}\right)^2 = 0, \tag{7.30}$$

$$g''' + fg'' \cdot f'g' + We\left(fg^{iv} - f'g''' + f''g'' - f'''g'\right) - A\gamma = 0, \tag{7.31}$$

$$\theta'' + \Pr f\theta' = 0, \tag{7.32}$$

$$y = 0: \quad f(y) = 0, \ f'(y) = 1, \ g(y,0) = 0, \ g'(y,0) - \varepsilon, \ \theta(y,0) = 1,$$

$$y \to \infty: \quad f'(y) = a/c, \ g''(y,0) = \gamma, \ \theta(y,0) = 0. \tag{7.33}$$

To find the solution of Eqs. (7.30)–(7.33), first we convert the Eq. (7.30) into a linear form by

using Newton's linearization process. For $(i+1)$th iterates, we write

$$f_{i+1} = f_i + \delta f_i, \tag{7.34}$$

and similarly for all other dependent variables, where δf_i represents a very small change in

f_i. Using Eq. (7.34) in (7.30) and dropping the quadratic and higher order terms in δf_i, we

obtained

$$c_{0,i}\delta f_i^{iv} + c_{1,i}\delta f_i''' + c_{2,i}\delta f_i'' + c_{3,i}\delta f_i' + c_{4,i}\delta f_i = R_i, \tag{7.35}$$

subject to boundary conditions

$$\delta f_i(0) = -f_i(0), \ \delta f_i'(0) = a/c - f_i'(0), \ \delta f_i'(\infty) = 1 \cdot f_i'(\infty). \tag{7.36}$$

The coefficients $c_{j,i}(j = 0,1,2,3,4)$ and R_i are

$$c_{0,i} = Wef_i, \ c_{1,i} = 1 - 2We f_i', \ c_{2,i} = f_i + 2We f_i''$$

$$c_{3,i} = -2f_i' - 2We f_i''', \ c_{4,i} = f_i'' + We f_i^{iv}, \tag{7.37}$$

$$R_i = -We\left(f_i f_i^{iv} - 2f_i' f_i''' + (f_i'')^2\right) - f_i''' - f_i f_i'' + (f_i')^2 - (a/c)^2.$$

121

Now the solution of obtained linear equations can calculated by employing the same steps as elaborated in chapter 4. Once the solution of Eqs. (7.30)–(7.33) is calculated for steady case ($t = 0$), we proceeded further to next time steps by taking step size $\Delta t = k = \pi/90$. The time derivative in Eqs. (7.21)–(7.24) is replaced by backward finite difference scheme $\left(\text{e.g. } \frac{\partial}{\partial t}()_n = \frac{1}{k}\left(()_n - ()_{n-1}\right) \right)$, the Eqs. (7.21)–(7.24) take the following form

$$\left(f'''\right)_n + (f)_n \left(f''\right)_n - \left(f'^2\right)_n + We\left((f)_n \left(f^{iv}\right)_n - 2\left(f'\right)_n \left(f'''\right)_n + \left(f''^2\right)_n\right) + (a/c)^2 = 0,$$
(7.38)

$$\left(\frac{\partial^3 g}{\partial y^3}\right)_n + (f)_n \left(\frac{\partial^2 g}{\partial y^2}\right)_n - \left(f'\right)_n \left(\frac{\partial g}{\partial y}\right)_n + We\left((f)_n \left(\frac{\partial^4 g}{\partial y^4}\right)_n - \left(f'\right)_n \left(\frac{\partial^3 g}{\partial y^3}\right)_n + \left(f''\right)_n \left(\frac{\partial^2 g}{\partial y^2}\right)_n\right.$$
$$\left. - \left(f'''\right)_n \left(\frac{\partial g}{\partial y}\right)_n\right) - \frac{\beta^*}{k}\left(\left(\frac{\partial g}{\partial y}\right)_n - \left(\frac{\partial g}{\partial y}\right)_{n-1}\right) - \frac{We\beta^*}{k}\left(\left(\frac{\partial^3 g}{\partial y^3}\right)_n - \left(\frac{\partial^3 g}{\partial y^3}\right)_{n-1}\right) - A\gamma = 0,$$
(7.39)

$$\left(\frac{\partial^2 \theta}{\partial y^2}\right)_n + \Pr\left((f)_n \left(\frac{\partial \theta}{\partial y}\right)_n - \frac{\beta^*}{k}(\theta_n - \theta_{n-1})\right) = 0,$$
(7.40)

$$y = 0: (f)_n = 0, \ (f')_n = 1, \ (g)_n = 0, \ \left(\frac{\partial g}{\partial y}\right)_n = \varepsilon \cos(nk), \ (\theta)_n = 1 + \varepsilon_1 \sin(nk),$$
(7.41)

$$y \to \infty: (f')_n = a/c, \ \left(\frac{\partial^2 g}{\partial y^2}\right)_n = \gamma, \ (\theta)_n = 0, \ t_n = nk \text{ where } n = 1, 2, 3\ldots .$$

As the Eq. (7.38) is independent of time, so solution of $(f)_n$ is known for all $n \geq 0$, then Eqs. (7.39), (7.40) became linear and are solved by employing differentiation matrix D directly [88–90]. For $n=1$, Eqs. (7.39), (7.40) take the following form

$$\left(\frac{\partial^3 g}{\partial y^3}\right)_1 + (f)_1 \left(\frac{\partial^2 g}{\partial y^2}\right)_1 - \left(f'\right)_1 \left(\frac{\partial g}{\partial y}\right)_1 + We\left((f)_1 \left(\frac{\partial^4 g}{\partial y^4}\right)_1 - \left(f'\right)_1 \left(\frac{\partial^3 g}{\partial y^3}\right)_1 + \left(f''\right)_1 \left(\frac{\partial^2 g}{\partial y^2}\right)_1\right.$$
$$\left. - \left(f'''\right)_1 \left(\frac{\partial g}{\partial y}\right)_1\right) - \frac{\beta^*}{k}\left(\left(\frac{\partial g}{\partial y}\right)_1 - \left(\frac{\partial g}{\partial y}\right)_0\right) - \frac{We\beta^*}{k}\left(\left(\frac{\partial^3 g}{\partial y^3}\right)_1 - \left(\frac{\partial^3 g}{\partial y^3}\right)_0\right) - A\gamma = 0,$$
(7.42)

$$\left(\frac{\partial^2 \theta}{\partial y^2}\right)_1 + \Pr\left((f)_1 \left(\frac{\partial \theta}{\partial y}\right)_1 - \frac{\beta^*}{k}(\theta_1 - \theta_0)\right) = 0,$$
(7.43)

$$y = 0: (f)_1 = 0, \ (f')_1 = 1, \ (g)_1 = 0, \ \left(\frac{\partial g}{\partial y}\right)_1 = \varepsilon \cos(k), \ (\theta)_1 = 1 + \varepsilon_1 \sin(k),$$
(7.44)

$$y \to \infty: (f')_1 = a/c, \ \left(\frac{\partial^2 g}{\partial y^2}\right)_1 = \gamma, \ (\theta)_1 = 0.$$

122

In Eqs. (7.42–7.44), the values of f_0, g_0 and θ_0 are known from the previous step ($t = 0$) and

the values of unknown f_1, g_1 and θ_1 are found by employing Chebyshev Spectral Collocation

Method, as it has been done in steady case ($t = 0$). Similarly for $n=2$, the values of unknown

f_2, g_2 and θ_2 are found. We continued this process up to required range of t. For the computa-

tion purpose, a numerical code in MATLAB 2010a is developed and used.

7.3   Results and discussion

The non-linear partial differential equations (7.21–7.23) subject to the boundary conditions

(7.24) are solved numerically for the different values of dimensionless parameters namely

Wiessenberg number We, velocities ratio parameter a/c, obliqueness parameter γ, unsteady

parameter β^*, Prandtl number Pr, amplitude of oscillating plate ε and amplitude of imposed

temperature oscillation ε_1, for required range of t. The Comparison of $f''(0)$, and $-\theta'(0)$

for some values of the parameters with those of previous studies are given in Tables 7.1 and

7.2. It is found that the computed results are convergent and highly accurate. In Table 7.3, the

values of skin friction coefficient and local Nusselt number are presented for different values

of pertinent parameters. Computed solution in term of velocity, temperature profiles, skin

friction coefficient and Nusselt number are plotted for sundry parameters in Figs. 7.2–7.9.

In Fig. 7.2, the dimensionless velocity component $u(y,t)$ is plotted against y at different time

steps, $t = 0$, $\pi/4$, $\pi/2$ and π for $\varepsilon = 1$, $\gamma = 2$, $\beta^* = 0.2$, $We = 0.1$. The solid lines are drawn for

$a/c - 0.1$ and the dashed lines are for $a/c = 1.2$. It is seem that due to no-slip condition fluid

oscillates with the velocity of plate. Since for fixed $\varepsilon = 1$, the oscillation velocity of the plate is

$u(y,t) = 1 + \cos t$, its least value is 0 and maximum value is 2. It is further observed that with

increase of time, the velocity of the fluid decreases against y and at $t = \pi$ it comes to zero, and

again starts increasing for $t = \pi$ to 2π. It is also noted that the velocity of the fluid increases

with increase in the values of a/c. In Fig. 7.3, the temperature profile is plotted against y at $t = 0, \pi/4, \pi/2$ and π for $\varepsilon = 1, \varepsilon_1 = 1, \gamma = 2, \beta^* = 0.2, We = 0.1, Pr = 1$. The solid lines are drawn for $a/c = 0.1$ and the dashed lines are for $a/c = 1.2$. For $\varepsilon_1 = 1$, the temperature of the fluid oscillates from 0 to 2. It is observed that the temperature decreases with increase in the values of a/c in the boundary layer region. In Fig. 7.4, the values of skin friction coefficient $(Re_x C_f)$ are plotted against t, for $\varepsilon = 0, 1, 2, 3$ at $We = 0.1, \gamma = 2, \beta^* = 0.2, \varepsilon_1 = 1$. The solid lines are drawn for $a/c = 0.1$ and the dashed lines are for $a/c = 1.2$. The values of skin friction coefficient oscillate about its mean value -0.384 for $a/c = 0.1$ and 1.981 for $a/c = 1.2$ respectively. The value $Re_x C_f = -0.384$ is at $\varepsilon = 0, a/c = 0.1, We = 0.1, \gamma = 2, \beta^* = 0.2, \varepsilon_1 = 1$ and $Re_x C_f = 1.981$ is at $\varepsilon = 0, a/c = 1.2, We = 0.1, \gamma = 2, \beta^* = 0.2, \varepsilon_1 = 1$ for all time t. It is importantly noted that with increase in the values of ε, the amplitude of skin friction coefficient increases. In the region $0 < t < \pi/2$ the skin friction coefficient decreases with increase of ε, where in the region $\pi/2 < t < 3\pi/2$ an opposite behavior is observed. Again in the region $3\pi/2 < t < 2\pi$ the skin friction coefficient decreases with increase of ε. The behavior of skin friction coefficient continues for all values of t. The amplitude of skin friction coefficient against t increases due to increase in the values of a/c. In Fig. 7.5, the values of skin friction coefficient $(Re_x C_f)$ are plotted against t for $\gamma = 0, 0.5, 1, 2$ at $We = 0.1, \beta^* = 0.2, \varepsilon = 0$ and $\varepsilon_1 = 1$. The values of skin friction coefficient increases with increase of obliqueness parameter γ. In this figure, the solid lines are drawn for Newtonian case $(We = 0)$ and dotted lines are for non-Newtonian case $(We = 0.2)$. It is also noted that amplitude of skin friction coefficient decreases with increase in the values of Non-Newtonian parameter We. In Fig. 7.6, the values of local Nusselt number $\left(Re_x^{-1/2} Nu_x\right)$ are plotted against t for $\varepsilon_1 = 0, 1, 2, 3$ at $\varepsilon = 1, We = 0.1, \beta^* = 0.2, \gamma = 2, Pr = 1$. The solid lines are drawn for $a/c = 0.1$ and the dashed lines are for $a/c = 1.2$. The heat transfer rate is observed periodic

function of time t and amplitude of oscillation can further be increased by increasing the values of ε_1 as shown in Fig. 7.6. It is further noted that the increase in the amplitude of oscillation can further be increased by increasing the values of velocities ratio parameter a/c. In general, both parameters help to increase the heat transfer rate in the boundary layer region near the oblique stagnation point flow over an oscillating stretching surface. The effect of Prandtl (Pr) on heat transfer rate is shown from Fig. 7.7. It is plotted for $\varepsilon = 1, a/c = 0.1, \beta^* = 0.2, \gamma = 2, \varepsilon_1 = 1$ and for different important values of $Pr = 0.1, 0.7, 1, 7$. The solid lines are drawn for $We = 0$ (Newtonian case) and the dashed lines are for $We = 0.2$ (non-Newtonian case). The heat transfer rate enhances due to increase in Pr and the amplitude of the oscillation become larger for large Prandtl number. It is also seen that in non-Newtonian fluid, the heat transfer decreases as compare to Newtonian fluid case. In Fig. 7.8, the values of skin friction coefficient $(Re_x C_f)$ are plotted against t over one period of oscillation, for $\beta^* = 0, 0.2, 0.4$, at $\varepsilon_1 = 1, \varepsilon = 1, a/c = 0.1, \gamma = 2, We = 0.1$ and $Pr = 1$. With increase of unsteady parameter β^*, the amplitude of the skin friction increases. It is also observed that with increase of β^*, the skin friction coefficient coefficient increases in the region $0^o < t < 195^o$ and decreases in the region $195^o < t < 378^o$. Fig. 7.9 shows the time variation of local Nusselt number $\left(Re_x^{-1/2} Nu_x\right)$ over one period of oscillation for $\beta^* = 0, 0.2, 0.4$ at $\varepsilon_1 = 1, \varepsilon = 1, a/c = 0.1, \gamma = 2, We = 0.1$ and $Pr = 1$. It is observed that the amplitude of the local Nusselt number is proportional to unsteady parameter β^* i.e increase in the values of β^* results in increase the amplitude of $Re_x^{1/2} Nu_x$. In Fig.7.10, the streamlines are plotted for $\gamma = 0, 0.5, 1, 2$ at $\varepsilon_1 = 1, \varepsilon = 1, \beta^* = 0.2, We = 0.1, a/c = 0.2$. It is noted that with increase in the values of γ, the amplitude of oscillation decreases. From the trend of streamlines, it is predicted that for larger values of γ, amplitude of oscillating streams tends to zero. In Fig.7.11, isotherms are plotted for $\varepsilon_1 = 0, 0.5, 1, 2$ at $\varepsilon = 1, \gamma = 1, \beta^* = 0.2, We = 0.1, a/c = 0.2$ and $Pr = 0.7$. It is seen

from the figures (a-d) the oscillation in temperature increases with increase in the values of ε_1.

Table 7.1: Comparison of $f''(0)$ and $\theta'(0)$ against different values of a/c with Nazar et al. [25] and Mahapatra and Gupta [24] when $We = 0$, $\varepsilon = 0$, $\varepsilon_1 = 0$, $\gamma = 0$, $\beta^* = 0$ and $Pr = 1.5$.

	$f''(0)$			$\theta'(0)$	
a/c	Present	Mahapatra and Gupta [24]	Nazar et al. [25]	Present	Mahapatra and Gupta [24]
0.1	−0.96939	−0.9694	−0.9694	−0.77680	−0.777
0.2	−0.91810	−0.9181	−0.9181	−0.79712	−0.797
0.5	−0.66726	−0.6673	−0.6673	−0.86479	−0.863
2.0	2.01750	2.0175	2.0176	−1.17810	−1.171
3.0	4.72928	4.7293	4.7296	−1.35194	−1.341

Table 7.2: Comparison of $f''(0)$ against different values of a/c and We with Husain et al. [52]. The others parameters are fixed at $\varepsilon = 0$, $\gamma = 0$, $\beta^* = 0$.

|	Present	Husain et al. [52]	Present	Husain et al. [52]	Present	Husain et al. [52]
a/c	$We = 0.1$		$We = 0.2$		$We = 0.3$	
0.1	−1.0273	−1.0271	−1.0956	−1.0955	−1.1778	−1.1777
0.5	−0.7300	−0.7299	−0.8102	−0.8101	−0.9142	−0.9141
1.1	0.1918	0.19177	0.2393	0.2392	0.3520	0.35198
1.2	0.3993	0.3992	0.5140	0.5139	0.9103	0.8499

Table 7.3: Values of Re_xC_f and $(Re_x)^{-1/2}Nu_x$ for the various parameter a/c, γ, ε_1, ε, β^*, Pr and We.

Pr	γ	ε₁	ε	a/c	We	β*	Re_xC_f				$\left(Re_x^{-1/2}Nu_x\right)$
							$t=0$	$t=\pi/4$	$t=\pi/2$	$t=\pi$	
0.7	0	0	0	0	0	0	-1.000 (0.4544)	-1.000 (0.4544)	-1.000 (0.4544)	-1.000 (0.4544)	
	0.5						-2.0344 (0.4544)	-2.0344 (0.4544)	-2.0344 (0.4544)	-2.0344 (0.4544)	
		0.5	0.5				-2.5130 (0.4544)	-2.3728 (0.6151)	-2.0344 (0.6817)	-1.5559 (0.4544)	
				0.3			-1.0819 (0.5250)	-0.9250 (0.7106)	-0.5463 (0.7875)	-0.0106 (0.5250)	
					0.1		-0.8216 (0.5170)	-0.7273 (0.6998)	-0.4256 (0.7755)	-0.0811 (0.5170)	
						0.1	-0.8216 (0.5170)	-0.7137 (0.7254)	-0.4018 (0.7788)	-0.0856 (0.4839)	
1.0							-0.8216 (0.6380)	-0.7137 (0.8930)	-0.4018 (0.9607)	-0.0856 (0.6000)	
		1					-0.5971 (0.6380)	-0.4891 (0.8930)	-0.1772 (0.9607)	0.3101 (0.6000)	
		1	1				-1.0040 (0.6380)	-0.7881 (1.1479)	-0.1643 (1.2833)	0.8104 (0.5620)	
				0.8			-0.4983 (0.7536)	-0.2593 (1.3314)	0.4461 (1.5115)	1.5685 (0.6942)	
					0.2		-0.3760 (0.7487)	-0.3023 (1.3234)	0.2216 (1.5017)	1.3019 (0.6889)	
						0.15	-0.3760 (0.7487)	-0.2936 (1.3467)	0.2411 (1.5052)	1.3092 (0.6593)	
7.0							-0.3760 (2.0422)	-0.2936 (3.6613)	0.2411 (4.1037)	1.3092 (1.8138)	
	2.0						0.1641 (2.0422)	0.2465 (3.6613)	0.7812 (4.1037)	1.8494 (1.8138)	
		1.5	1.5				-0.2154 (2.0422)	-0.0918 (4.4709)	0.7103 (5.1345)	2.3125 (1.6995)	
				1.1			-0.1081 (2.1487)	-0.0253 (4.6711)	0.9064 (5.3969)	2.6808 (1.8295)	
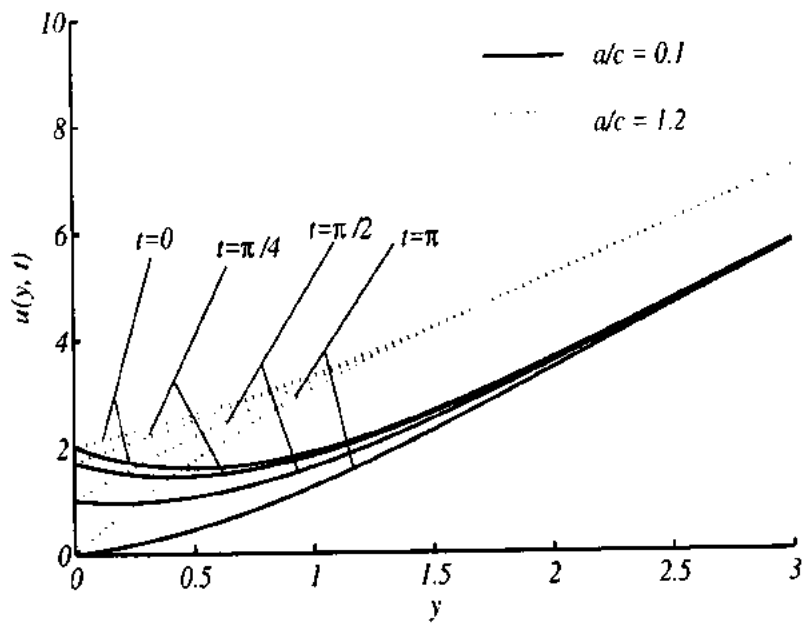
Figure 7.2: Velocity profile $u(y,t)$ against y at different time steps.
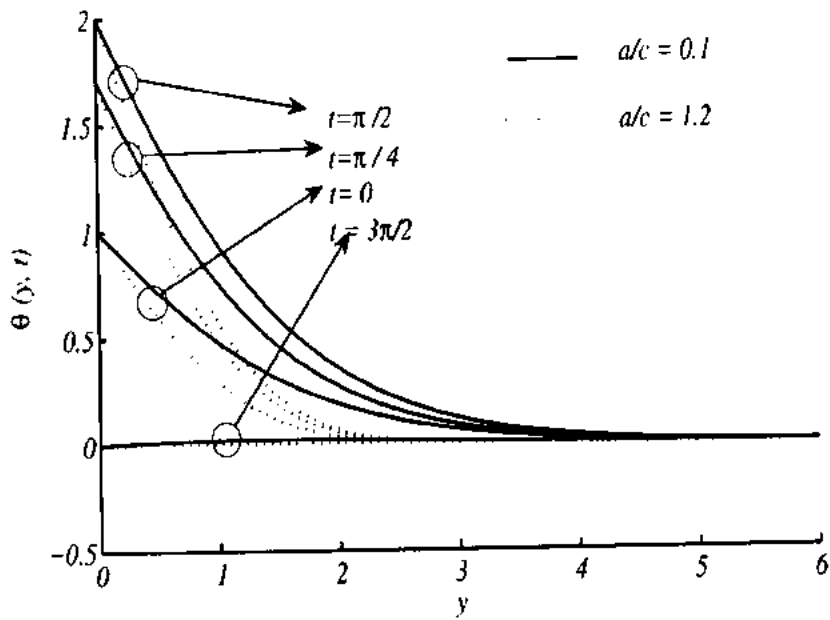
Figure 7.3: Temperature profile $\theta(y,t)$ against y at different time steps.

128
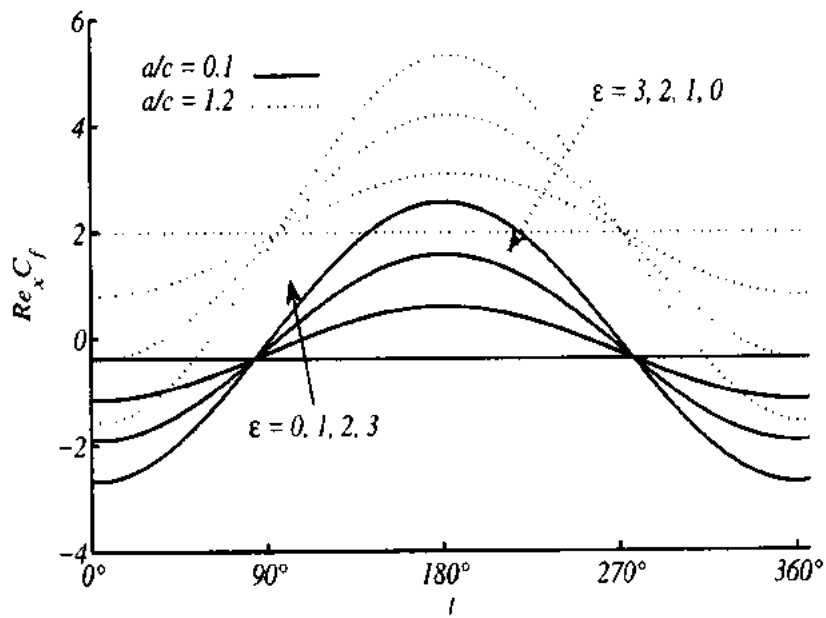
Figure 7.4: Variation of skin friction coefficient Re_xC_f against t for different values of ε and a/c.
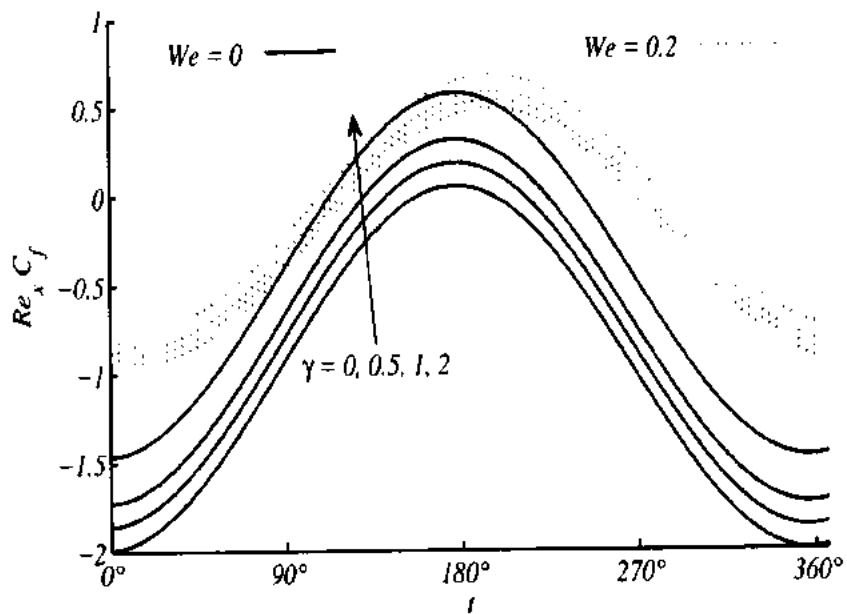
Figure 7.5: Variation of skin friction coefficient Re_xC_f against t for different values of γ and We.
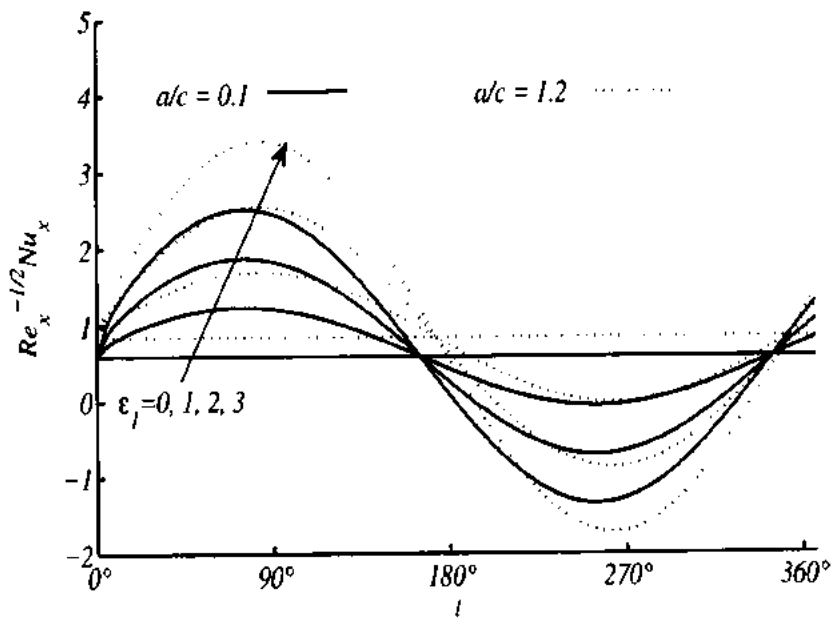
Figure 7.6: Variation of Nusselt Number $Re_x^{-1/2}Nu_x$ against t for different values of ε_1 and a/c.
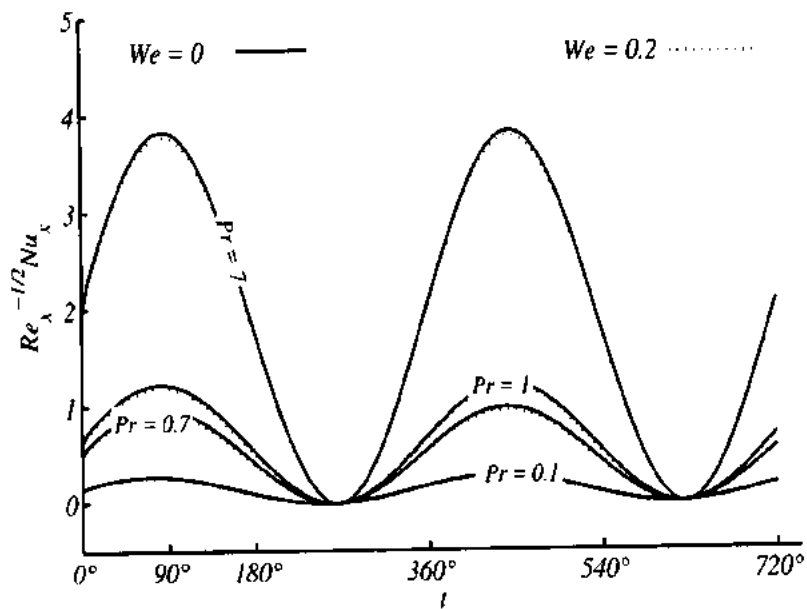
Figure 7.7: PVariation of Nusselt Number $Re_x^{-1/2}Nu_x$ against t for different values of Pr and We.

130
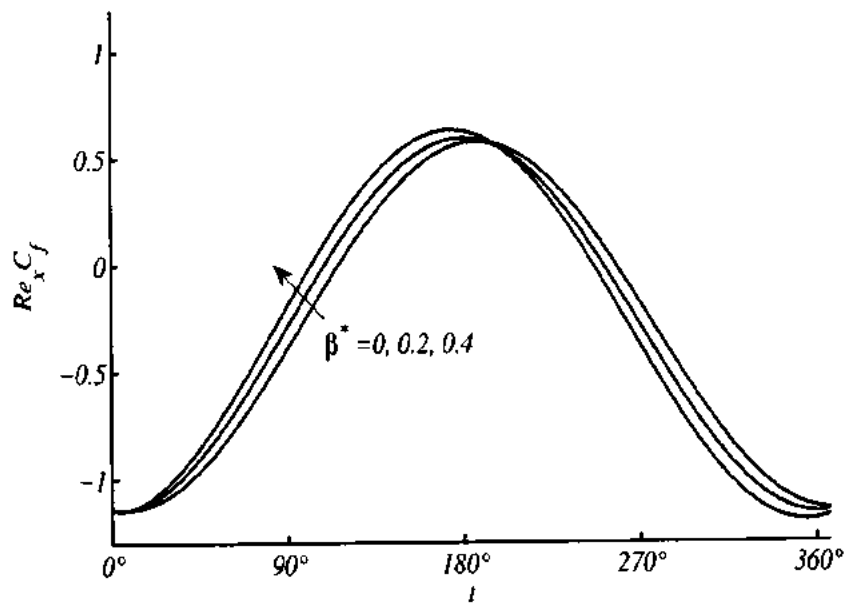
Figure 7.8: Variation of skin friction coefficient $Re_x C_f$ against t for different values of β^* .

Figure 7.9: Variation of Nusselt Number $Re_x^{-1/2} Nu_x$ against t for different values of β^* .

131
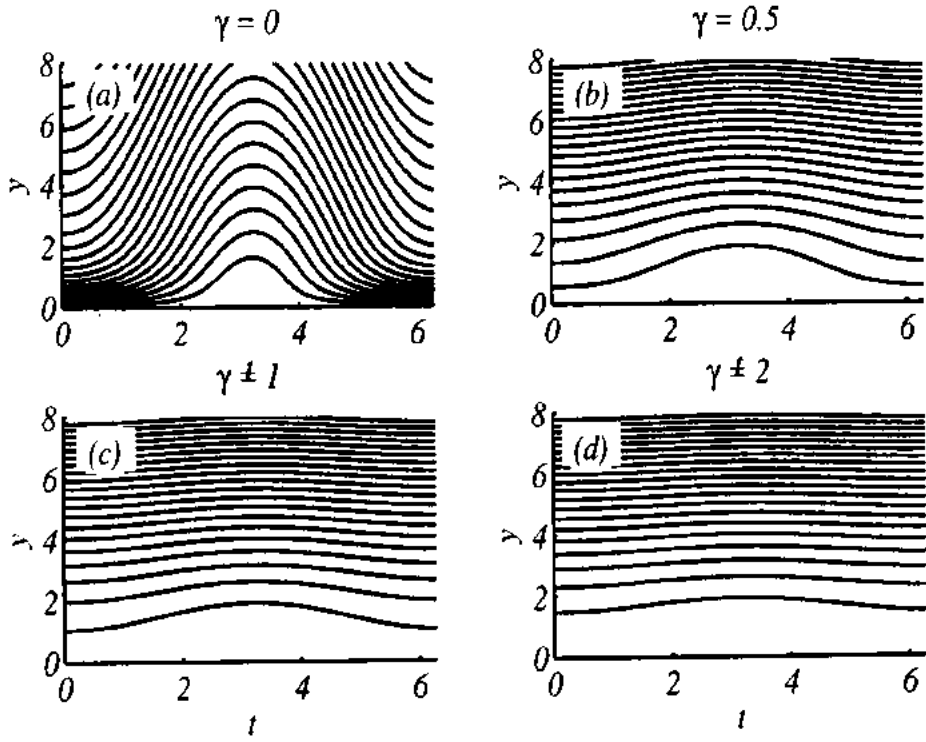
Figure 7.10: Stream lines for different values of γ.
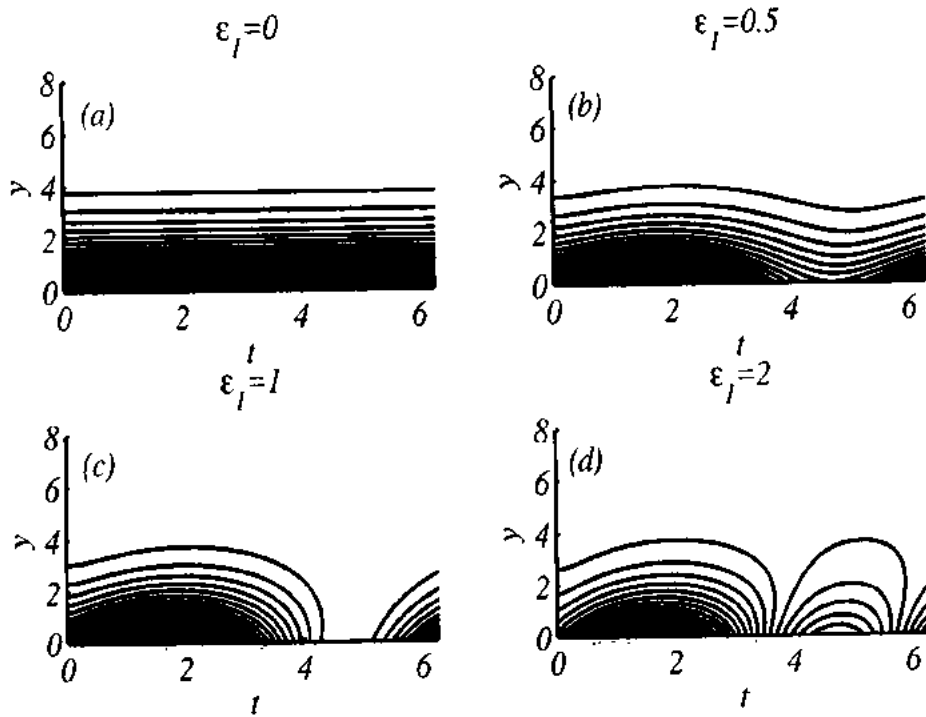
Figure 7.11: Isotherms for different values of ε_1.

132

7.4 Conclusions

In this chapter, unsteady oblique stagnation point flow of elastico-viscous fluid over an oscillating-stretching surface with sinusoidal wall temperature is considered. The governing partial differential equations are transfo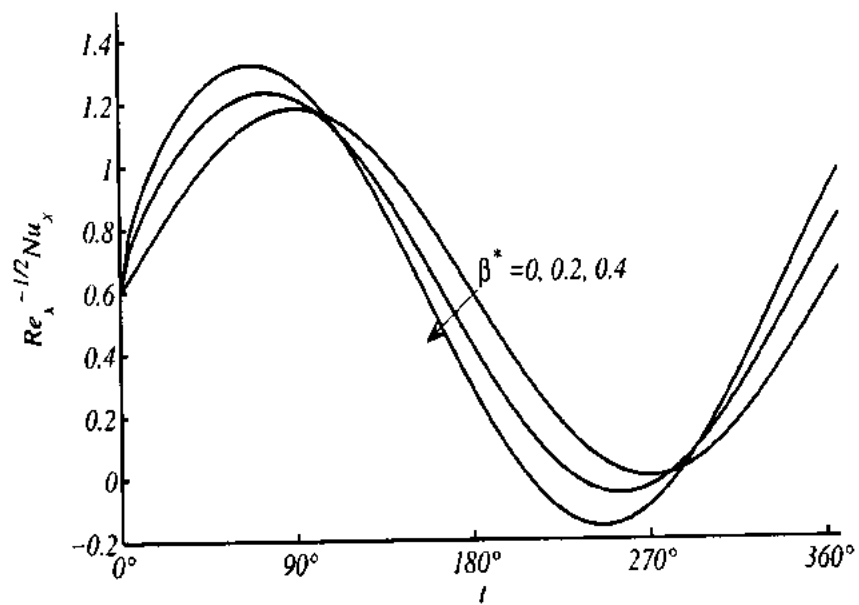rmed into dimensionless form. The obtained system of partial differential equations is solved numerically by using Chebyshev Spectral Newton Iterative Scheme (CSNIS). The numerical results are compared with the previous studies in limiting sense, which are highly accurate and have excellent agreement with published results. The results are shown graphically for sundry parameters. Velocity, temperature, skin friction coefficient and local Nusselt number oscillate periodically due to sinusoidal nature of the plate oscillation and surface temperature. This study concludes that

- The velocity of the fluid increases with increase in the values of a/c in the boundary layer region, while the temperature is observed a decreasing function of a/c.

- The values of skin friction coefficient increases with the increase of obliqueness parameter γ.

- Amplitude of skin friction coefficient decreases with increase in the values of We.

- The heat transfer rate enhances due to increase of Prandtl number (Pr) in the boundary layer region near the stagnation point.

- Heat transfer rate decreases in non-Newtonian fluids as compare to Newtonian fluids.

- The amplitude of the local Nusselt number $\left(Re_x^{-1/2} Nu_x\right)$ and skin friction coefficient $\left(Re_x C_f\right)$ is proportional to unsteady parameter β^*.

Bibliography

[1] K. Hiemenz, Die grenzschitcht an einem in den gleichformigen flussigkeitsstrom einge-

tauchten geraden kreiszylinder, Dingler polytech. J., 326 (1911) 321 – 324.

[2] L. Howarth, On the calculation of the steady flow in the boundary layer near the surface

of a cylinder in a stream, ARC-RM, 164 (1935) 16–32.

[3] S. Goldstein, Modern Developments in Fluid Dynamics, Oxford University Press (1938).

[4] F. Homann, Der einuss grosser zahigkeit bei der stromung um den zylinder und um die

kugel, Z. Angew Math. Mech. (ZAMM), 16 (1936) 153–164.

[5] L. Howarth, The boundary layer in three-dimensional flow. Part-II: the flow near a stagna-

tion point, Philos Mag., 42 (1951) 1433–1440.

[6] A. Davey, Boundary layer flow at a saddle point of attachment, J. Fluid Mech., 10 (1961)

593–610.

[7] E.R.G. Eckert, Die berechnung des warmeuberganges in der laminaren grenzschicht um-

stromter korper, VDI forschungsheft, Berlin, (1942).

[8] P.R. Nachtsheim and P. Swigert, Satisfaction of asymptotic boundary conditions in numer-

ical solution of systems of non-linear equations of the boundary layer type, NASA TN D

3004, October (1965).

[9] N. Rott, Unsteady viscous flow in the vicinity of a stagnation point, Quarterly J. Appl. Math., 13 (1956) 444–451.

[10] M.B. Glauert, The laminar boundary layer on oscillating plates and cylinders, J. Fluid Mech., 1 (1956) 97–110.

[11] J. Watson, The two-dimensional laminar flow near the stagnation point of a cylinder which has an arbitrary transverse motion, Quarterly J. Mech. Appl. Math., 12(2) (1959) 175–190.

[12] J.T. Stuart, Double boundary layers in oscillatory viscous flow, J. Fluid Mech., 24 (1966) 673–687.

[13] T.J. Pedley, Two-dimensional boundary layers in a free stream which oscillates without reversing, J. Fluid Mech., 55 (1972) 359–383.

[14] C.E. Grosch and H. Salwen, Oscillating stagnation point flow, Proceedings of the Royal Society of London, Series A, Math. Physical Sci., 384 (1982) 175–190.

[15] G.J. Merchant and S.H. Davis, Modulated stagnation point flow and steady streaming, J. Fluid Mech., 198 (1989) 543–555.

[16] A.L. Hazel and T.J. Pedley, Alteration of mean wall shear stress near an oscillating stagnation point, J. Biomech. Eng., 120 (1998) 227.

[17] L.J. Crane, Flow past a stretching plate, Z. Angew. Math. Phys., 21 (1970) 645-647.

[18] P.S. Gupta and A.S. Gupta, Heat and mass transfer on a stretching sheet with suction or blowing, Can. J. Chem. Eng., 55 (1977) 744-746.

[19] C.Y. Wang, The three dimensional flow due to a stretching at surface, Phys. Fluids, 27 (1984) 1915–1917.

[20] C.Y. Wang, Fluid flow due to a stretching cylinder, Phys. Fluids, 31 (1988) 466–468.

[21] C.Y. Wang, Liquid film on an unsteady stretching sheet, Quart. Appl. Math., 48 (1990) 601–610.

[22] T. C Chiam, Stagnation point flow towards a stretching plate, J. Phys. Soc. Jpn., 63 (1994) 2443–2444 .

[23] T. R. Mahapatra and A. S. Gupta, Magnetohydrodynamic stagnation point flow towards a stretching sheet, Acta Mech., 152 (2001) 191–196.

[24] T.R. Mahapatra and A.S. Gupta, Heat transfer in stagnation point flow towards a stretching sheet, Heat Mass Transfer, 38 (2002) 517–521.

[25] R. Nazar, N. Amin, D. Filip and I. Pop, Stagnation point flow of a micropolar fluid towards a stretching sheet, Int. J. Nonlin. Mech., 39 (2004) 1227–1235.

[26] G. C. Layek, S. Mukhopadhyay and S. K. A. Samad, Heat and mass transfer analysis for boundary layer stagnation point flow towards a heated porous stretching sheet with heat absorption/generation and suction/blowing, Int. Commun. Heat Mass, 34 (2007) 347–356.

[27] T. Hayat, T. Javed, and Z. Abbas, MHD flow of a micropolar fluid near a stagnation point towards a non-linear stretching surface, Nonlinear Anal-Real, 10 (2009) 1514–1526.

[28] J. Zhu, L. Zheng and Z. G. Zhang, Effects of slip condition on MHD stagnation point flow over a Power-law stretching sheet, Appl. Math. Mech., 31 (2010) 439–448.

[29] G. C. Shit, R. Haldar and Sinha, Unsteady flow and heat transfer of a MHD micropolar fluid over a porous stretching sheet in the presence of thermal radiation, J. Mech., 29 (2013) 559−568.

[30] K. Bhattacharyya, Heat transfer analysis in unsteady boundary layer stagnation point flow towards a shrinking/stretching sheet, Ain Shams Eng. J., 4 (2013) 259−264.

[31] J.T. Stuart, The viscous flow near a stagnation point when the external flow has uniform vorticity, J. Aerospace Sci., 26 (1959)124−125.

[32] K.J. Tamada, Two-dimensional stagnation point flow impinging obliquely on a plane wall, J. Phys. Soc. Jpn., 46 (1979) 310−311.

[33] T. C Chiam, Two-Dimensional Flow Impinging Obliquely on a Moving Plane Wall. Z. angew. Math. Mech., 62 (1982) 708−709.

[34] J.M. Dorrepaal, An exact solution of the Navier-Stokes equation which describes non-orthogonal stagnation point flow in two dimensions, J. Fluid Mech., 163 (1986) 141−147.

[35] M.J. Lyell and K.D. Cronin, Extinction properties of a premixed laminar flame in oblique stagnation flow in the region of the stagnation point, Comput. Method. Appl. M., 95(1) (1992) 71−86.

[36] F. Labropulu, J. M. Dorrepaal and O. P. Chandna, Oblique flow impinging on a wall with suction or blowing, Acta Mech., 115 (1) (1996) 15−25.

[37] B. S. Tilley and P. D. Weidman, Oblique two-fluid stagnation point flow, Eur. J. Mech. − B/Fluids, 17 (2) (1998) 205−217.

[38] M. Amaouche and D. Boukari, Influence of thermal convection on non-orthogonal stagnation point flow, Int. J. Therm. Sci. 42 (3) (2003) 303−310.

[39] P. D. Weidman and Putkaradze, Axisymmetric Stagnation Flow Obliquely Impinging on a Circular Cylinder, Eur. J. Mech. - B/Fluids, 22 (2003) 123-131.

[40] P. D. Weidman and Putkaradze, Erratum to axisymmetric stagnation flow obliquely impinging on a circular cylinder, Eur. J. Mech.- B/Fluids, 24 (2004) 788-790.

[41] F. Labropulu and M. Chinichian, Unsteady oscillatory stagnation point flow of a viscoelastic fluid, Int. J. Eng. Sci. 42 (2004) 625-633.

[42] M. Reza, A.S. Gupta, Steady two-dimensional oblique stagnation point flow towards a stretching surface, Fluid Dyn. Res., 37 (2005) 334-340.

[43] Y. Y. Lok, N. Amin and I. Pop, Non-orthogonal stagnation point flow towards a stretching sheet, Int. J. Non-Linear Mech., 41 (2006) 622-627.

[44] M. Reza and A.S. Gupta, Some aspects of non-orthogonal stagnation point flow towards a stretching surface, Engineering, 2 (2010) 705-709 .

[45] P. Drazin and N. Riley, The Navier-Stokes equations, a classification of flows and exact solutions, London Mathematical Society, Lecture notes series, Cambridge University Press, (2007).

[46] T.R. Mahapatra, S. Dholey and A.S. Gupta, Oblique stagnation point flow of incompressible visco-elastic fluid towards a stretching sheet, Int. J. Non-Linear Mech. 42 (2007) 484- 499.

[47] R. M. Tooke and M. G. Blyth, A note on oblique stagnation point flow, Phys. Fluids, 20 (2008) 1-3.

[48] T. Grosan, I. Pop, C. Revnic and D.B. Ingham, magnetohydrodynamic oblique stagnation point flow, Acta Mech., 44 (2009) 565-572.

[49] P. Singh, N. S. Tomer, S. Kumar and D. Sinha, MHD oblique stagnation point flow towards a stretching sheet with heat transfer, Int. J. Appl. Math. Mech. 1. 6(13) (2010) 94−111.

[50] Y. Y. Lok, I. Pop and D. B. Ingham, Oblique stagnation slip flow of a micropolar fluid, Meccanica, 45 (2010) 187−198.

[51] P.D. Weidman and M.A. Sprague, Flows induced by a plate moving normal to stagnation point flow, Acta Mech., 219 (2011) 219−229.

[52] I. Husain, F. Labropulu and I. Pop, Two-dimensional Oblique stagnation point flow towards a stretching surface in a viscoelastic fluid, Cent. Eur. J. Phys., 9 (2011) 176−182.

[53] T.R. Mahapatra, S.K. Nandy and A.S. Gupta, Oblique stagnation point flow and heat transfer towards a shrinking sheet with thermal radiation, Meccanica, 47 (2012) 1325−1335.

[54] L.V. Yajun and Z. Liancun, MHD Oblique stagnation point flow and heat transfer of a micro polar fluid towards to a moving plate with radiation, Int. J. Eng. Sci. Innovative Tech., 2 (2013) 200−209.

[55] J. Buongiorno and L.W. Hu, Nanofluid coolants for advanced nuclear power plants, Proceedings of ICAPP, Seoul, Paper No. 5705 (2005) 15−19.

[56] J. C. Maxwell, A Treatise on Electricity and Magnetism, 2nd Edition, Oxford Univ. Press, Cambridge, (1904).

[57] S.U.S. Choi, Enhancing thermal conductivity of fluids with nanoparticles, in: Developments and Application of Non-Newtonian Flows, ASME ,FED-Vol. 231/MD-vol. 66 (1995) 99−105.

[58] J. Buongiorno, Convective Transport in Nanofluids, ASME J. Heat Transf., 128 (2006) 240–250.

[59] A.V. Kuznetsov and D.A. Nield, Natural convective boundary layer flow of a nanofluid past a vertical plate, Int. J. Therm. Sci., 49 (2010) 243–247.

[60] A.V. Kuznetsov and D.A. Nield, Double-diffusive natural convective boundary layer flow of a nanofluid past a vertical plate, Int. J. Therm. Sci., 50 (2011) 712–717.

[61] O.D. Makinde and A. Aziz, Boundary layer flow of a nanofluid past a stretching sheet with a convective boundary condition, Int. J. Therm. Sci., 50 (2011) 1326–1332.

[62] M. Hassani, M. Mohammad Tabar, H. Nemati, G. Domairry and F. Noori, An analytical solution for boundary layer flow of a nanofluid past a stretching sheet, Int. J. Therm. Sci., 50 (2011) 2256–2263.

[63] P. Rana and R. Bhargava, Flow and heat transfer of a nanofluid over a nonlinearly stretching sheet: a numerical study, Commun. Nonlinear Sci., 17 (1) (2012) 212–226.

[64] M.A.A. Hamad and M. Ferdows, Similarity solution of boundary layer stagnation point flow towards a heated porous stretching sheet saturated with a nanofluid with heat absorption/generation and suction/blowing: a Lie group analysis, Commun. Nonlinear Sci., 17(1) (2012) 132–140.

[65] M. Sheikholeslami, M. Hatami and G. Domairry, Numerical simulation of two phase unsteady nanofluid flow and heat transfer between parallel plates in presence of time dependent magnetic field, J. Taiwan Inst. Chem. E., 46 (2015) 43–50.

[66] M. Turkyilmazoglu, Nanofluid flow and heat transfer due to a rotating disk, Comput. fluids, 94 (2014) 139–146.

[67] M.M. Rahman, A.V. Roscab and I. Pop, Boundary layer flow of a nanofluid past a permeable exponentially shrinking/stretching surface with second order slip using Buongiornos model, Int. J. Heat Mass Tran., 77 (2014), 1133–1143.

[68] M.M. Rashidi, N. Vishnu Ganesh, A.K. Abdul Hakeem and B. Ganga, Buoyancy effect on MHD flow of nanofluid over a stretching sheet in the presence of thermal radiation, J. Mol. Liq., 198 (2014) 234–238.

[69] P.K. Kameswaran, S. Shaw, P. Sibanda and P.V.S.N. Murthy, Homogeneous–heterogeneous reactions in a nanofluid flow due to a porous stretching sheet, Int. J. Heat Mass Tran., 57 (2013) 465–472.

[70] F.M. Abbasi, T. Hayat and A. Alsaedi, Peristaltic transport of magneto-nanoparticles submerged in water: Model for drug delivery system, Phasica E, 68 (2015) 123–132.

[71] N. Bachok, A. Ishak and I. Pop, boundary layer flow of nanofluids over a moving surface in a flowing fluid, Int. J. Therm. Sci., 49(9) (2010) 1663–1668.

[72] S.M. Sebdani, M. Mahmoodi and S. Mohammad Hashemib, Effect of nanofluid variable properties on mixed convection in a square cavity, Int. J. Therm. Sci., 52 (2012) 112–126.

[73] M.M. Rashidi, E. Momoniat, M. Ferdows and A. Basiriparsa, Lie group solution for free convective flow of a nanofluid past a chemically reacting horizontal plate in a porous media, Math. Probl. Eng., (2014), Article ID 239082.

[74] Mohammad H. Abolbashari, N. Freidoonimehr, F. Nazari and Mohammad M. Rashidi, Entropy analysis for an unsteady MHD flow past a stretching permeable surface in nanofluid, Powder Technol., 267 (2014) 256–267.

[75] O.D. Makinde, Analysis of Sakiadis flow of nanofluids with viscous dissipation and Newtonian heating, Appl. Math. Mech., (Engl Ed) 33(12) (2012) 1545–1554.

[76] N. Takemitsu and Y. Matunobu, Unsteady stagnation point flow impinging obliquely on an oscillating flat plate, J. Phys. Soc. Jpn. 47 (1979) 1347.

[77] T. Cebeci, and P. Bradshaw, Physical and computational aspects of convective heat transfer, Springer New York (1984).

[78] H.B. Keller and T. Cebeci, Numerical methods in boundary layer theory, Annu. Rev. Fluid Mech. 10 (1978) 417–433.

[79] P.D. Ariel, Hiemenz flow in hydromagnetics, Acta Mech. 103 (1994) 31– 43.

[80] M. Sajid, Z. Abbas,T. Javed and N. Ali, Boundary layer flow of an Oldroyd−B fluid in the region of stagnation point over a stretching sheet, Can. J. Phys., 88 (2010) 635–640.

[81] F. Labropulu, D. Li and I. Pop, Non-orthogonal stagnation point flow toward a stretching surface in a non-Newtonian fluid with heat transfer, Int. J. Therm. Sci., 49 (2010) 1042–1050.

[82] J.A. Shetz, Boundary Layer Analysis, Prentice Hall, New Jersey, (1993).

[83] H. Schichting, Boundary Layer Theory, sixth ed., McGraw-Hill, New York, (1964).

[84] T. Cebeci and H. B. Keller, shooting and parallel shooting methods for solving the Falkner-Skan boundary layer equation, J. Comput. Phys., 7 (1971) 289–300 .

[85] K. Vafai, Handbook of Porous Media, second ed. Taylor & Francis, New York, (2005).

[86] H. A. Attia, Hiemenz Flow through a Porous Medium of a Non-Newtonian Rivlin-Ericksen Fluid with Heat Transfer, Tamkang J. Sci. Eng., 12 (2009) 359–364.

[87] M.A. Hossain, H.S. Takhar, Radiation effect on mixed convection along a vertical plate with uniform surface temperature, Int. J. Heat Mass Tran., 31 (1996) 243–248.

[88] S. S. Motsa, P. G. Dlamini, and M. Khumalo, Spectral Relaxation Method and Spectral Quasi-linearization Method for solving unsteady boundary layer flow problems, Adv. Math. Phys., (2014), Article ID 341964.

[89] T. Javed and I. Mustafa, Effects of unsteady expansion / contraction of Wang's cylinder problem with suction near a stagnation point, Asia-Pac. J. Chem. Eng., Asia Pacific J. Chem. Eng., 10 (2015) 184–192.

[90] A. Majeed, T. Javed, A. Ghaffari and M.M. Rashidi, Analysis of heat transfer due to stretching cylinder with partial slip and prescribed heat flux: A Chebyshev Spectral Newton Iterative Scheme, Alexandria Eng. J., 54 (2015) 1029–1036.

[91] L.N. Trefethen, Spectral Methods in MATLAB, Society for Industrial and Applied Mathematics, SIAM ,Philadelphia, Pa, USA, (2000).

[92] D. Li, F. Labropulu and I. Pop, Oblique stagnation point flow of a viscoelastic fluid with heat transfer, Int. J. Non-Linear Mech., 44 (2009) 1024–1030.

[93] D. W. Beard and K. Walters, Elastico-viscous boundary layer flows, I. Two-dimensional flow near a stagnation point, Math. Proc. Cambridge, 60 (1964) 667–674.

[94] V.K. Garg and K.R. Rajagopal, Flow of a non-Newtonian fluid past a wedge, Acta Mech., 88 (1991) 113.

[95] K. Vajravelu and T. Roper, Flow and heat transfer in a second grade fluid over a stretching sheet, Int. J. Non-linear Mech., 34 (1999) 1031–1036.

[96] T. Hayat, S. Asad, M. Mustafa and Hamed H. Alsulami, Heat transfer analysis in the flow of Walter's B fluid with a convective boundary condition, Chinese, Phys. B, 23 **(2014)** 084701.

[97] P.D. Weidman, D.G. Kubitschekb and A.M.J. Davis, The effect of transpiration on self-similar boundary layer flow over moving surfaces, Int. J. Eng. Sci., 44 **(2006)** 730−737.

[98] J. Paullet and P. Weidman, Analysis of stagnation point flow toward a stretching sheet, Int. J. Nonlinear Mech., 42 **(2007)** 1084−1091.

[99] A.V. Rosca, and I. Pop, Flow and heat transfer over a vertical permeable stretching/ shrinking sheet with a second order slip, Int. J. Heat Mass Tran., 60 **(2013)** 355−364.

[100] J.H. Merkina and I. Pop, Free convection near a stagnation point in a porous medium resulting from an oscillatory wall temperature, Int. J. Heat Mass Tran., 43 **(2000)** 611−621.

[101] E. Magyari, A. Pantokratoras, Note on the effect of thermal radiation in the linearized Rosseland approximation on the heat transfer characteristics of various boundary layer flows, Int. Commun. Heat Mass, 38 **(2011)** 554−558.

[102] Y.Y. Lok, N. Amin and I. Pop, Mixed convection flow near a non-orthogonal stagnation point towards a stretching vertical plate, Int. J. Heat Mass Tran. 50 **(2007)** 48554863.